

Republic of Iraq  
Ministry of Higher Education  
and Scientific Research  
University of Baghdad  
College of Education For Pure  
Science / Ibn Al-Haitham



# Study the Structural and Optical Properties of (SnO<sub>2</sub>) Thin Film and analyzing it by Using Image Processing Technique

A thesis

Submitted to the College of Education for Pure Science / Ibn  
Al-Haitham - University of Baghdad in Partial Fulfillment of the  
Requirements for the Degree of Master of Science in Physics

By

**Noor Ali Hameed**

Bachelor of Science in Physics / 2013

Supervised by:

**Dr. Inbethaq Mohammed Ali**

بِسْمِ اللَّهِ الرَّحْمَنِ الرَّحِيمِ

﴿وَسَأَلُوهُنَّ عَنِ الرَّوحِ ۗ قُلِ الرُّوحُ مِنْ أَمْرِ رَبِّي وَمَا أُوتِيتُمْ مِنَ الْعِلْمِ إِلَّا قَلِيلًا﴾

﴿وَسَأَلُوهُنَّ عَنِ الرَّوحِ ۗ قُلِ الرُّوحُ مِنْ أَمْرِ رَبِّي وَمَا أُوتِيتُمْ مِنَ الْعِلْمِ إِلَّا قَلِيلًا﴾

صدق الله العظيم

سورة الاسراء

الآية 85

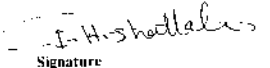


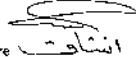
Committee Certification

We certify that we have read this thesis " Study the Structural and Optical Properties of (SnO<sub>2</sub>) Thin Film and analyzing it by Using Image Processing Technique " submitted by (Noor Ali Hameed) and as examining committee examined the student in its content and that in our opinion it is adequate with standard as thesis for the Degree of Master of Science in Physics.

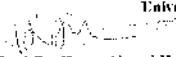
Signature S. A. MAKI  
Name: Dr. Namir A. Maki  
Address: University of Baghdad.  
Title: Professor  
(Chairman)  
Date: / / 2018

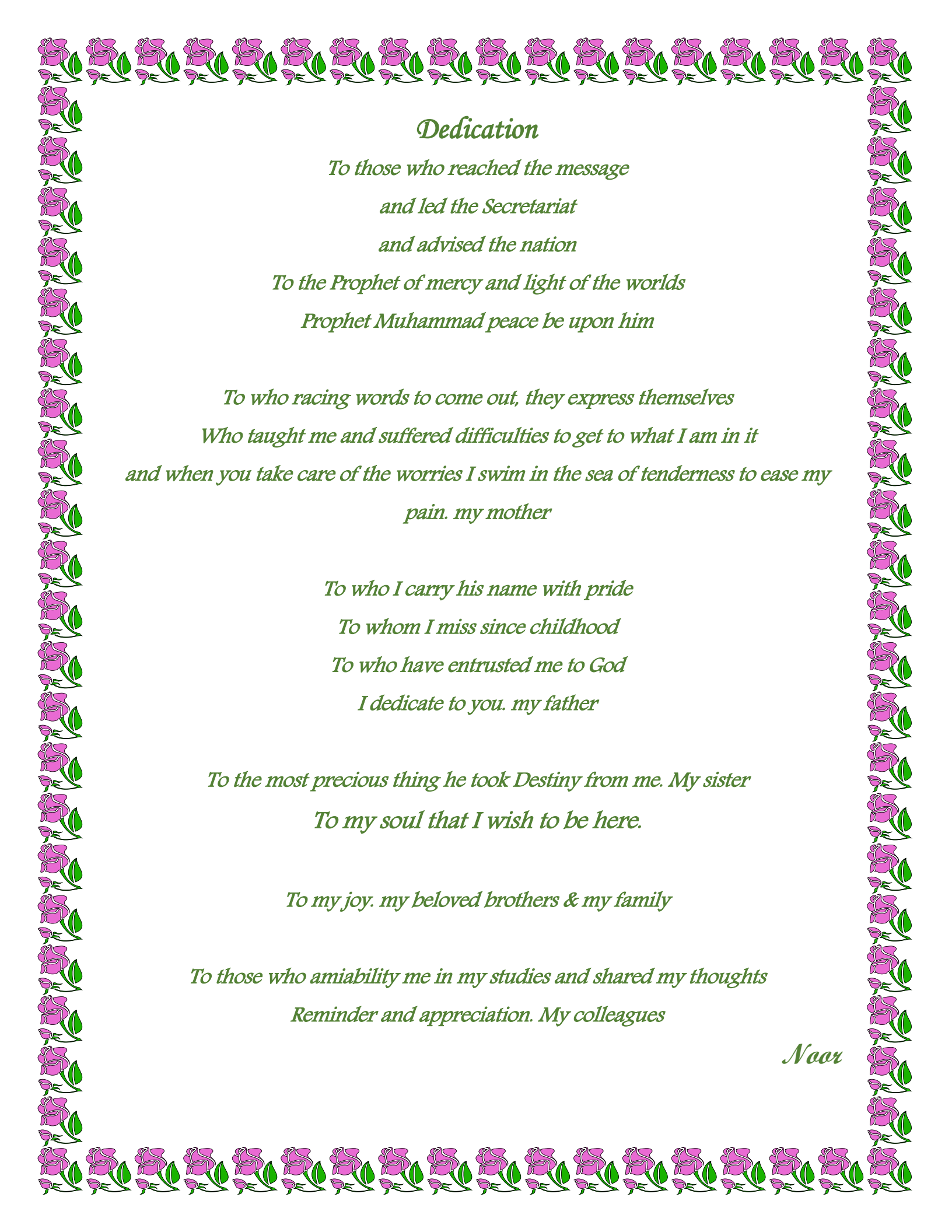
Signature   
Name: Dr. Radha S. Hammodi  
Title: Professor  
Address: Al-Mustansiriyah University  
(Member)  
Date: / / 2018

Signature   
Name: Instr. Dr. Ikhlās H. Shalal  
Title: Professor  
Address: University of Baghdad  
(Member)  
Date: / / 2018

Signature   
Name: Instr. Dr. Inbethaq Mohammed Ali  
Address: University of Baghdad  
Title: Instructor  
(Member-Supervisor)  
Date: / / 2018

Approved by the Council of the College of Education for Pure Sciences Ibn Al-Haitham /  
University of Baghdad

Signature   
Name: Prof. Dr. Hasan Ahmed Hasan  
Address: Dean of college  
Date: 5/ 15/ 2018



## *Dedication*

*To those who reached the message  
and led the Secretariat  
and advised the nation*

*To the Prophet of mercy and light of the worlds  
Prophet Muhammad peace be upon him*

*To who racing words to come out, they express themselves  
Who taught me and suffered difficulties to get to what I am in it  
and when you take care of the worries I swim in the sea of tenderness to ease my  
pain. my mother*

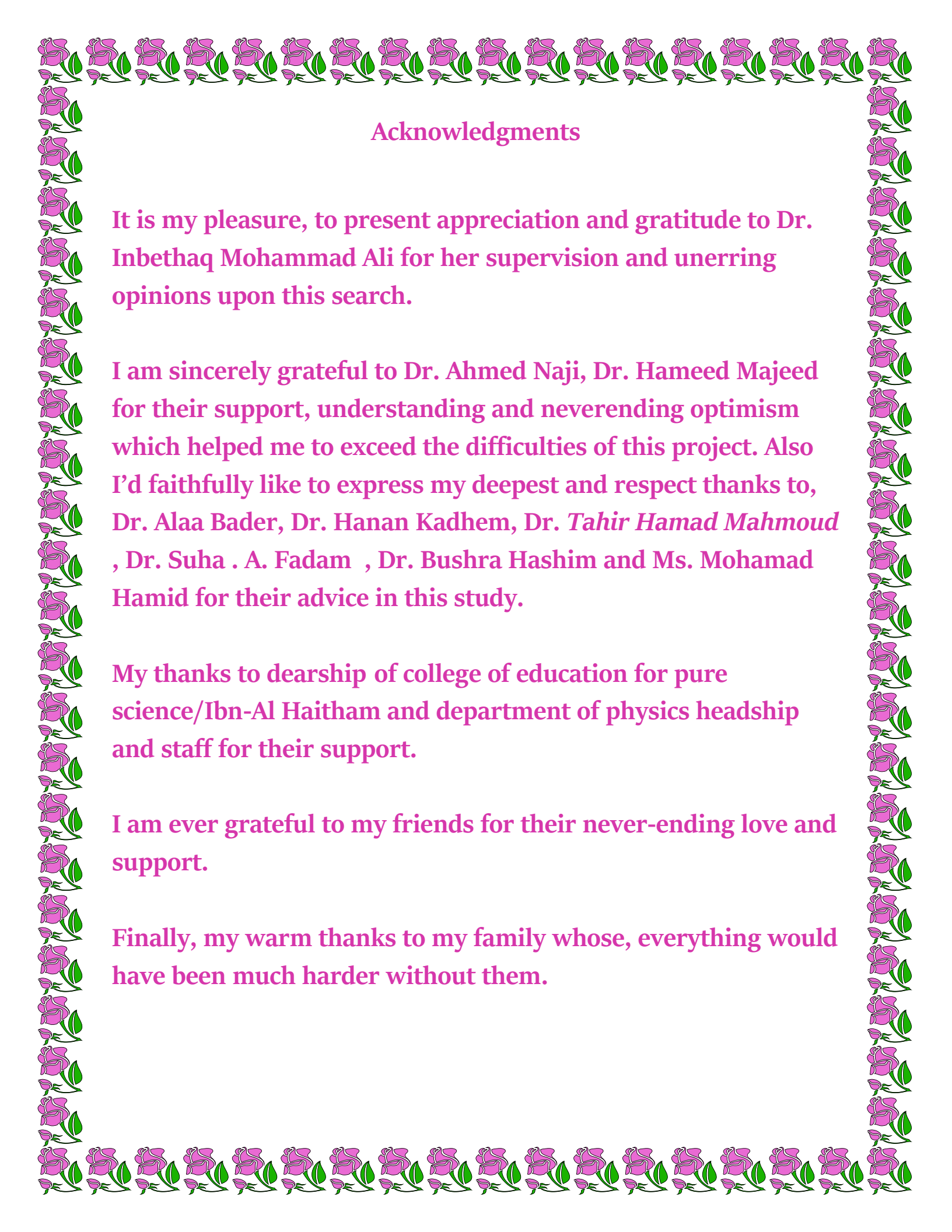
*To who I carry his name with pride  
To whom I miss since childhood  
To who have entrusted me to God  
I dedicate to you. my father*

*To the most precious thing he took Destiny from me. My sister  
To my soul that I wish to be here.*

*To my joy. my beloved brothers & my family*

*To those who amiability me in my studies and shared my thoughts  
Reminder and appreciation. My colleagues*

*Noor*



## Acknowledgments

It is my pleasure, to present appreciation and gratitude to Dr. Inbethaq Mohammad Ali for her supervision and unerring opinions upon this search.

I am sincerely grateful to Dr. Ahmed Naji, Dr. Hameed Majeed for their support, understanding and neverending optimism which helped me to exceed the difficulties of this project. Also I'd faithfully like to express my deepest and respect thanks to, Dr. Alaa Bader, Dr. Hanan Kadhem, Dr. *Tahir Hamad Mahmoud* , Dr. Suha . A. Fadam , Dr. Bushra Hashim and Ms. Mohamad Hamid for their advice in this study.

My thanks to dearship of college of education for pure science/Ibn-Al Haitham and department of physics headship and staff for their support.

I am ever grateful to my friends for their never-ending love and support.

Finally, my warm thanks to my family whose, everything would have been much harder without them.

## **ABSTRACT**

In this research, undoped SnO<sub>2</sub> films were prepared by thermal vacuum evaporation method, in which the films were deposited on glass substrates with different thicknesses [450, 525 and 600] nm.

The surface morphology and topography of the prepared films was studied using the Scanning electron microscopy (SEM) and the Atomic force microscopy (AFM). The study showed that the surface structure of the deposited films was nanostructures with grain size of (60-71) nm. It was found that the surface roughness increased with changing thickness from (0.9 – 1.9) nm. General characterization includes study surface topography (grain size and roughness) using AFM images and explores the relationship with an advanced set of roughness parameters obtained from the SEM images, these averaging amplitude parameters  $S_a$ ,  $S_q$  and extreme amplitude parameters  $S_p$ ,  $S_v$  and  $S_z$  explain of surface profile the height. The parameters  $S_{sk}$  and  $S_{ku}$  refer to the distribution of the amplitudes and the symmetry of the surface heights about the mean plane.

Results showed that all thin films prepared by X-ray, with the dominance orientation (111), it was found that the prepared SnO<sub>2</sub> films were of polycrystalline structure of an orthorhombic type and full width at half maximum values peaks (FWHM) of these films decreased with increasing thickness.

The optical properties including the measuring of absorbance and transmittance spectra as a function of wavelength in the range (300-1100) nm for all samples, the transmission decreased with increment of thickness. The energy band gap for direct transition decreased from (3) to (2.2) eV, values with increasing thicknesses.

## *Symbols & Abbreviations*

<i>Symbol</i>	<i>Description</i>	<i>Unit</i>
$a, b, c$	<i>Lattice constants</i>	$\text{Å}^\circ$
$hkl$	<i>Miller indices</i>	-
$d_{hkl}$	<i>Lattice plane</i>	$\text{Å}$
$\delta$	<i>Dislocation density</i>	$\text{Line}/\text{cm}^2$
$N_o$	<i>Number of crystals</i>	$\text{Crystal}/\text{nm}^2$
$E_{\text{gap}}^{\text{opt}}$	<i>Optical energy gap</i>	$\text{eV}$
$D$	<i>Crystallite size</i>	$\text{nm}$
$n$	<i>Refractive index</i>	-
$q$	<i>Wave vector of the absorbed photon</i>	$\text{cm}^{-1}$
$h$	<i>Planck constant</i>	$\text{J}\cdot\text{s}$
$K_B$	<i>Boltzmann constant</i>	$\text{J}/\text{K}$
$T$	<i>Transmittance</i>	%
$t$	<i>Film thickness</i>	$\text{nm}$
$h\nu$	<i>Incident photon</i>	$\text{eV}$
$A$	<i>Absorbance</i>	-
$R$	<i>Reflection</i>	-
$\lambda$	<i>Photon wavelength</i>	$\text{nm}$
$c$	<i>Speed of light</i>	$\text{m}/\text{s}$
$\alpha$	<i>Absorption coefficient</i>	$\text{cm}^{-1}$

$\nu$	<i>Frequency</i>	<i>Hz</i>
$2\theta$	<i>Diffraction angle</i>	<i>Degree</i>
$\theta$	<i>Bragg's angle</i>	<i>degree</i>
$I_A$	<i>Intensity of absorbed radiation</i>	<i>eV/m<sup>2</sup>.sec</i>
$I_o$	<i>Intensity of incident radiation</i>	<i>eV/m<sup>2</sup>.sec</i>
$I$	<i>Intensity of transmitted radiation</i>	<i>eV/m<sup>2</sup>.sec</i>
$IR$	<i>Infrared</i>	<i>-</i>
$\lambda_{cut\ off}$	<i>Cut off wavelength</i>	<i>nm</i>
$\beta_{FWHM}$	<i>Full width at half maximum</i>	<i>Rad</i>
$E_i$	<i>Primary energy of electron</i>	<i>eV</i>
$E_f$	<i>Final energy of electron</i>	<i>eV</i>
$K_i$	<i>Primary wave vector of electron</i>	<i>cm<sup>-1</sup></i>
$K_f$	<i>Final wave vector of electron</i>	<i>cm<sup>-1</sup></i>
$K_p$	<i>Wave vector of phonon</i>	<i>cm<sup>-1</sup></i>
$UV$	<i>Ultraviolet</i>	<i>-</i>
$ASTM$	<i>American standard of testing material</i>	<i>-</i>
$XRD$	<i>X-ray diffraction</i>	<i>-</i>
$AFM$	<i>Atomic force microscopy</i>	<i>-</i>
$FTIR$	<i>Fourier transformation infrared spectroscopy</i>	<i>-</i>
$VIS$	<i>Visible</i>	<i>-</i>
$R.M.S$	<i>Root mean square</i>	<i><math>\mu m</math></i>

<i>SEM</i>	<i>Scanning electron microscopy</i>	-
<i>l</i>	<i>Length of sample</i>	-
<i>S<sub>a</sub></i>	<i>Average roughness</i>	<i>μm</i>
<i>S<sub>z</sub></i>	<i>Ten point roughness</i>	<i>μm</i>
<i>S<sub>m</sub></i>	<i>Maximum peak</i>	<i>μm</i>
<i>S<sub>v</sub></i>	<i>Maximum depth of the profile</i>	<i>μm</i>
<i>S<sub>p</sub></i>	<i>Maximum height of the profile</i>	<i>μm</i>
<i>S<sub>ku</sub></i>	<i>kurtosis describes sharpness</i>	-
<i>S<sub>sk</sub></i>	<i>Skewness</i>	-
<i>k</i>	<i>Solidity factor</i>	-
<i>S<sub>vm</sub></i>	<i>Mean depths of valleys</i>	<i>μm</i>
<i>S<sub>pm</sub></i>	<i>Mean height of peaks</i>	<i>μm</i>
<i>AA</i>	<i>Arithmetic average</i>	<i>μm</i>
<i>CLA</i>	<i>Centre line average</i>	-

# CONTENTS

Chapter One	Introduction	Page
1-1	Introduction	1
1-2	The physical properties of SnO <sub>2</sub>	3
1-3	Uses of SnO <sub>2</sub>	3
1-4	Literature survey	5
1-5	The aim of research	8
Chapter Two	Theoretical part	
2-1	Introduction	10
2-2	Nanoscience	10
2-3	Nanomaterials	11
2-4	Classification of Nanomaterial	11
2-5	Semiconductor concept	13
2-6	Structure of Semiconductors	14
2-7	Crystal Growth for Films	19
2-8	Structural properties of prepared thin film	21
2-8-1	X – Ray Diffraction (XRD)	21
2-8-2	Atomic Force Microscopy (AFM)	25
2-8-3	Fourier transformation infrared spectroscopy (FTIR)	26
2-8-4	Scanning Electron Microscope (SEM)	26
2-9	Optical Properties of thin film prepared	28
2-9-1	Optical Absorption	29
2-9-2	Optical absorption Coefficient ( $\alpha$ )	31
2-9-3	Fundamental Absorption Edge	32
2-10	Optical constants	38
2-10-1	Absorption	38
2-10-2	Transmittance	39
2-10-3	Reflectance	39
2-10-4	Refractive Index	40
2-11	Surface roughness	41
2-12	Roughness gauges	41

2-12-1	Roughness average ( $S_a$ )	41
2-12-2	Ten-point mean roughness ( $S_z$ )	43
2-12-3	Mean of maximum peak to height valley ( $S_{tm}$ )	44
2-12-4	Kurtosis ( $S_{ku}$ )	45
2-12-5	Skewness ( $S_{sk}$ )	47
2-12-6	Root Mean Square ( $S_q$ )	48
2-12-7	Maximum height of peaks ( $S_p$ )	49
2-12-8	Maximum depths of valleys ( $S_v$ )	49
2-12-9	Mean height of peaks ( $S_{pm}$ )	49
2-12-10	Mean depth of valleys ( $S_{vm}$ )	49
2-12-11	Maximum height of the profile ( $S_t$ )	50
2-12-12	Solidity factor of the profile ( $k$ )	51

## 4

### Chapter Three Experimental part

3-1	Introduction	53
3-2	Thermal Evaporation Under Vacuum Method	55
3-3	Thermal Evaporation System	56
3-3-1	Evaporation Chamber	57
3-3-2	Vacuum unit	58
3-3-3	Vacuum gauges	59
3-3-4	Cooling System	59
3-4	Advantage of Thermal Evaporation Under Vacuum Method	60
3-5	Disadvantage of Thermal Evaporation Under Vacuum Method	60
3-6	The Parameters that Influence on the Prepared Films Homogeneity	62
3-7	Cleaning Substrates	62
3-8	Preparing SnO <sub>2</sub> Thin Films	63
3-8-1	Deposition of Pure Material	63
3-8-2	Thermal Oxidation	65
3-9	Investigation the Structural of Prepared Films by (XRD) Technique	66
3-10	Infrared Spectroscopy Measurement	66
3-11	Atomic Force Microscopy measurements	67
3-12	Scanning Electron Microscopy measurements	67
3-13	Optical Measurement	68

## Chapter Four Results & Discussion

4-1	Introduction	69
4-2	Structural Properties of SnO <sub>2</sub>	69
4-2-1	X-Ray Diffraction	69
4-2-2	FTIR spectrum investigation	72
4-3	Optical Properties	75
4-3-1	Absorption spectrum	75
4-3-2	Transmittance Spectrum	76
4-3-3	The Optical Energy Gap Calculation	78
4-3-4	Reflectance & Refractive spectrum	80
4-4	Introduction of surface roughness	82
4-5	Atomic Force Microscope Results	84
4-6	Scanning Electron Microscopy results	87
4-7	New method to calculation the surface roughness for SnO <sub>2</sub> films	91
4-8	Conclusions	99
4-9	Future works	100
	Reference	

**(1-1) Introduction**

Nanomaterials and their applications are intensive research because of their unique chemical and physical properties which make them interesting in terms of their technological importance in improving the properties of the material, as well as their scientific value to understand these properties [1,2].

The most important factors in which nanomaterials differ from the bulk materials (i) surface effects (causing smooth properties scaling due to the fraction of atoms at the surface) and (ii) quantum effects (showing discontinuous behavior due to quantum confinement effects in materials with delocalized electrons) are chemical reactions and physical properties (mechanical, optical, electrical, and magnetism) will be affected by these factors [3].

Nanotechnology sciences is a generic term for applications deal with materials of too small in atomic and molecular boundaries. In this size of the material, the physical, chemical and biological properties differ from those in the microstructure and the wider ranges. This includes production, physical and chemical applications, and biological systems at levels ranging from atoms or molecules to single-dimensional nanoparticles, resulting in larger systems similar to quasi-technology conductors, and information technology or cellular and molecular technology. Nanotechnology is important in many areas, such as, manufacturing materials, electronics, medicine, health care, energy, biotechnology, information technology, national security and others. Many scholars saw it as the next industrial revolution [4,5].

In this work, it has focused on thin film technology which is one of the most important techniques that participated in semiconductors study, and

gave an idea of many physical and chemical properties, because they contributed effectively to the practical side [6]. The term thin film is usually called to a layer of multilayer atoms of a certain thickness not exceeding one micron. It is the result of the intensification of atoms, molecules or ions that have different important properties compared to a thick mass in terms of physical and engineering properties [7]. Due to the low thickness and easy cracking of these films, they were deposited as sediment bases of various materials such as glass, quartz, silicon, aluminum and other metals based on the nature of the study and its applications [8]. Thin films therefore have an industrial and technical importance. They are included in the most electronic applications, used in magnetic memory devices, integrated circuits, transistors, rectifiers,) digital calculators, detectors, solar-cells and gas sensors. In addition to these multiple applications, thin films were used in optical applications, photographic reproduction and optical filters which give benefit to the photovoltaic industry (photo cells), reflective mirrors [9,10].

The concept of digital image processing refers to the processing of images using a computer. The need for image processing is therefore to facilitate the interpretation process and improve its clarity providing visual information which is difficult to obtain from its sources and is free from defects and noise due to imaging systems, for measurement errors which are referred to as noise or analysis ability due to many chemical and optical effects [11]. Therefore, the digital image processing field has grown rapidly in recent time, using multiple techniques to improve the visual information for analysis and interpretation purposes. Therefore, the importance of these images and their wide applications spread in various areas of daily life of man such as military fields, improving thermal

images, infrared images, techniques for improving X-ray images and ultrasound images [12].

### **(1-2) The physical properties of (SnO<sub>2</sub>) thin film**

Tin oxide semiconductor SnO<sub>2</sub> has been found in nature which called (Cassiterite), it's a white powder tends to gray with a large band gap, its crystalline structure is an orthorhombic as shown in figure (1-1) and the lattice constants of the compound are (a=4.714 nm) (b=5.727 nm) (c=5.214 nm). The concentration of free electrons is (10<sup>16</sup>cm<sup>-3</sup>) [13] [14].

SnO<sub>2</sub> is a non-stoichiometric compound due to the presence of oxygen vacancies, so the thin film form of this material is SnO<sub>2</sub> [15]. It belongs to groups (IV) in the periodic Table with (n-type), Table (1-1) shows physical properties of SnO<sub>2</sub>. Due to its characteristic properties such as, optical transmittance, homogeneity, mechanical rigidity, in addition to the reliability of thermal treatment and electrostatic behavior [16], therefore suitable for the following applications:

### **(1-3) Applications of tin oxide(SnO<sub>2</sub>): -**

1. In gas sensors
2. In solar cells, due to, the concentration of free electrons.
3. In transparent coating and hot mirrors (in buildings due to Low thermal emission)
4. In integrated circuits within devices made of micro silicon
5. As an element of sensitivity in micro-detection systems
6. In lithium-ion batteries

7. Its photovoltaic is used in powerful capacities and light emitting diodes
8. In projectors. [17, 18]

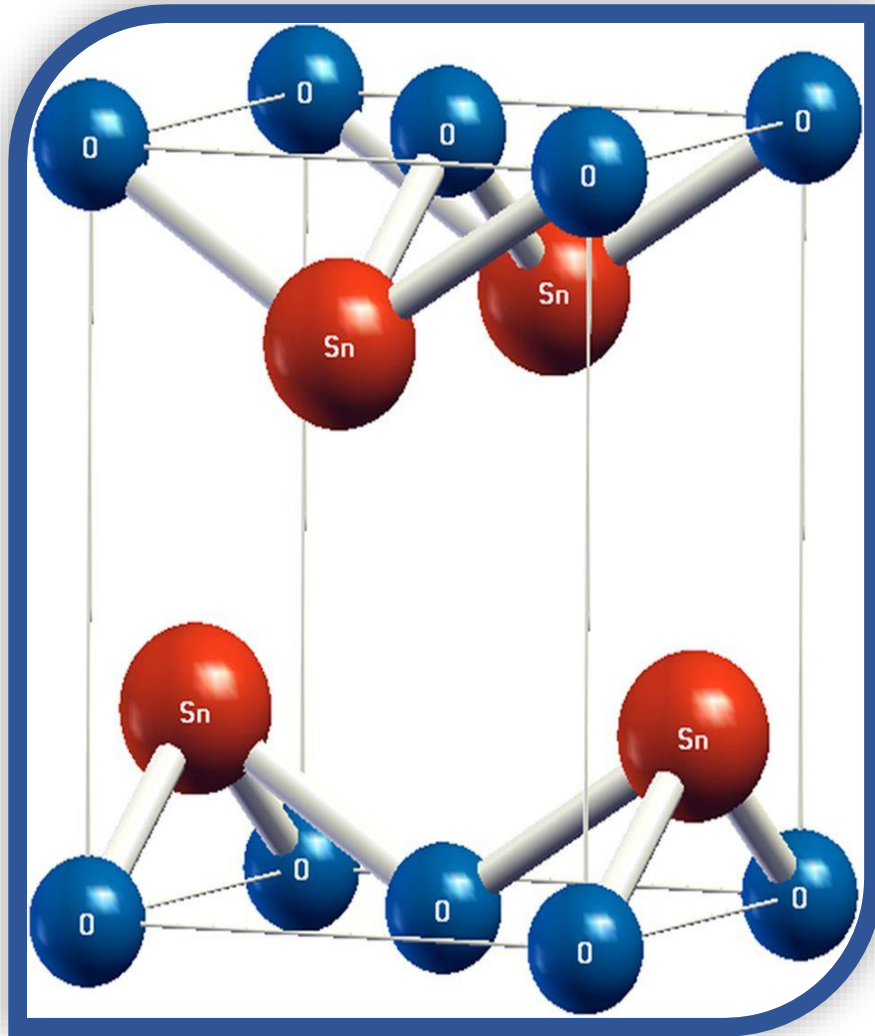


*Figure (1-1) the crystalline structure of tin dioxide (SnO<sub>2</sub>) [19].*

Table (1-1) some physical properties of tin dioxide [20].

<u>Chemical formula</u>	<i>SnO<sub>2</sub></i>
<u>Appearance</u>	<i>White to grey</i>
<u>Molar mass</u>	<i>150.69 g·mol<sup>-1</sup></i>
<u>Density</u>	<i>6.95 g/cm<sup>3</sup> (20 °C)</i>
<u>Melting point</u>	<i>1630 °C ; (1900 K)</i>
<u>Boiling point</u>	<i>(1800–1900 °C); (2070–2170 K)</i>
<u>Crystal structure</u>	<i>Rutile tetragonal</i>

**(1-4) Literature survey:**

- ❖ *Reem Sami et al in (2010)* prepared the pure and doped cadmium oxide films, structural properties have been studied before and after the annealing process using a number of image processing techniques by studying the change in film color with changing the size, number and shape of the film granules. A number of digital image techniques have been applied to the images using Matlab such as contours, stained glass, film grain, smudge stick and pixel pointillist paintings [21].

- ❖ *A.A. Hussain and Jebor in (2010)* prepared pure SnO<sub>2</sub> by chemical pyrolysis methods. Optical and structural properties have been studied for pure SnO<sub>2</sub> thin films at different thicknesses (100, 200, 300 nm). (XRD) showed that the (SnO<sub>2</sub>) films were polycrystalline with tetragonal type. Optical properties measurements, absorbance (A) and transmittance (T) of SnO<sub>2</sub> film showed that they had a high transmittance of up to (80%) in the wavelength range (300 - 800) nm [22].
  
- ❖ *Saikia et al in (2011)* prepared SnO<sub>2</sub> by atmospheric pressure chemical vapor deposition on glass substrate temperature of (400-500) C°, studied structural properties of (XRD) results have been shown that the preferred direction was (110), it had a tetragonal structure. Optical properties such as transmittance, absorbance and reflectance spectra between  $\lambda=254$  nm to 1400 nm have been calculated. The results showed transmitted visible light was ~94% [23].
  
- ❖ *R. O. Mahdi in (2012)* studied the optical and structural properties of SnO<sub>2</sub> nanostructures prepared by simple and classical method on glass substrate, the results showed that the film had high transmission in the visible and near infrared regions and the value of the energy gap was (3.82) eV, the structural properties of the X-ray diffraction showed the Bragg angle at ( $2\theta=30.24$ ). The results of AFM tests showed that nanoparticles and particle size was in range of (15-140 nm) and the root mean square value was (5.72 nm). [24]

- ❖ *N. S. Sabri et al in (2012)* prepared pure and doped SnO<sub>2</sub> with manganese by chemical method. They studied optical and structural properties of nanoparticles studied by using (XRD, UV-VIS spectrometer), they found that the manganese particles were substituted in a tin oxide and the results showed displacement peaks of intensities in the (XRD), there was shrink in the lattice constant by increasing manganese, and the shift in the energy gap values was attributed to sp-d exchange interaction or increase in grain size [25].
  
- ❖ *G.R. Kandhasamy et al in (2013)* studied the surface of ZnO thin film using scanning electron microscopy (SEM) to determine the pores of thin film by various edge detection techniques such as Sobel, Canny, Prewitt and Roberts. Their results had showed that the best technique has been given the best information of porosity of (ZnO) thin film was Canny edge detection. Those results taken to find peak signal to noise ratio values to identify the particular place of pores [26].
  
- ❖ *R. Barougui in (2014)* prepared SnO<sub>2</sub> nanoparticles and doped them with zinc by chemical deposition, synthesis and optical properties have been studied by (XRD) tests revealed that all samples prepared in the rutile phase and electron microscopy analyzes decreased with increasing the doping, the energy gap was proportional with grain size [27].

- ❖ *A. R. Razeghizadeh et al in (2015)* studied the optical and structural characteristics of tin oxide doped with aluminum, the properties were investigated using (XRD, FTIR, SEM and UV-visible). It has concluded that no change in the quaternary phase of SnO<sub>2</sub>, in addition to the intensity and granular size decrease in samples doped with aluminum. the samples showed high permeability in the visible region, and energy gap increased with increasing of (Al), because it increment of (Al) reduced the size of grains and improved absorbance at short wavelengths [28].
  
- ❖ *Jahnavi et al in (2016)* Studied the structural, optical and morphological properties of SnO<sub>2</sub> using thermal evaporation method they observed that when the annealing temperature of SnO<sub>2</sub> film increased, the energy gap increased. UV-visible of these films indicated that in the visible region high transmittance of 99% has been found [29].

### (1-5) The aim of the research

1. Study the physical properties of SnO<sub>2</sub> thin films, then analyzed the results by using image processing technique and focused to the structural properties obtained for SnO<sub>2</sub> thin film which was prepared in vacuum evaporation, including the images of Atomic Force Microscopy and Scanning Electron Microscopy, in terms of calculation surface roughness and grain size.

2. Studying the structural properties of SnO<sub>2</sub> thin film and calculating the grain size, the density of the defects, the number of crystals per unit area using XRD, AFM, SEM.
3. Studying the optical properties of SnO<sub>2</sub> thin film, including absorption measurements of the prepared samples, transmittance, the absorption coefficient and the optical energy gap using visible UV devices.
4. Studying the surface topography of the thin film (grain size and roughness) using atomic force microscopy (AFM) images.
5. Calculation of adopted roughness parameters for scanning electron microscopy (SEM) image.
6. Finally, comparing and reading the obtained results by MATLAB technique implemented in SEM images and performed measurement using AFM images such as  $S_a$ ,  $S_q$ ,  $S_p$ ,  $S_v$  and  $S_z$ .

### **(2-1) Introduction**

This chapter includes the theoretical aspects of the subject of research, in terms of theoretical concepts, whether in laws and mathematical relations or in scientific interpretations or definition of terms that have been adopted to clarify, the practical aspect of research.

### **(2-2) Nanoscience**

Nanoscience is a science deals basically with the synthesis, characterization, exploration and exploitation of nanostructured materials. These materials have a single dimension of nanometer range in nanoscience, nanoparticles are part of a billion (part of a thousand million), and nanometers are used to measure a length unit of very small objects which can be seen by an electronic microscope. This unit is used to express the diameters of the materials particles, their atoms and microscopic particles such as bacteria and viruses [30,31]. Shrink materials to nanoscale may suddenly exhibit very different characteristics than those on the micro scale, resulting in unique applications where dark material may become transparent such as copper, inert materials become with catalysts properties such as aluminum, solids are converted to liquids at room temperature (such as gold), the insulating materials are converted to conductive materials (such as silicon). Inert substances in their natural chemical composition (such as gold) may also convert into chemical catalysts when shrink to nanomaterials [32].

### **(2-3) Nanomaterials**

Nanomaterials define as the material can be produced and processed with particle dimensions of smaller or equal to the critical dimension ( $D \leq D^*$ ) when ( $D^*=10^2\text{nm}$ ). The small size and measurements of these materials have led to behavior unlikely traditional large-size materials increase their dimensions (resulting in a volume effect). It is used in many industries such as pure nanotubes used for corrosion resistant tires and nano-fibers for insulating and backing in overlapped materials. Iron oxide is used to generate magnetic materials used in the disks. Titanium and zinc as ultraviolet rays use nanostructures and thin nanoparticles to make the product lighter, more powerful and more connective. There are many applications for nanomaterials in biology and medicine, for example gold in its normal size, which is an excellent conductor for heat, electricity, and less affected for light. But properly constructed nanoparticles begin to absorb light and can convert it to sufficient heat to behave as a miniature thermometer to kill unwanted cells in the body, such as cancer cells. Nanomaterials also depend on the sources of their production, but they vary in origin, such as organic, inorganic, natural and processed materials [33, 34].

### **(2-4) Classification of nanomaterial**

Nanomaterial are classified into four kinds:

#### ***i. Installation of zero dimension***

Nanoparticle or a nanoscale contains nanocluster. In other words, nanoparticles are isolated from each other. A good example is the

difference in hardness between the phase shift of diamond to the graphite as shown in figure (2-1 a) [35].

*ii. Nanomaterials in one dimension*

All Materials in this category at least, one of dimension should be measured which is called nanofilms i.e., have only one nanodimension as shown in figure (2-1 b). Examples of such materials are chips or membranes (Thin Layers), such as nanoparticles used in surface coatings (Surface Nano coating) [36].

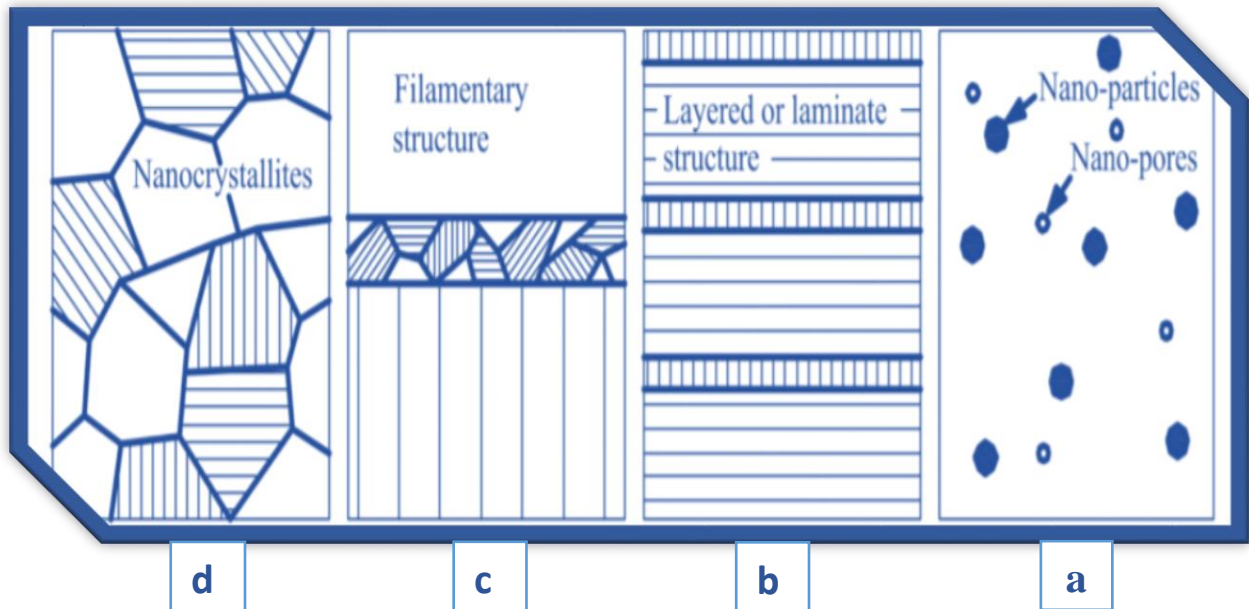
*iii. Nanomaterials in two dimension*

Nanomaterials in this category at least, two of its dimensions should be measured. Carbon nanotubes, and nanowires are important models for this class of materials, as shown in figure (2-1 c). They can be used as supporting and reinforcing materials for metals increase its strength and improve its mechanical properties, especially resistance against collapse. They also, combine other unique properties such as super thermal and electrical conductivity [36].

*iv. Nanomaterials in three dimension*

Spheres nanoparticles and ultra-smooth filament powders as shown in figure (2-1 d). It is worth to mention that this category of nanomaterials with three dimensions is the most important one because of its versatility in technological fields due to the global production of modern nanoparticles in general besides of and their applications. For example, nanocrystalline metal oxides powder are of great economic importance, such as silicon oxide which enters in modern medical sector and replaces

materials, pharmaceuticals, traditional electronics, and contribute to increased product quality [36].



*a- Nanomaterial in zero dimension b- in 1-dimension c - in 2 dimension  
d- in 3-dimension*

*Figure (2-1) the schematic classification of nanomaterials [35].*

### **(2-5) Semiconductor concept**

Semiconductors define as materials with properties between conductors and insulators according to their electrical conductivity. They are insulating materials, with no electrical conductivity, at very low temperatures (at absolute zero temperature), but once they become warmer near room temperature or more for a certain period, the electrical conductivity begins increasing and makes current increasing, through which an external electric field is exposed, similar to this behavior of conductive materials (behavior conduction) [37].

### **(2-6) Structure of semiconductors**

The energy gap between the equivalence and conduction bands is different between semiconductors and insulators, the difference in the value for single conductor whether it has single or polycrystalline structure or amorphous structure, depending on methods and conditions of preparation during its crystal development process. Therefore, semiconductors can be classified depending on their crystalline structure nature during crystalline development to crystalline and random semiconductors [38, 39].

#### ***1. Crystalline semiconductors***

It is classified into two categories: -

##### ***i. Single crystal semiconductors***

These materials are characterized by the fact that their atoms are assembled in rows and arranged periodically forming a three-dimensional configuration with repetitive symmetry, that is to say, its crystalline structure can be considered as a result of repeating the model or cell of the three-dimensional unit, thus the long range structure order achieving the least possible internal energy potential of its atoms' system as shown in figure (2- 2 a), [40, 39] .

##### ***ii. Polycrystalline semiconductors***

These materials are in a form of multiple crystals (Polycrystalline) where the crystalline model consists of a large number of very small and individual crystals called "grains" as shown in figure (2-2 b), they have polymorphic materials

characteristics on the basis of which these substances are identical in all directions (Isotropic), so that each grain represents a small individual crystal in itself, thus having a long-range system in the order of its atoms the interior is unlike what it is in the crystalline model as a whole and monolithic from this grain group. Where it will have a short-term system in the order of its constituents (short range order) structure as a result of the variation of the atomic orientation of its crystalline grains, the formation of a crystalline system with free internal energy is greater than that of the crystallization of monocrystalline materials [39]. The surfaces of the crystalline grains meet with each other and the periodic arrangement is interrupted each grain is called the grain boundary, which is a type of surface crystal imbalance is not balanced for what it possesses these limits of large energy range between (1.25 - 6.25) eV / nm and so these crystals materials are always dependent on reducing the area of their granular boundaries in order to reduce the free energy of the system its internal atoms [37, 41].

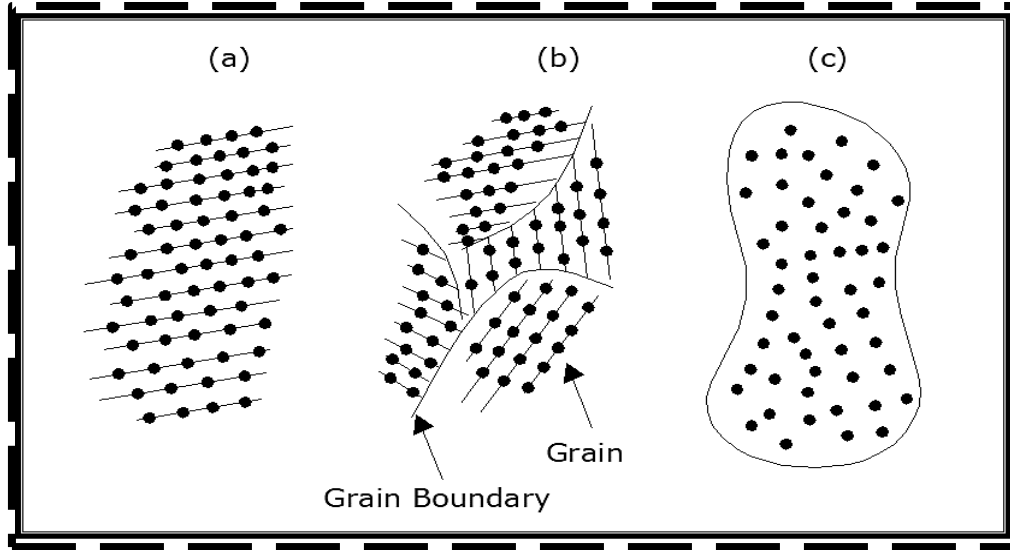


*Figure (2-2) the arrangement of atoms in the material [45].*

*a- single crystalline   b- polycrystalline   c- amorphous*

## **2. Amorphous semiconductor**

Also called super cooled liquids because of their similarity with liquids in terms of random atoms in their order, but the atoms of these materials are of fixed sites and do not move as in liquids, this is (super cooled liquid) [37,40]. The atomic system of these materials does not have a uniform crystalline structure. atoms accumulate randomly and irregularly forming a complex composition cannot be considered a result of repeating any non-crystalline material model (or unit cell) as shown in fig (2-2 c), it is the most common materials (regular window glass) [42]. The long-range system in the atomic order is missing from structural formations that the arrangement in its general sense is not completely and definitively missing, but is limited to its appearance in these substances and in (liquids) within a limited number of atoms, especially neighboring atoms or surrounding a

certain atom if that atom is taken as a base or a reference , and the farther away from it the distribution of the rest of the atoms in relation to them becomes a completely random distribution, so these materials are often characterized by having a short-range system in its atomic order for short periods only within the material and the arrangement is clearly visible in x-ray diffraction [37]. With X-ray diffraction of the sample prepared from the material and from observing the diffraction pattern the body has bright spots or concentric loops and concentric high sharp lighting and broad but poor lighting - the crystalline structure of the prepared material can then be judged whether it is a substance crystalline monocrystalline or polycrystalline or random synthesis [43].

The random state is thermodynamically unstable state, so it crystallizes when the causes of its random composition vanish or has the freedom to lose excess energy, then the atoms return to the state of relaxation and micro-energy [44], it should be noted that some elements and semiconductors examples such as germanium, silicon, beryllium fluoride and boron oxides are found in two structural forms, crystallized solids and non-crystalline solids resulting due to properties way of these materials or how they are formed. When the atoms have an opportunity to arrange themselves with less energy, they can produce crystalline matter. When atoms do not have the chance to arrange themselves to accumulate at random and are larger than those atoms assembled in a system that produces a non-crystalline or non-periodic solid material, these materials are

eventually identical in all directions (*Isotropic*), as are semiconductor polymers, but that reverse in semiconductors monocrystalline, which have different properties (*Anisotropic*) [39].

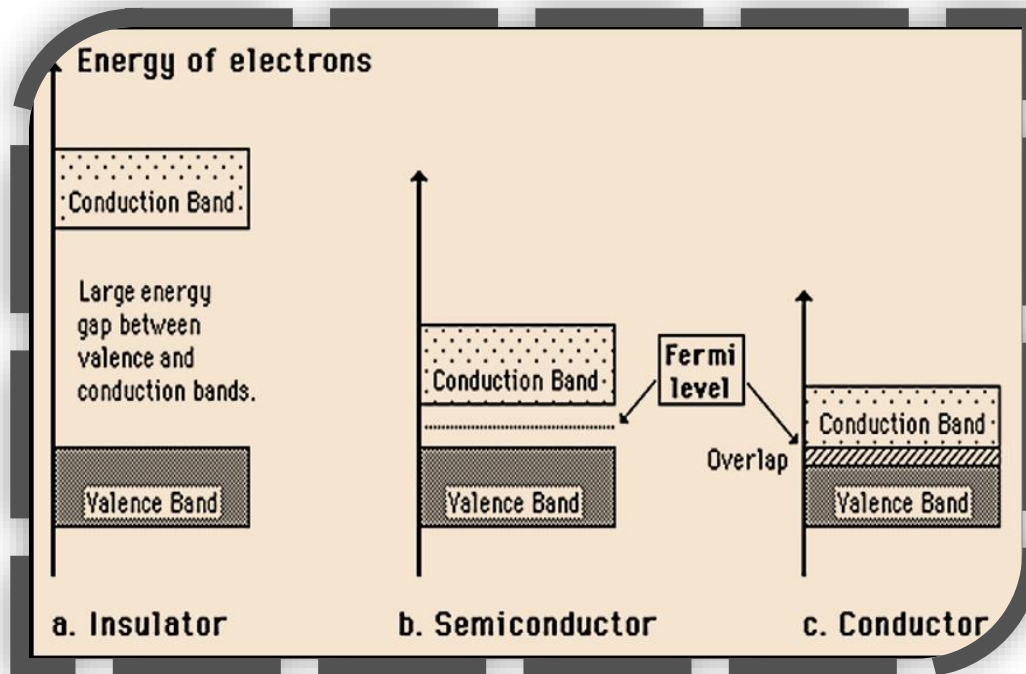


*Figure (2-3) energy bands scheme in Solids [46].*

Figure (2-3) shows the energy bands schemes for three classes of solids, dielectric, semiconductor, and conductor. In Fig (2-3 a), the energy of the forbidden gap in the insulator material is large. All the energy levels in the valence band are full with the electrons, while all the energy levels in the conduction band are vacant. Neither the thermal energy nor the electric field can lift the electrons to the top of the valence band to conductive pack. Therefore, such materials cannot transmit electricity.

Figure (2-3 b) shows that the gap energy in semiconductor is not in the capacity of the gap in the insulating material. The semiconductor behaves as insulator at absolute zero temperature, where the valence band is fully filled with electrons while the conduction band is completely empty. A small amount of energy (thermal or electric field) acquired by the electrons in the valence band may be transferred through the power of the forbidden gap to the conduction band leaving behind holes in the valence band [47,48].

When an electric field is applied, the electrons in the conduction band and the holes in the valence band, acquire kinetic energy contributes to the electrical conductivity. The conductive materials, such as metals, are either partially filled with electrons, or intertwined with the valence band, as shown in figure (2-3 c). So, the high electrons in partially occupied bands or electrons at the top of the valence band can move to higher energy levels when they acquire kinetic energy from the electrolytic field, so the current can easily transfer [49].

### **(2-7) Crystal growth for films**

After the film material in the melting boat reaches its melting point, its vapor atoms begin to volatilize in all directions inside the evaporation chamber, and collide with the substrates prepared for deposition, to face one of the possibilities:

1. The recoil may be repeated again by its high energy (therefore the deposition rate goes to be slight), because of

the difference in thermal expansion coefficient of both sediment particles and atoms of base material or because of the high temperature of the base. The base is a source of evaporation, the holes are created of making the films thickness less than the material density from which it comes [50, 51].

2. The material atoms move on the base associated with energy loses as heat hardening to connect them with the base in unstable manner. This link is accompanied by a relatively long distance movement during which the atoms look for low energy positions to settle down, and then begin to assemble and adhere the substrate surface by atomic bonding forces among atoms of the sediment. Besides that, atoms of the base material form small clusters called "nucleus" or "nucleation centers" their composition depends on several factors such as including deposition rate, base temperature, and chemical impurities that are added to the substance. When evaporation method is used to form the membrane the sedimentation rate increases. Increasing the density of the nuclei formed by the base, make the nucleation process increasing, this results in a small membrane granule volume. When sedimentation base temperature increases the large sizes granules due to the time increment of the atoms move on the base. This gives the atom a greater chance to addition a low-energy site. They do not only increase the nucleus but act as barriers to the grains growth [50 ,52 ,53].

Growth of three-dimensional nuclei with the dominance of growth in surface dimensions (parallel to the sediment base) was due to the surface propagation of the atoms [54]. As sedimentation is continuous, these nuclei increase (the number of atoms within a group increases which lead to increase the nucleus size). From the granular growth process to the active granular phase, which is then ready to join with its peers of similar size grains in a behavior similar to the behavior of the contact between two drop forming the connected film. This is in the case that the granules are identical in terms of their atomic orientations, single crystal. If these grains are different in terms of their atomic orientation, so-called granular boundaries, which are the characteristic properties of polycrystalline materials on the one hand, and some types of surface defects on the other (50, 55).

### **(2-8) Structural properties of prepared thin film**

#### ***(2-8-1) X – ray diffraction (XRD)***

X-ray is an electromagnetic wave with specific wavelength between the ultraviolet (UV) and gamma ray (0.1-10 Å). Therefore, it is preferable to use in most crystalline diffraction experiments. In general, diffraction depends on crystalline structure, wavelength used should be equal to or approximate to lattice constant [56]. X-ray diffraction provides important information about the shape and specification of the unit cell and the crystalline structure of the films prepared whether they are *single crystalline polycrystalline or amorphous* [43]. Bragg supposed that the

crystal is a large groups of parallel surfaces of atoms repeat itself periodically in three-dimensional space and the space between any two successive surfaces is "d" so he imagined the crystal as shown in figure (2-4). Therefore, Bragg assumed the X-ray of wavelength with monochromatic from source falls on the sample to be examined at an angle ( $\theta$ ) in (degree) and reflected at an angle value of twice the fall angle recorded on the detector, the fall angle changed once after ( $160^\circ$ ) depending on the need for this range.

This technology provides information on characteristic peaks locations which represent the direction of crystalline growth prevailing within the crystal lattice, the mid-width represents the greatest level of intensity through which granular boundary information can be obtained the knowledge of growth in granular size of the test sample [57].

As a result of construction interferences, X-Ray diffraction peaks characteristic of the prepared films are between the reflected rays from the characteristic surfaces groups of the prepared films at specific angles called "Bragg's angles", the characteristic surfaces of a similar phase which the optical path difference between them equals to an integer number of wavelengths with monochromatic X-Ray [39].

Bragg deduce the following law [58]:

$$n\lambda = 2 d_{hkl} \sin\theta \dots\dots\dots(2-1)$$

where

n : integer number representing diffraction order

$\lambda$  : X-ray wavelength (1.5406 Å)

d : distance between two successive levels

hkl : Miller index

$\theta$  : Bragg diffraction angle

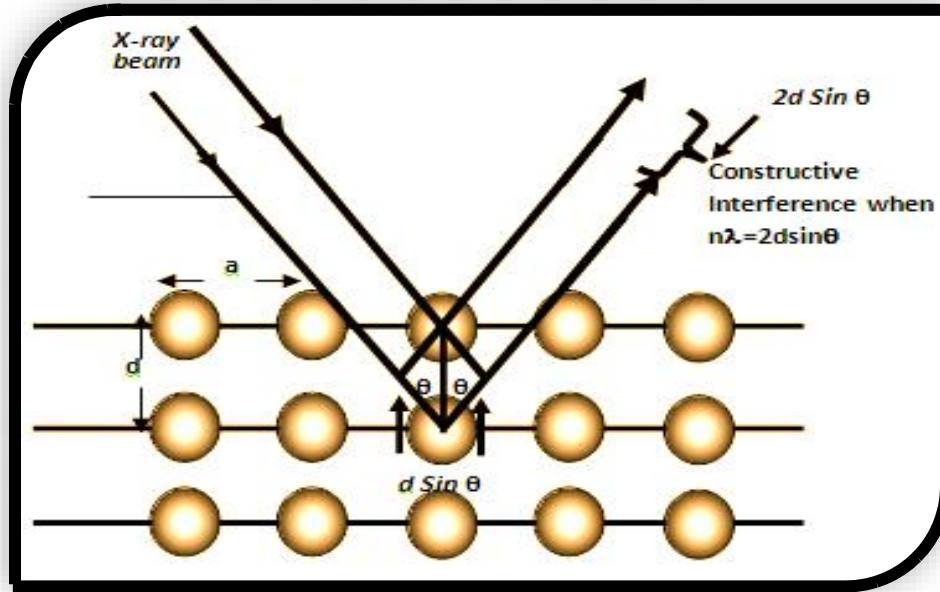


Figure (2-4) crystalline diffraction Bragg's law [57].

(2-8-1-1) Crystallite size (D)

The average grain size can be calculated using Scherer's equation. The amount of exposure to characteristic peaks ( $\beta$ ) can be found based on the FWHM (Full Width at Half Maximum) measured in radians, average grain size will be in (nm) according to the following formula (sheerer's formula) [59,60]

$$D = \frac{(0.94\lambda)}{\beta_{FWHM} \cdot \cos \theta} \dots \dots \dots (2 - 2)$$

Where

$\beta_{FWHM}$  : the full width at half maximum (in radians)

$\theta$ : Bragg's angle in degree

In orthorhombic system the lattice constant values can be calculated from the following formula using the Miller incident (hkl) and the inter-planar spacing (d) [61]

$$\frac{1}{d^2} = \frac{h^2}{a^2} + \frac{k^2}{b^2} + \frac{l^2}{c^2} \dots\dots\dots(2-3)$$

**(2-8-1-2) Dislocation density**

It is the number of lines showing the dislocations within the crystalline structure of the material in unit area measured in (m<sup>2</sup>), the quality of crystal structure can be found from the following relationship [39]:

$$\delta = \frac{1}{(D)^2} \dots\dots\dots (2-4)$$

δ : dislocations density in (dislocation Line /nm<sup>2</sup>) units

**(2-8-1-3) Crystals number (N<sub>o</sub>)**

It is the number of grains in unit volume (m<sup>3</sup>)

$$(N_o) = \frac{t}{(D)^3} \dots\dots\dots (2-5)$$

t : is thickness of the film measured in (nm) [62].

**(2-8-1-4) Full width at half maximum (β)**

The curve width can be measured at the midpoint of the greatest intensity of the prevailing direction, and then converted from grades to (rad) units when applied in particle size law [63].

### **(2-8-2) Atomic force microscopy (AFM)**

A type of scanning probe microscope (SPM) that is developed using the scanning tunneling microscope (STM), which is used to measure the insulators and conductor's surfaces, it also provides very accurate information about surface roughness and rate (RMS), besides the grain sizes and numbers of grains [64]. Figure (2-5) shows an atomic force microscope (AFM), this technique maximizes the film surface image in very complex and modern manner. The atomic power microscope features high analysis capacity is (0.1-1.0) nm and magnification power ( $5 \times 10^2$ - $10^8$ ), with possibility of operating at atmospheric pressure without need for high discharge [65]. The microscope is made of a cantilever with a probe of sharp head a tiny end known as (tip) used to survey the sample surface. Cantilever is made of Silicon nitride ( $\text{Si}_3\text{N}_4$ ) with radius does not exceed a few nanometers. Atomic force microscopy is usually used to measure the range of physical properties of insulators, conductor's and semiconductors surfaces, providing very accurate information about surface roughness and rate (RMS), as well as grain sizes [66].

The atomic force microscopy acts when cantilever movement in 3D creates with a piezoelectric scanner which is one of the key element in high resolution of the AFM. AFM feedback systems tries to keep the cantilever in a similar position compared to the sample surface by moving the sample up and down. The surface height data is generated from the sample up and down movement. AFM is a multitask instrument can be used to image the surface, measure 3D roughness (profiling technique), separate different surface properties and measure force interactions [67].

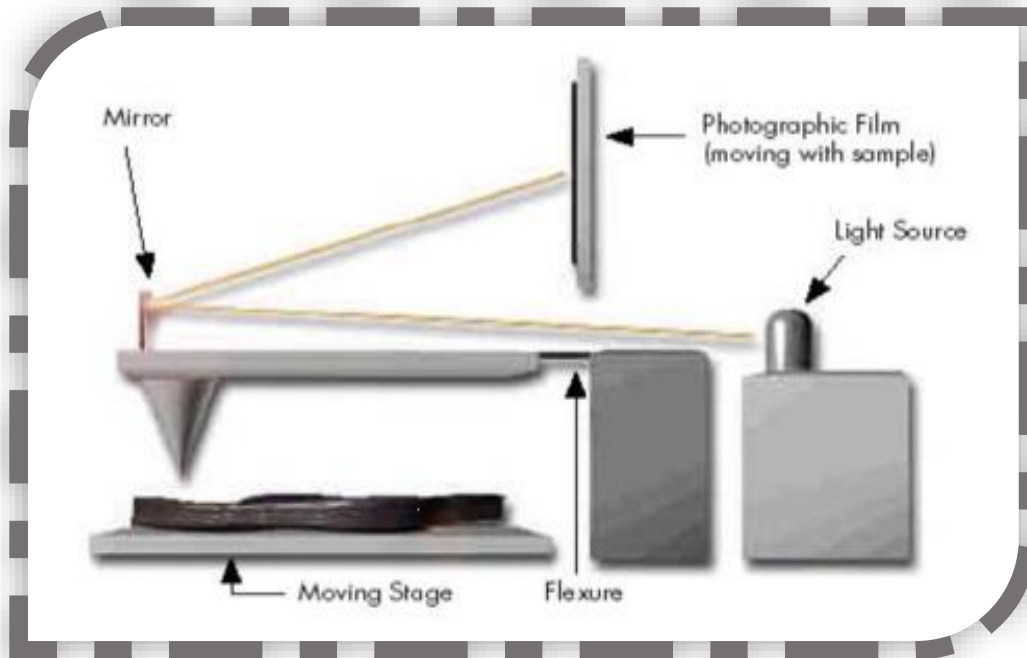


*Figure (2-5) cross section of the atomic force microscope [68].*

### **(2-8-3) Fourier transformation infrared spectroscopy (FTIR)**

Infrared passes through the sample, the process of absorption and penetration of some of the fallen radiation through the sample resulting spectrum represents a molecular fingerprint on the sample, but no molecular structures produced by the same infrared spectrum, so the analysis of this technology distinct from the rest of the analysis [69].

### **(2-8-4) Scanning electron microscope (SEM)**

The SEM electron microscope gives a magnified image for the thin film surface up to  $(10^6)$  times, thus, it is clear that there is difference in the nature and shape of the different parameters in the film and the surface

smoothness, as well as for the detection of structural defects such as large gaps and isolated clusters because of the different preparatory conditions and method of preparation of films. There is no need to cut the sample into slices for examination [57], the device function is illustrated in Figure (2-6) when an electron beam falls on the sample surface, it creates different kinds of electrons and electromagnetic waves can be analyzed. In SEM the electron beam is used as a “probe” and the surface is scanned line by line with the electron beam. The SEM image describing surface shapes is usually a result of secondary electrons emitted from the surface. The image is a computer generated figure of the electron signals (matrix of data points), not image of light and shadows. Other signals emitted from the sample surface can also be used to create SEM images and other data. Other commonly used signals in SEM analysis are backscatter electrons and X-ray emission signals [70]. Backscatter electrons contrast is affected by the atom mass of the elements on the surface and X-ray emission signals can be used in element analysis. Backscatter, X-ray emission signals are useful in surface homogeneity / heterogeneity study or when certain elements have to be identified on the surface. Typically, SEM has a horizontal (spatial) resolution of ~5 nm and vertical resolution of 10-20 nm [71]. Scanning microscope means that it does not photograph the sample at one time but rather focuses the electron beam on a small spot of the sample and takes its image, then pick them up and so follow, the SEM has a large field depth compared to traditional microscopes, which means access to and analysis of three-dimensional images, while the optical microscope provides only two-dimensional surface images [72].

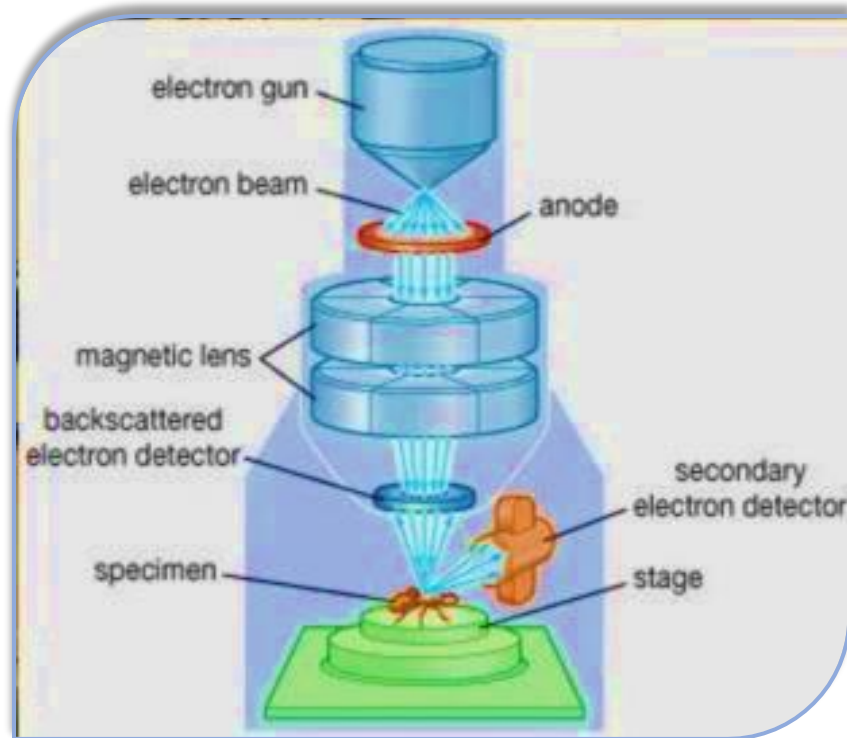


*Figure (2-6) A diagram of the scanning electron microscope (SEM). [73]*

### **(2-9) Optical properties of prepared thin film**

The study of semiconductors optical properties has a great importance in recognition of optical applications for films prepared from those materials, as well as providing important information on optical energy gap value (under certain preparatory conditions) such as the nature of the package installation and type of electronic transitions whether directly or indirectly by studying the values of their absorption coefficient besides of knowledge other optical constants values.

**(2-9-1) Optical absorption**

The absorption spectrum results from the energy loss due to the interaction between the falling light and the material charges as shown in figure (2-7), which shows how the valence electron cannot move from completely filled levels (valence band) to empty levels completely (conduction band) unless they possess energy efficiency required to complete this transition by absorbing photons, as is explained in the following relationship [37, 39]:

$$(h\nu)_{\text{photon}} \leq E_{\text{gap}} \dots \dots \dots (2 - 6)$$

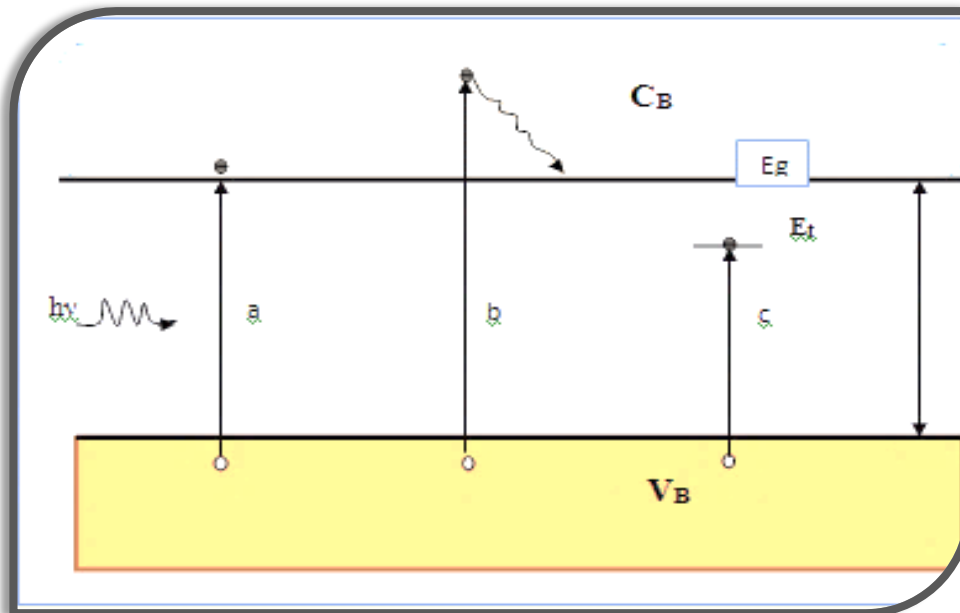


*Figure (2-7) the absorption of semiconductors [74].*

When the photon energy is larger than the forbidden gap energy

$(h\nu_{\text{photon}} > E_g)$  a pair of (electron-hole) will be generated, the extra power dissipates  $(h\nu - E_g)$  as heat, if photon

photovoltaic energy was less than forbidden gap energy of pure semiconductor ( $h\nu < E_g$ ) electronic transition would not occur (it happens in impure semiconductor with help of local levels of added impurities) [74]. If the photon energy value equals the forbidden gap energy of the pure semiconductor, ( $\lambda_{\text{cut off}}$ ) would get an (electron-hole) pairs arrange as in equation

[75, 39]: -

$$h\nu_{\text{photon}} = E_{\text{gap}} = \frac{hc}{\lambda_{\text{cut off}}} \dots\dots\dots (2-7)$$

Where

h : Planck constant ( $6.626 \times 10^{-34}$  J.sec)

c : speed of light in a space ( $3 \times 10^8$  m/sec)

Substitute the constant's values, equation (2-7) becomes as:

$$\lambda_{\text{cut off}} \text{ (nm)} = \frac{1240}{E \text{ (eV)}} \dots\dots\dots (2-8)$$

( $\lambda_{\text{cut off}}$ ) represents cutting wave length which defines as the corresponding wavelength of the forbidden energy gap of pure semiconductor, at which the optical absorption process starts thus showing the fundamental absorption edge [75,37]. In figure (2-7) (a) and (b) are called "intrinsic transition" or "band-to-band transition", the third transition (c), is not in the pure semiconductor, but with presence of local levels of impurities within the forbidden gap, it is called "extrinsic transition" [75].

**(2-9-2) Optical absorption coefficient ( $\alpha$ )**

It is defined as the percentage of decrement in falling beam intensity to distance unit towards wave propagation center. It depends on:

- ❖ Photon energy ( $h\nu$ ) in (eV).
- ❖ Characteristics of semiconductor in relation to semiconductor gap energy and type of electronic transitions.

When light beam falls on a thin film, part of it is reflected and part is transmitted and remained part is absorbed by the film material, the reflected and transmitted energies depends on:

- ❖ The nature of thin film material and its surface.
- ❖ The wavelength of incident light beam.

The absorption coefficient value indicates the susceptibility of the film material to absorb the falling radiation energy. If the intensity light falling ( $I_0$ ) on the material thickness ( $t$ ) and the absorption coefficient ( $\alpha$ ), the light intensity ( $I$ ) is given according to (Beer- Lambert) equation [76,77]:

$$I_T = I_0 e^{(-\alpha t)} \dots \dots \dots (2-9)$$

From above equation:

$$\alpha t = \ln\left(\frac{I_0}{I}\right) \dots \dots \dots (2-10)$$

By converting the natural logarithm to decimal produces:

$$\alpha = 2.303 (A/t) \dots\dots\dots (2-11)$$

$(I_0), (I_T)$  : represent the intensity of the incident and penetrated radiation from the membrane, respectively

$\alpha$  : absorption coefficient in  $(\text{cm}^{-1})$

$t$  : film thickness in  $(\text{nm})$

$A$  : absorptance

### (2-9-3) Fundamental absorption edge

The basis absorption edge is a semiconductors characteristic has a forbidden gap energy as one of the basic parameters of the membrane material which its required location must be studied within the electromagnetic spectrum, so because of its importance to locate the semiconductor forbidden gap energy it determines the kind of application that can harness the film material in its service and gives important information about the material properties of the energy packages and the type of electronic transitions, it is defined as the amount of absorption increment when the resulting electromagnetic radiation for photon has the same forbidden gap energy between the semiconductor valence and conduction bands [78]. Equation (2-9) gives the equivalent value of a forbidden gap energy but not in all semiconductors, it is sharp in single crystalline semiconductors while they are less in polycrystalline semiconductors [79] as shown in figure (2-8).

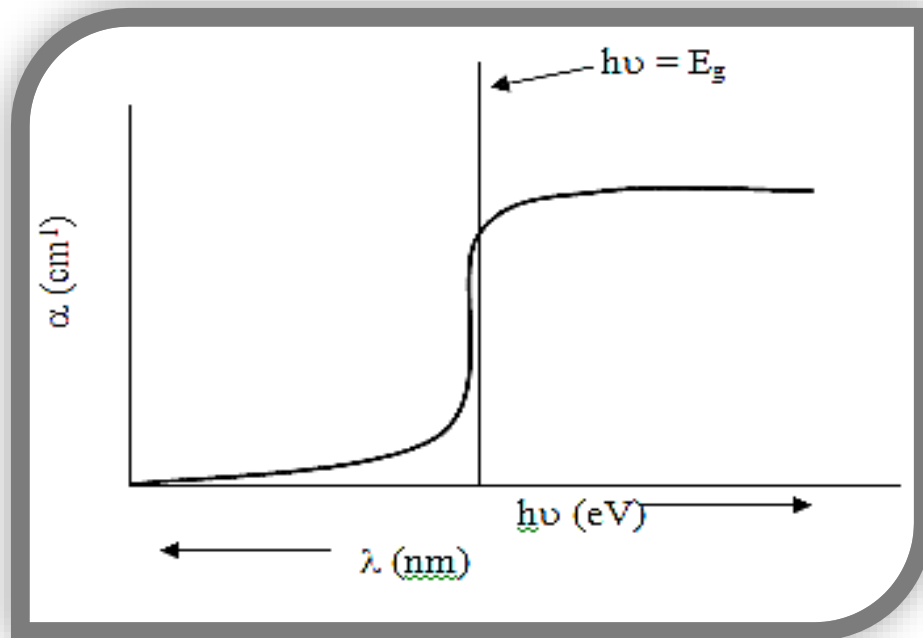


**Figure (2-8) the amount of absorption coefficient before and after the absorption edge [45].**

The reason is that the peak of the some semiconductors valence band do not fall directly under the conduction band , as it may first match the position of the valence band peak (V.B) in K-wave space with the bottom of conduction band, when this mismatch occurs, the semiconductor is said to have a (**Direct Intrinsic Gap**), but if this match does not occur, the semiconductor has an (**Indirect Intrinsic Gap**) [37,39], according to this, there are two kinds of electronic transitions in semiconductors, the direct type occurs when the difference ( $E_{gap}^{opt}$ ) between the highest point at the top of valence band is less than the lowest point at the bottom of the conduction band (**the edge of the basic absorption**), these transitions are : -

**i. Direct transition**

It occurs directly in semiconductors of direct self-space from the highest point at the top of the valence band to the lowest point at the bottom of the conduction band, where the wave vector is constant for each of the two dots (because they are on one straightness in the vector space) [39,80] as shown in figure (2-9).

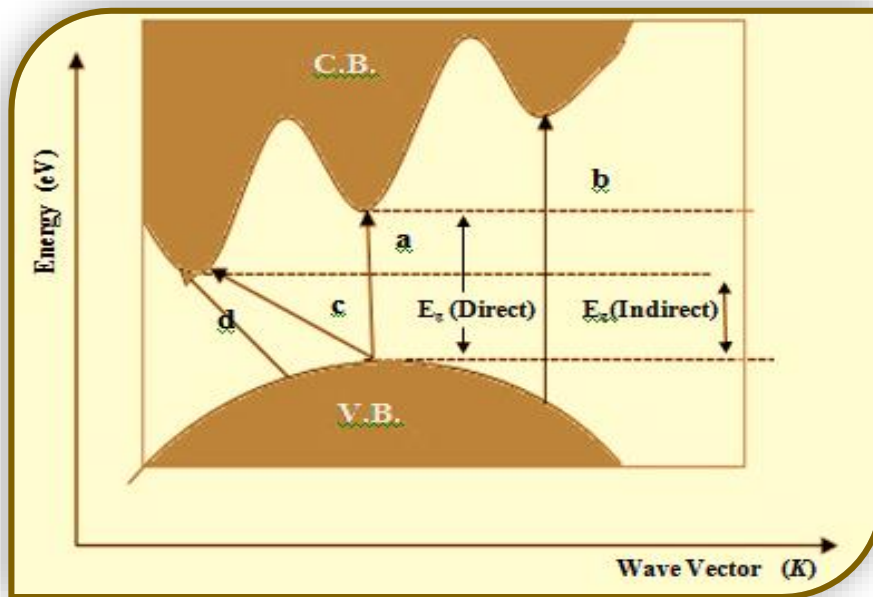


*Figure (2-9) electronic transitions: a: direct allowed*

*b: direct forbidden c: indirect allowed d: indirect forbidden [81].*

(K = 0), so both momentum and energy are stored in this type of transition [82], as in the following equations [37, 39]

$$E_f = E_i + h\nu_{photon} \dots \dots \dots (2 - 12)$$

$$K_f = K_i + q_{\text{photon}} \dots \dots \dots (2 - 13)$$

$E_i, E_f$  : Primary and final electron energy in the valence and conductive bands, respectively.

$K_i, K_f$ : The primary and final wave vector of the electron in both the valence and conduction bands, respectively.

$h\nu_{\text{photon}}$ : The energy of the incident photon (absorbed by the electron valence).

$q_{\text{photon}}$ : The wave vector of the absorbed photon, its value is small compared to the wave vector of moving electron because the wavelength of the falling photon is long depending the relationship

$$q_{(\text{photon})} = \frac{2\pi}{\lambda_{\text{photon}}} \dots \dots \dots (2 - 14)$$

therefore,  $q_{\text{photon}}$  can be neglected from equation (2-13) above and become as follows: -

$$K_f = K_i \dots \dots \dots (2-15)$$

The absorption coefficient for this type of transfer is given by Tauc equation [83,84]: -

$$\alpha h\nu = \beta (h\nu - E_{\text{gap}}^{\text{opt}})^{\left(\frac{1}{2}\right)} \dots \dots \dots (2 - 16)$$

of which the direct gap energy of all prepared films was calculated.

$h\nu$  : the energy of the absorbed photon

$\beta$  : constant

$E_{gap}^{opt}$  : optical gap energy

$r$  : the exponential coefficient depends on the type of transition, its value is  $(1/2)$  for direct allowed transition [85]. There is a movement between the points located in the adjacent areas to that of allowed direct movement, the wave vector value remains constant, ie ( $\Delta K = 0$ ), then the transition is called "direct forbidden transition". Absorption coefficient for this type of transfer is given in the following relationship [83,84]

$$(\alpha h\nu) = \beta (h\nu - E_{gap}^{opt})^{\left(\frac{3}{2}\right)} \dots \dots \dots (2 - 17)$$

$r = (3/2)$  for the forbidden direct transition [85], referring to both types of the transition do not depend on the temperature [39,86].

## ii. Indirect transition

It appears in semiconductors have indirect intrinsic gap, when a far-reaching energy position, in waveguide space, is from the valence beam peak position ( $\Delta K \neq 0$ ), figure (2-9), this means that no (electron-hole) pairs in this case. By a pure single-step optical absorption process (unless directly in the process), either phonon absorption momentum [ $-\hbar (k_c - k_v)$ ], or the emission of its [ $\hbar (k_c - k_v)$ ], which is defined as the vibrational quantum energy unit of crystal lattice, its function is balanced the change in crystalline momentum as a result of momentum change in moving electron, thus momentum conservation law is maintained as in following equation[85, 87]:

$$K_i + q_{(\text{photon})} = K_f \pm K_p \dots \dots \dots (2 - 18)$$

Where (+ k<sub>p</sub>): is the wave vector of the absorbed phonon.

(-k<sub>p</sub>): is the wave vector of the emitted phonon.

The wave vector of the incident photon (q) is small compared to the wave vector of the emitted phonon, so that it can be neglected from the above equation to become as follows

$$K_i = K_f \pm K_p \dots \dots \dots (2 - 19)$$

The absorption coefficient for this type of transition is given in the relationship shown below [85,88]: -

$$(\alpha h\nu) = \beta_1 (h\nu - E_{gap}^{opt} \pm E_p)^r \dots \dots \dots (2 - 20)$$

Where (+E<sub>p</sub>): absorber phonon energy

(-E<sub>p</sub>): for the emitted Phonon energy

β<sub>1</sub>: constant depends on temperature and properties of conduction and valance band.

In above equation (r) depends on the type of transition. When the transition from the highest point at the top of the valence band to the lowest point in the indirect bottom of the conduction band, the transition is called "allow indirect transition", where the value of (r) equals 2. If the transition between the points are located in the vicinity of the allowed indirect transfer zones, it is called the "forbidden indirect transition" where the value of r equal to 3 [85].

Electronic transitions occur at all temperatures except for some indirect transitions accompanied with phonon absorption, where they cannot occur at low temperatures because there are no phonons available at these levels. Therefore, this type of transition is dependent on temperature [85, 86, 89].

**(2-10) Optical constants**

They are important functions from their values the applications of semiconductors or the optimal use of thin films can be determined.

These constants are:

**(2-10-1) Absorptance (A)**

It is the ratio between the intensity of absorbed radiation by the film ( $I_A$ ) to the original falling intensity on it ( $I$ ), absorptance is usually free of units, and is given by relationship [90].

$$A = \frac{I_A}{I_o} \dots \dots \dots (2 - 21)$$

**(2-10-2) Transmittance (T)**

It is the ratio between the intensity of the radiation from the film ( $I$ ) to the original falling intensity on it ( $I_0$ ) and it is free of units. It is obtained from the following relationship [91]

$$T = \frac{I_T}{I_o} \dots \dots \dots (2-22)$$

The permeability with absorption is related to the following relationship:

$$A = \log(1/T).....(2-23)$$

From which the values of permeability can be extracted after re-formulation with the following relation:

$$T = (10)^{-A} ..... (2-24)$$

The transmittance depends on several factors [92] :-

- a) Thickness of the prepared film: The greater the thickness of the film the less permeability and vice versa
- b) Impuriting rates: By increasing the Impuriting ratio, the number of local levels between valence and conduction bands increases, thereby increasing absorption and reducing permeability.

**(2-10-3) Reflectance (R)**

It is the ratio between the intensity of reflected radiation in a given direction to the original intensity for the electromagnetic radiation falling on the material, as in equation:

$$R = \frac{I_R}{I_o}..... (2-25)$$

As well as the possibility of finding value from spectroscopy absorption and permeability by the adoption of the law conservation energy is given in the following relationship:

$$R = 1 - A - T \dots \dots \dots (2 - 26)$$

From which the reflectivity of the membrane material was obtained for the falling wavelengths and for all the prepared films [91,52].

#### (2-10-4) Refractive index ( $n_o$ )

It is the ratio between the speed of light in the vacuum to the speed of light in any material medium, as in following relationship [37,91]:

$$n_o = c/v \dots \dots \dots (2-27)$$

Where

c : light speed in vacuum,

v : light speed in any material medium.

A refractive index is one of the optical constants, its amount varies from substance to another, depending directly on several basic factors [93]:

- i. Type of material
- ii. Crystalline structure
- iii. Particle size (D)
- iv. Light intensity (in nonlinear media)

The refractive index can be found by the following equation: [94]

$$n_o = \frac{1+R}{1-R} \dots \dots \dots (2-28)$$

### **(2-11) Surface roughness**

It is the finer irregularities of the surface texture, which usually originate from the production process or material conditions of the Surface [96]. Surface roughness is considered one of the important characteristics that must be available in practical applications, it is the degree of softness of the surfaces. It requires a high degree of smoothness so that the desired function performs with the best possible performance. The practical experience has proved that it is impossible to manufacture absolute smooth surfaces, regardless the modern machinery used for manufacturing surface roughness may be called in other terms such as irregularity, roughness, unevenness [97].

### **(2.12) Roughness gauges**

In order to describe surface roughness in a specific way, numerical gauges were agreed to reflect the degree of roughness of the surface. Therefore, specialists in the field of surface roughness agreed on a number of numerical measures to be used to distinguish surfaces with varying roughness, these gauges are:

#### ***(2-12-1) Roughness average ( $S_a$ )***

It is also known arithmetic average (AA) or centre line average (CLA) of the distance deviations from the actual average distance [97]. A sample of the studied surface is taken with sufficient length (L) contains an appropriate amount of aliasing, the average line is drawn so that the area of the protrusions above and below this line is equal, the value of

roughness average ( $S_a$ ) is determined [98]. From figure (2-10) describes surface roughness and how measured its average, where the region below the center line as shown in A is turned to the top of the center line in B, and the mean height of the resulting profile is ( $S_a$ ). This parameter does not distinguish surfaces of different kinds of profiles. This means if there were two different surfaces (different shapes) with same roughness values, this parameter would not be sufficient to measure surface roughness [99].

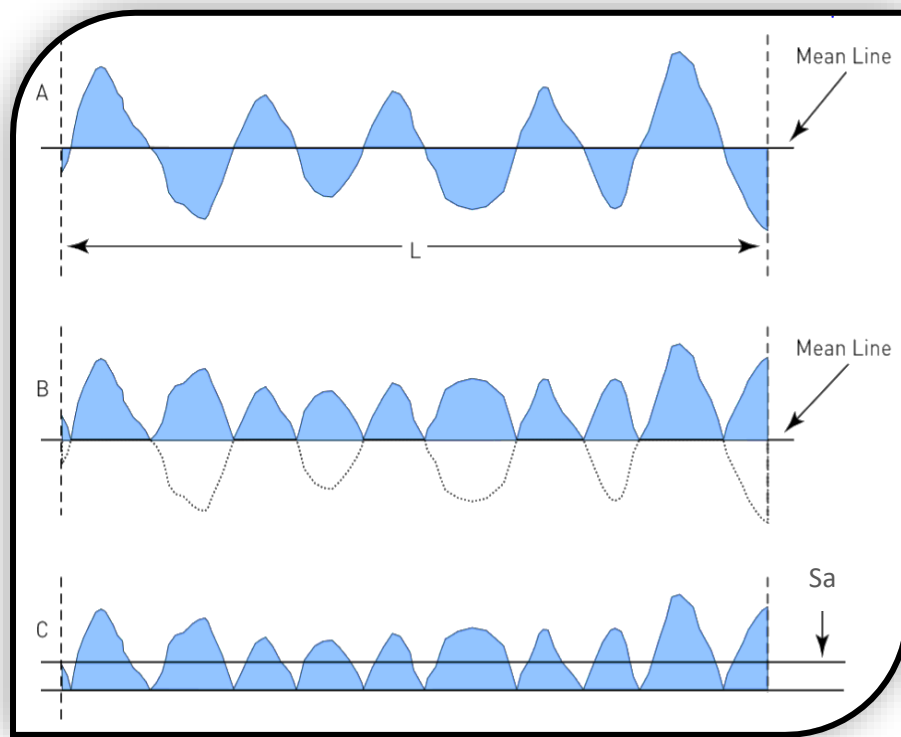


Figure (2-10) the arithmetic average of roughness [99].

The average roughness ( $S_a$ ) parameter is calculated from the height data according to Equation [100]:

$$S_a = \frac{1}{l} \int_0^l |y(x)dx| \dots\dots\dots(2 - 29)$$

Where

$S_a$  : average roughness

$l$  : samples length

**(2-12-2) Ten-point mean roughness ( $S_z$ )**

It is the mean difference between the top five deviations and the lowest five deviations in the measured sample [100]. At the average line drawn on the studied surface as shown in figure (2-11), it is considered more sensitive to high peaks or deep valleys than ( $S_a$ ), this parameter beneficial Especially at measuring very small lengths because it depends on ten points within the sampling length [98].

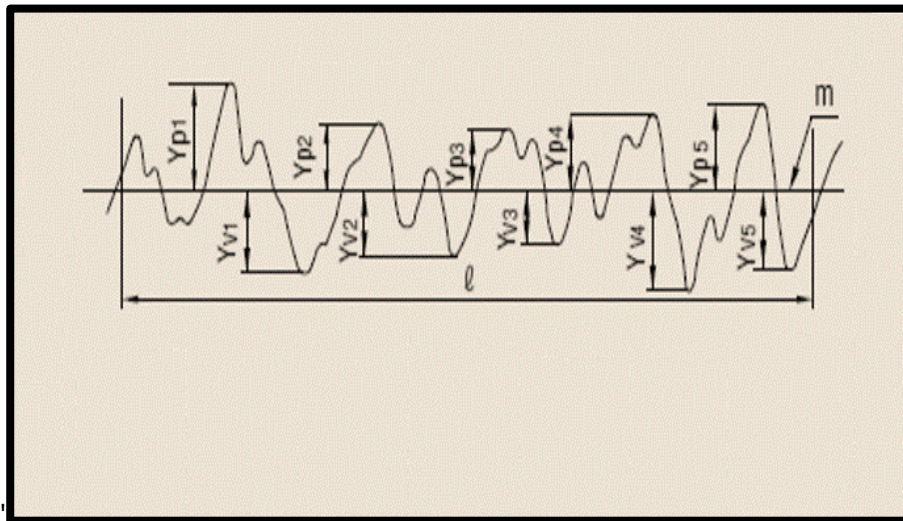


Figure (2-11) mean maximum surface deviations [98]

( $S_z$ ) is calculated from the height data according to equation [98].

$$S_z = \frac{1}{2n} \sum_{i=1}^n P_i - \sum_{i=1}^n V_i \dots \dots \dots (2 - 30)$$

Where

$n$  : is the number of samples along the mean line

$P_i$  : highest peaks

$V_i$  : lowest peaks

**(2-12-3) Mean of maximum peak to height valley ( $S_{tm}$ )**

It is all average heights of maximum peaks to valleys within the evaluation length of the profile as shown in figure (2-16), it can be expressed in mathematical form as following:

$$S_{tm} = \frac{1}{n} \sum_{i=1}^n S_{ti} \dots \dots \dots (2-31)$$

Where

$n$  : the number of samples along the evaluation length.

$S_{tm}$  represented in Fig (2-12) is: [100]

$S_{ti}$  : the vertical distance between the highest peak and lowest valley for each sampling length

$i$  : ranges from 1 to 5

$$S_{ti} = S_{pi} + S_{vi}$$

$$S_{t1} = S_{p1} + S_{v1}, \dots \dots \dots S_{t5} = S_{p5} + S_{v5}$$

$$S_{tm} = (S_{t1} + S_{t2} + S_{t3} + S_{t4} + S_{t5})/5$$

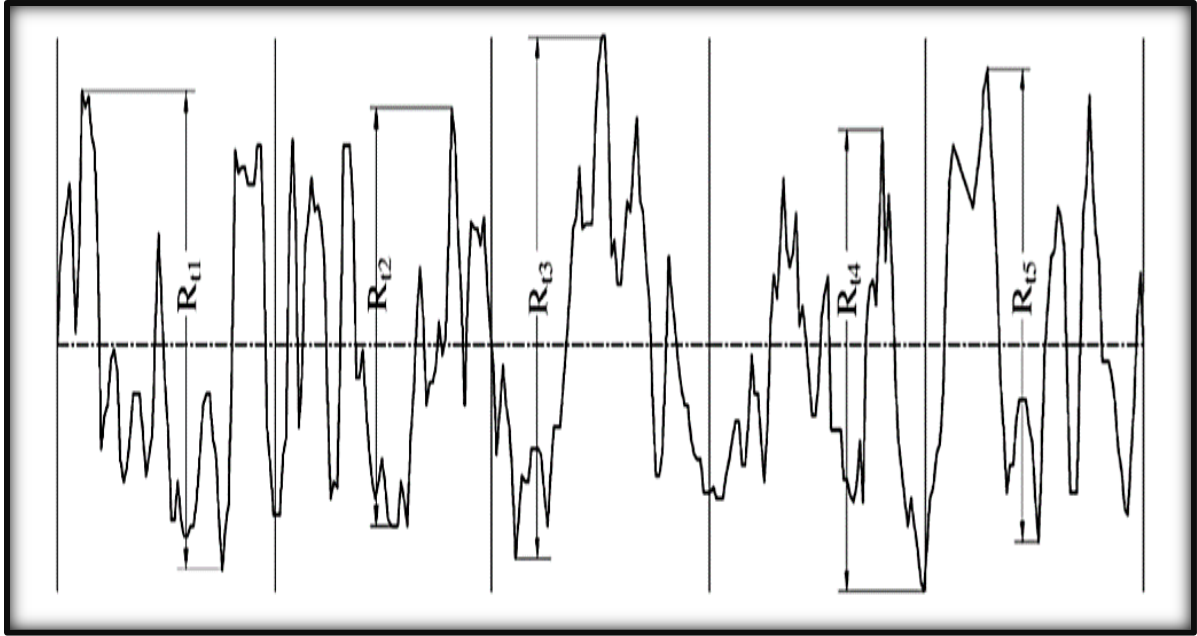


*Figure (2-12) mean of maximum peak to height valley [100].*

#### **(2-12-4) Kurtosis ( $S_{ku}$ )**

It describes the sharpness of the density probability of the profile, figure (2-13) and (2-14) show these two types of kurtosis

The kurtosis coefficient in the normal distribution equals 3, so the distribution curve can be described in terms of flattening, as follows:

- If  $k = 3$  the distribution curve will be moderate.
- If  $k > 3$  the distribution will be leptokurtotic curve, (has many high peaks and low valleys).
- If  $k < 3$  the distribution will be platykurtotic curve (overfed), (has few high peaks and low valleys) [100].

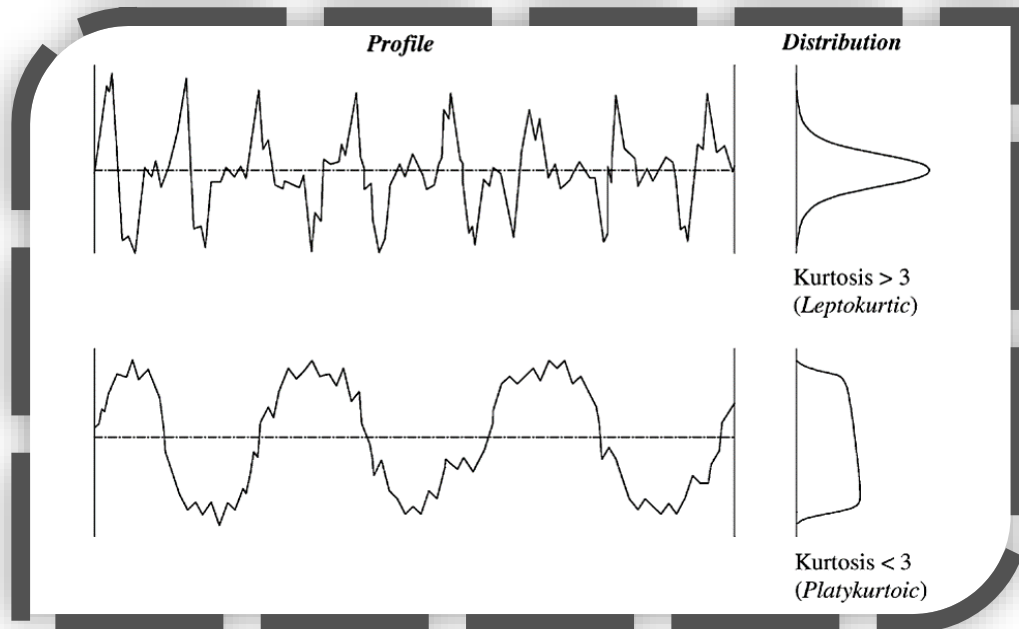


Figure (2-13) definition of kurtosis parameter [100].

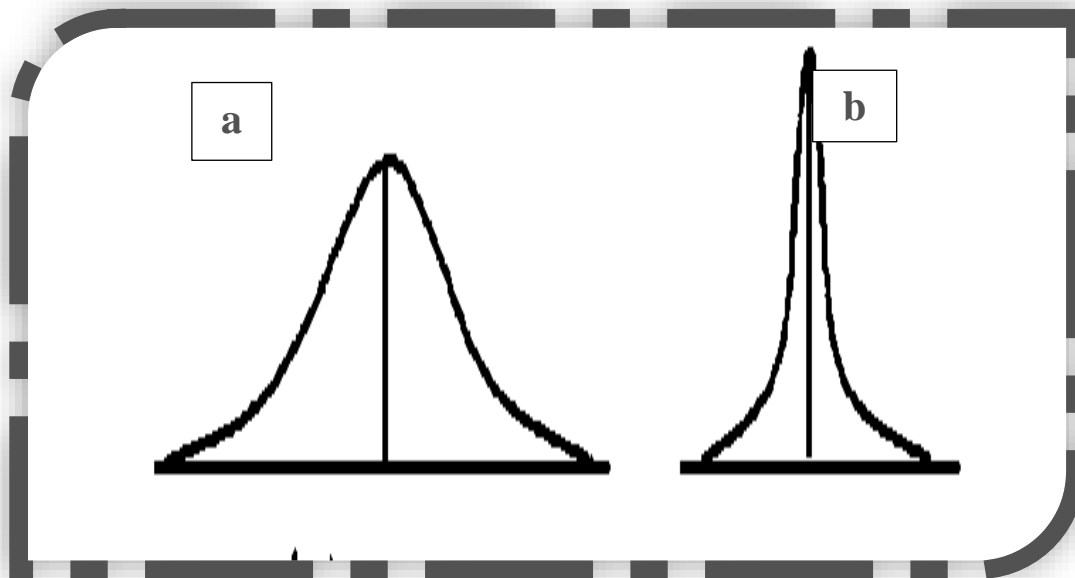


Figure (2-14) the forms of kurtosis

a- platykurtic curve

b- leptokurtic curve

The formula describes the kurtosis is :

$$S_{ku} = \frac{1}{NS_q^4} \sum_{i=1}^n Y_i^4 \dots\dots\dots (2-32)$$

Where

$S_{ku}$  : kurtosis value

$S_q$  : root mean square

$Y_i$  : the height of the profile at point number  $i$  [100].

### (2-12-5) Skewness ( $S_{sk}$ )

The Skewness distinguishes the degree of asymmetry in a given distribution around its mean. This parameter is sensitive to the deep valleys or high peaks, when there are two profiles with the same ( $S_a$ ,  $S_q$ ) the skewness is used to discriminate between these surfaces, can be the sign of the skewness determined in negative or positive cases according to presence the part of the material below the mean line (+) skewness or above the mean line (-) skewness, as shown in Figure (2-15), [100,101].

$$S_{sk} = \frac{1}{NS_q^3} \sum_{n=1}^N r_n^3 \dots\dots\dots (2 - 33)$$

Where

$S_{sk}$  : skewness value

$N$  : number of the height values

$S_q$  : standard deviation of the height values

$r_n$  : distance between mean line and individual height value

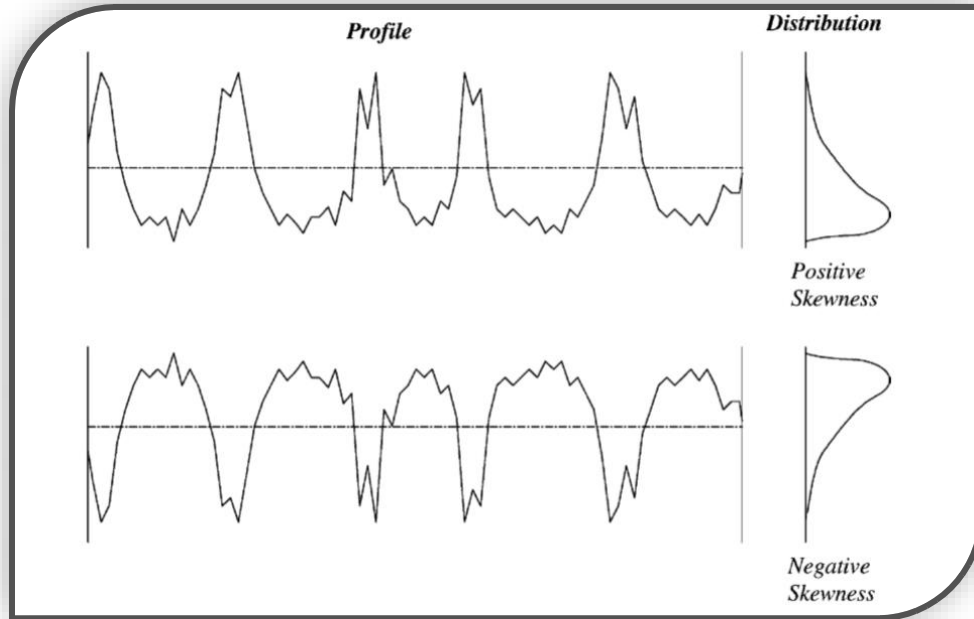


Figure (2-15) the amplitude distribution curve and skewness [100].

**(2-12-6) Root mean square ( $S_q$ )**

It is also known R.M.S which is another way to compute the average roughness value and is it obtained from squaring each value and gathering the mean square root, it represents the criterion deviations distribution of the surface heights. This parameter is more sensitive than the average roughness, ( $S_q$ ) characterizes the deviation of the measurement points to the centerline, this method describes the variability of the measured profile from centerline [101]. Where the parameters  $S_a$  and  $S_q$  are useful to evaluate the average heights and depths of surface profiles [100].

$$S_q = \sqrt{\frac{1}{l} \int_0^l \{y(x)\}^2 dx} \dots \dots \dots (2 - 34)$$

Where

$S_q$  : root mean square

$l$  : length of sample

***(2-12-7) Maximum height of peaks ( $S_p$ )***

It is the highest altitude of the profile above the center line within assessment length, as shown in fig (2-16)

Where

$S_{p3}$  : in figure (2-16) represents ( $S_p$ )

***(2-12-8) Maximum depths of valleys ( $S_v$ )***

It is known as the highest depths of the profile under the center line within assessment length, as shown in fig (2-16)

Where

$S_{v4}$  : in figure (2-16) represents the ( $S_v$ ), [100].

***(2-12-9) Mean height of peaks ( $S_{pm}$ )***

It is the average of the maximum height of peaks acquired for every sampling length of the assessment length, as shown in figure (2-16) [100].

Where

$$S_{pm} = \frac{S_{p1}+S_{p2}+S_{p3}+S_{p4}+S_{p5}}{5} \dots\dots\dots(2 - 35)$$

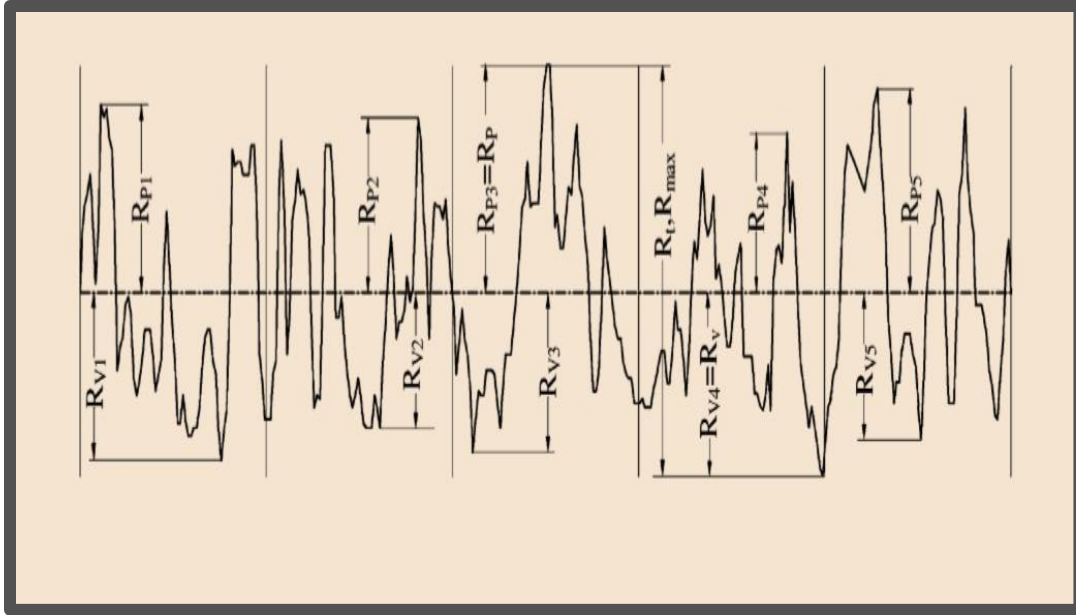


Figure (2-16) shows the  $(S_p)(S_v)(S_{pm})(S_{vm})(S_t)$  parameters [100].

**(2-12-10) Mean depth of valleys ( $S_{vm}$ )**

It is the average of the maximum depth of acquired for every sampling length of the assessment length, as shown in figure (2-16) [100].

Where

$$S_{vm} = \frac{S_{v1} + S_{v2} + S_{v3} + S_{v4} + S_{v5}}{5} \dots \dots \dots (2 - 36)$$

**(2-12-11) Maximum height of the profile ( $S_t$ )**

It is, sometimes, called ( $S_{max}$ ), it is the vertical distance between the highest and lowest points of the profile within the evaluation length as shown in fig (2-16), [99].

Where

$$S_t = S_p + S_v \quad \text{or} \quad S_{p3} + S_{v4} \dots \dots \dots (2-37)$$

Where this parameter is measured taking an adequate surface length of the sample ( $l$ ), then draw the average line to measure the heights values and decrease the average line on the Y-axis, ( $S_{max}$ ) equals to the total length of the highest peak and lowest valley from the evaluation length [97]. The problem with this parameter is the sensibility to outliers, since one exceptionally high or low height value has direct influence to this value [101].

### ***(2-12-12) Solidity factor of the profile ( $k$ )***

It can be calculated from the following equation

$$k = S_v/S_{max} \dots \dots \dots (2 - 38)$$

It represents the ratio between the maximum depth of valleys to the maximum height of the profile [100].

**(3-1) Introduction**

This chapter includes a review of preparation methods for thin films focusing on thermal evaporation in vacuum and its characteristics from other methods, being the method adopted in this study. This chapter also includes an accurate description of the devices used in synthetic and optical measurements of tin oxide ( $\text{SnO}_2$ ) films, surface roughness ( $S_a$ ), root mean square ( $S_q$ ) and average grain size was calculated using (AFM) images also with aid of AFM image by using SEM images on a large scale, the surface roughness of the thin film was calculated in terms maximum depths of valleys ( $S_v$ ), maximum height of peaks ( $S_p$ ), mean of maximum peak to height valley ( $S_{tm}$ ), ten point mean roughness ( $S_z$ ), kurtosis ( $S_{ku}$ ), skewness ( $S_k$ ), mean height of peaks ( $S_{pm}$ ), mean depths of ( $S_{vm}$ ), maximum height of the profile ( $S_t$ ) and solidity factor ( $k$ ) which evaluated using MATLAB software.

Figure (3-1) illustrates an outline of the action steps.

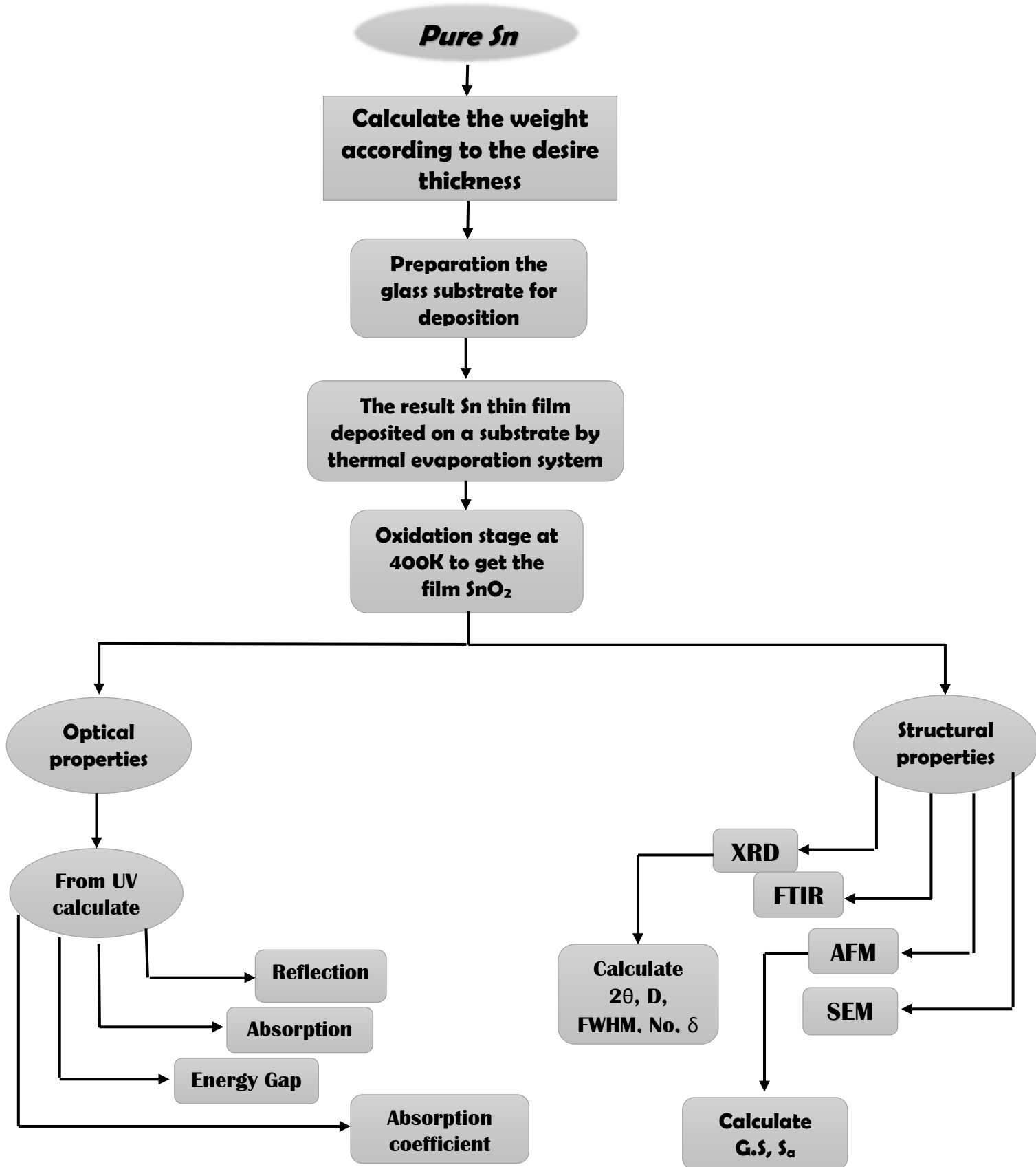


Figure (3-1) an outline of steps in practical part

### **(3-2) Thermal evaporation Technique**

Recently, this method is one of the most widely used methods in thin films preparation, as this method has its own characteristics that makes it different from other preparation methods. The most important of these is the absence of the possibility of chemical contamination inside the evaporation chamber, due to high evacuation and very low pressure during which sedimentation is performed, the chamber is evacuation from the air pressure between ( $10^{-9}$ - $10^{-6}$ ) mbar with help of both rotary and diffusion pumps means clearance. The chamber of gases and vapors majority in which interacts with the vapor from the deposited material, especially oxygen gas which is characterized by the oxidation of all the reactants with it. In this method, dust particles and other atoms present in evaporation chamber may cause defects in crystal structure of the prepared film [54,102].

To prepare a thin film in this method, material was heated by applying suitable voltage difference till evaporation happens putting the equivalent weight of the thickness required of the film material in the melting point (Boat), melting point must be higher than boiling point of the deposition material, besides the absence of any chemical reaction between them, then connect the ends tightly to an electrolytic pole to give a large current manually changed from one material to another depending on the nature of the sedimentation material and its melting temperature, as soon as the appropriate pressure is reached to precipitate and the material reaches its boiling temperature when its steam begins to rise to collide with the lower floors temperature and prepared for this purpose, thin film is formed by condensation process [52].

The method of thermal evaporation in vacuum is an appropriate method in metal membranes and semiconductors preparation, but it is inappropriate in the preparation of compounds membranes because of the elements tendency of these compounds to secrete during the gradual rise in temperature, and therefore, the evaporation method is used in the electronic package for films preparation such as this type of compound [103].

### **(3-3) Thermal evaporation system**

The coating system (Edwards 306) is used in films preparation under study. The system consists of the following basic parts:



***Figure (3-2) vacuum evaporation system***

### (3-3-1) Evaporation chamber

The evaporation chamber consists mainly of: -

- i. **The cover:** Cylinder is made of stainless steel material with high ability to resist rust, corrosion, high temperature tolerance and low pressure for deposition
- ii. **Heating poles:** A vaporizing vessel is installed and equipped with appropriate voltages to evaporate the material contains an electrode connected in parallel to the electrodes.
- iii. **Boil:** It varies in shape and type of manufacturing material, either in a spiral spring or in a small box with a perforated cover or otherwise depending on the quality of the sediment and its structure, whether it is Bulk or Powder, they are made of tungsten or molybdenum metal because of their high melting point. In this study, a locally made container of molybdenum (1cm<sup>3</sup>) was used to avoid volatilization of the material from the container during heating process.
- iv. **Substrate Holder:** Samples are stabilized so that the vertical distance between the samples and the source of evaporation is controlled by sliding vertically along an axial nail on the chamber floor. The sample carrier also contains the heater to temperatures that can be identified using a device (Thermocouple) with a thermal range (273\_1273) K.

### **(3-3-2) Vacuum unit**

The unit of discharge is the base of the work of thermal evaporation in vacuum system because of its low pressure and suitable for the sedimentation completion. This unit consists of two main pumps [101,103,104]:

- ***Mechanical roughing pump***

A vacuum pump acts as a supporting pump in the vacuum system uses two alternating pumps, it adjusts the pressure inside the evaporation chamber to suit the function of the diffuse pump. It evacuation atmospheric pressure from the chamber to a pressure of about ( $10^{-1}$ ) Pascal or ( $10^{-3}$  mbar), which represents the minimum pressure required to start the second pump to reduce it to appropriate pressure for deposition.

- ***Diffusion pump***

It is easy to design with very high vacuum, reduces the pressure inside the evaporation chamber to about ( $10^{-7}$ ) mbar or less, thus it is complementary to the rotary pump work as well as working without noise or vibration movements. The high degree of vacuum is the distinguishable by character of the diffusion pump which is due to air particle's capture efficiency and other gases were purified by condensate oil vapor at the top of the pump chamber. So, the type of oil used in the pump chamber (in terms of density, purity, boiling point, and molecular weight of its droplets) will be with effective and significant role in obtaining the required discharge degrees in short time. The fault this pump is the possibility of leakage in evaporated oil particles into the evaporation

chamber during the deposition process, which adversely affects the purity of the prepared membranes and their adhesion to the base. To prevent this, the matter should treat by cooling the pump walls using liquid nitrogen or cooled water.

### ***(3-3-3) Vacuum gauges***

There are two vacuum gauges were used in this system: -

- i. Pirani gauge: It is within ( $1^{-3}$ ) Torr range and suitable for mechanical pumps.
- ii. Penning gauge: It operates within ( $10^{-2}$ - $10^{-6}$ ) Torr range and suitable for diffusion pumps.

### ***(3-3-4) Cooling system***

It is the part of thermal evaporation system which has a great effect to obtain low temperatures and the required discharge to compress the air during short time periods, this work depends on the efficiency and type of the used liquid for cooling process either to be cooled water or Fluid nitrogen.

**(3-4) Advantage of vacuum thermal evaporation**

Thermal evaporation in vacuum is a highly efficient procedure to obtain excellent films purity (depending on the purity of the base material and the degree of air discharge).

- ❖ One of the confident methods to obtain films as few stress centers (or internal tension) as possible resulting from the presence of exotic atoms or dust particles the evaporation chamber.
- ❖ This method is highly discharge technology, it is reducing the probability of collisions or scattering between the vapors and other gases in evaporation area.
- ❖ Simple in preparation.
- ❖ Ensures that no thermal oxidation associated with presence of oxygen gas.
- ❖ Has the least surface damage for deposition substrate.
- ❖ Does not produce ionized radiation.
- ❖ Reduces the material melting point by increasing pressure falling.
- ❖ The possibility of completing multiple samples with uniform conditions (for one evaporation) in a short time [75,102,105] .

**(3-5) Disadvantage of vacuum thermal evaporation**

- ❖ The possibility of pollution from the heater " Boat "
- ❖ Thermal evaporation in vacuum is one of the most common preparation methods imperfection are created in deposited atomic layers of the prepared thin films. Point defects are some of these imperfections, especially the type called the "vacancies". Any membrane in this method must contain a number of those holes

(vacancies) depending on both the base temperature, and the deposition rate.

- ❖ It is a limited evaporation method for low-melting compounds such as Al, Cd Sn, Pb, In, Zn, Cu.
- ❖ Loss of vaporized matter during evaporation due to the spherical propagation mechanism of evaporated atoms in evaporation chamber.
- ❖ It is difficult to evaporate electrically (Dielectric Materials).
- ❖ The prepared films density adhesion degree of with the prepared slides for deposition are weak when compared with sputtering method.
- ❖ Large-scale films cannot be prepared.
- ❖ The samples of the single deposition vary in thickness, due to the engineering design of both the evaporation chamber and the sampling carrier.

The cause of these defects (especially vacancies) is explained as a process of extinguishing the state of the material (*Quenching Process*) from the vapor state to the solid state and the subsequent membrane cooling leads to stabilization of such defects in the crystalline structure of the prepared membranes to cause high stress, which can be later discarded by annealing [75,50,105].

**(3-6) The parameters that influence on the prepared films homogeneity**

- ❖ Air pressure inside evaporation chamber (discharge degree).
- ❖ The vertical distance between the evaporation boat and the substrate prepared for deposition.
- ❖ substrate temperature.
- ❖ Deposition rate.
- ❖ Clean of chamber evaporation.
- ❖ Shape of the boat type of manufactured material [106].

**(3-7) substrate preparation**

The substrate cleaning process is necessary to ensure that the films are suitable for study with minimal contamination. The process of cleaning the substrate is done in several steps:

- i. It is first washed with running water and a cleaning powder to get rid of stains or residue of material or soil stuck to it.
- ii. Immerse in a tank of distilled water for washing with an ultrasonic device for 15 minutes. Figure (3-3) shows a picture of used ultrasonic device.
- iii. Immerse in the same tank of pure ethanol alcohol to wash automatically with an ultrasonic device for the same period.
- iv. Then dried with filter paper and then subjected to a dry air stream.
- v. Put it to the sample holder and then placed inside the evaporation chamber to be ready for deposition.



*Figure (3-3) ultrasonic device*

### ***(3-8) Preparing( $\text{SnO}_2$ ) thin films***

#### ***(3-8-1) Deposition of pure material***

( $\text{SnO}_2$ ) is characterized by its composition as a compound with a high melting temperature (about  $1630\text{ C}^\circ$ ), which is large compared to the melting temperature of the tin element of melting temperature of ( $231.9\text{ C}^\circ$ ), purity (99.9%) in the preparation of the films in this study, this stage includes the following steps:

- 1) The weight of the material was calculated using a sensitive electronic balance of (Precisa) with a sensitivity range of ( $10^{-4}$ ) gm and an equivalent weight for required thickness of films [450, 525 and 600]

720 nm in the boat of molybdenum metal was locally manufactured high temperature, as shown in Figure (3-4)



*Figure (3-4) shape of the used molybdenum*

- 2) The substrates are set up in the sample holder, the vertical distance between the evaporation source and the sample carrier is changes to obtain greater adhesion strength and better homogeneity of the formed film. The carrier sat up at a vertical distance away from the evaporation source at a distance of 9 cm, which was the best distance for achievement.
- 3) After the pressure inside the evaporation chamber reached ( $3.5 \times 10^{-5}$  mbar), the material starts to evaporated at a deposition rate of ( $2.5 \pm 0.1$ ) (nm / sec).
- 4) The samples should be left after the deposition process in the evaporation chamber until the temperature reached the room temperature to ensure that the crystallization process was complete and the prepared samples were not broken or cracked if they were suddenly cooled (temperature difference).
- 5) Finally, the samples are prepared for the thermal oxidation stage.

**(3-8-2) Thermal oxidation**

To get the final form of thin films, the pure tin films prepared by thermal evaporation in vacuum were placed in a (Kilns furnaces) described in Figure (3-5) at (400) K with existing air flow for an hour. leave the samples in oven to cool until the temperature reaches the room temperature, then structural and optical tests are applied using devices prepared for this purpose.



*Figure (3-5) oxidation electric furnace*

**(3-9) Investigation of prepared films structure by using (XRD) technique**

To determine the crystalline structure of the studied film material ( $\text{SnO}_2$  thin films), whether it is crystalline, single crystalline, polycrystalline, or amorphous structure use an x-ray diffraction device type:

*Table (3-1) shows device specification of x-ray diffraction*

<i>X-Ray Tube</i>	<i>Scanning</i>
<b>Target : Cu <math>\alpha</math></b>	<b>Scan Mode : continuous Scan</b>
<b>Voltage : 40 k Volt</b>	<b>Axis : Theta-(<math>2\theta</math>)</b>
<b>Wavelength<sub>(x-ray)</sub>= 1.5406 <math>\text{\AA}</math></b>	<b>Range : 10_80 (deg)</b>
<b>Current : 30 mA</b>	
<b>Speed : 5 (deg/min)</b>	

**(3-10) Fourier infrared spectroscopy measurement (FTIR)**

This technique is used to determine the chemical bonds of the compounds to be studied, when the infrared ray falls on the particles interference between the electric field of the infrared radiation occurs with the generated electric field by the diode dipole. If the electric field frequency of an infrared ray corresponds with the field frequency in the molecule, the molecule absorbs the beam energy, which moves it from a low vibration level a higher level. When the energy is lost and the part is returned to the level of its "ground" vibration, When the

energy is lost and the part of molecules is returned to the level of its "ground" vibration, emission of recorded infrared light that be by a sensitive detector, this data is recorded on a machine draws on a graphic paper representing the image of the infrared spectrum. The FTIR measurements were performed using a (SHIMADZU-8400S) device within a range between (400-4000)  $\text{cm}^{-1}$ .

### **(3-11) Atomic force microscopy measurements (AFM)**

AFM technique identifies the effect of thickness change in surface topography and calculation of roughness, average roughness, and knowledge the root mean square using a type device (SPM-AA3000 contact mode spectrometer, Angstrom) supplier from company (Advanced Inc. company, USA), for getting a two and three-dimensional image describing the surface and grain size.

### **(3-12) Scanning electron microscopy measurements (SEM)**

This technique identifies the extent of the surface regularity, showing the shape of the granules and their homogeneity and arrangement within the crystalline structure of the surface. The microscope was SAI2300C and its origin: USA - (VEGA3-TESCAN model).

### **(3-13) Optical measurement**

The optical measurements include spectral spectrometry (A) and prepared films transmission (T) using (UV-visible 1800 spectrophotometer), figure (3-6). The absorptance and transmittance values of the prepared films were measured as a functions of wavelength change within range of (400-1100) nm by inserting deposited glass slide to measure its transmittance as a reference chip, and then insert another slide deposited on it with same type, subtracting values of transmittance of non-deposited slice from transmittance values of the deposited slice shows the transmittance values of the prepared films only. From the transmittance spectrum, absorbance and absorption coefficient were, as well as the type of electronic transitions, optical constants and energy gap were calculated.



***Figure (3-6) the UV-VIS device***

### **(4-1) Introduction**

This chapter deals with the results of structural tests using x-ray diffraction technology of pure thin ( $\text{SnO}_2$ ) material, oxidized at ( $400^\circ$ ) C, and deposited on glass substrate using vacuum evaporation method with multiple thicknesses (450, 525, 600 nm), with deposition rate of ( $2.5 \pm 0.1$ ) nm / s. Structural and optical characteristics of prepared films, crystalline structure and study of its optical properties by measuring the transmission spectrum, the absorption coefficient, the optical energy gap, refractive index and the calculation of reflective, are presented in this chapter as well.

### ***(4-2) Structural properties of ( $\text{SnO}_2$ )***

#### **(4-2-1) X-ray diffraction**

The results of the X-ray diffraction spectroscopy were shown that the films have a polycrystalline nature with (Orthorhombic) type with preferred orientation along (111), the XRD pattern results showed that the films were of good match with the card number JCPDS (Joint Committee on powder Diffraction Standards) and appeared extreme approximation between the illustrated practically recorded peaks with the values of the numbered card (00-029-1484) with about ( $2\theta$ ) and ( $d_{hkl}$ ), figure (4-1) shows the X-ray spectrum of deposited  $\text{SnO}_2$  film on a glass substrate by evaporation method in vacuum at Bragg angle range between ( $10-70^\circ$ ). From figure (4-1) the prepared film with thickness (450 nm) has a sharp peak in (111) direction ( $2\theta=29.4^\circ$ ) , when the thickness of the film increases to (525nm) and (600nm), a clear increase of the intensity reflects in the first peak with increasing the thickness of prepared film, this

indicates enhancement of crystallinity of these films by increasing their thickness, where the atoms of the deposited layers tend to arrange themselves, later, in the least internal energy to get rid of their excess energy direction and reach the stable state from follow vaporized atoms to arrange themselves in that direction, the Sheerer equation (2-2) was extracted the dominant peak of crystalline size. The peaks used at the angles (24.2), (29.4), (32.8), (34.01) and (35.7) are in (110), (111), (020), (002) and (021) directions, respectively. Therefore, the crystalline size increases from (14.5 to 15.8) and number of crystal layers from (1.44 to 1.50), but the decrease in dislocation density from (46.9 to 39.7) as shown in Table (4-2). As it is believed, the cause of other phases emergence with increasing thickness leads to exchange the sites of oxygen atoms.

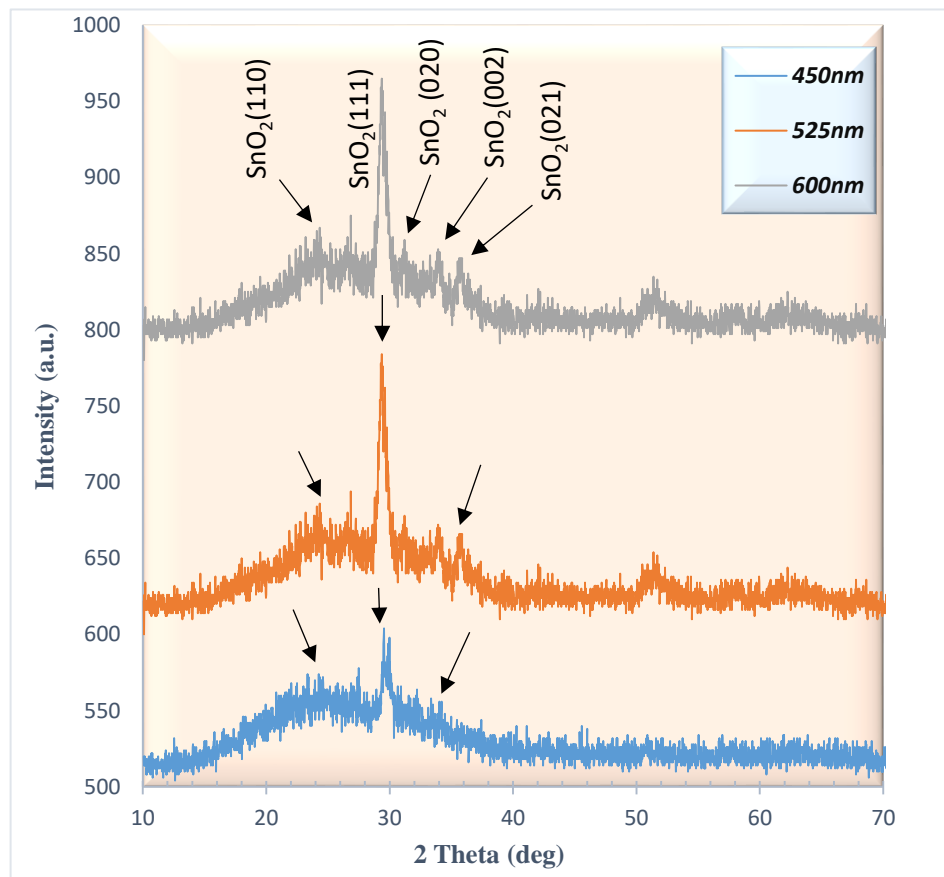


**Fig. (4-1) XRD spectra of SnO<sub>2</sub> films for 3-thicknesses**

Table (4-1) comparison of the X-ray and card(ASTM) results for pure SnO<sub>2</sub> film

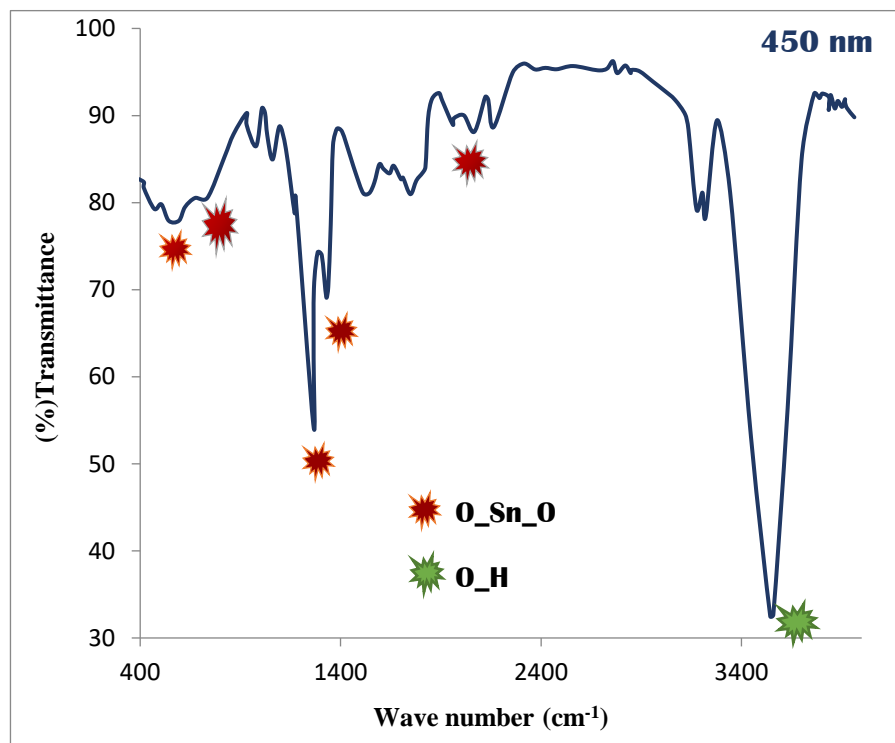
Thickness (nm)	2θ (ASTM)	2θ Observed	d(A) (ASTM)	d(A°) Observed	hkl planes ASTM
450	29.919	29.424	2.98	3.033	111
	34.343	34.018	2.60	2.633	002
	24.434	24.294	3.64	3.661	110
525	29.919	29.425	2.98	3.032	111
	24.343	24.127	3.64	3.685	110
	35.772	35.707	2.50	2.512	021
600	29.919	29.356	2.98	3.039	111
	34.343	33.929	2.60	2.639	002
	31.237	32.857	2.86	2.723	020

Table (4-2) the X-ray results of pure SnO<sub>2</sub> film for dominant peaks

Thickness (nm)	hkl	d (A°)	2 Theta (deg)	D (nm)	β(FWHM) (deg)	δ * 10 <sup>14</sup> lines . m <sup>-2</sup>	N <sub>o</sub> * 10 <sup>18</sup> crystal /m <sup>2</sup>
450	111	3.03	29.42	14.59	0.56	46.97	1.44
525	111	3.03	29.42	11.72	0.69	72.70	3.25
600	111	3.03	29.35	15.86	0.515	39.73	1.50

### (4-2-2) FTIR spectrum investigation

Fourier transformation infrared results give information about vibrational properties and the way in which oxygen is bound to metal ions. it may be observed that the (SnO<sub>2</sub>) film showed characteristic FTIR absorption peaks at (1263, 1328 and 2066) cm<sup>-1</sup> due to Sn–O vibrational and O–Sn–O stretching modes. In addition, there are absorption peaks due to O–H modes at (3558) cm<sup>-1</sup>. As shown in Figures (4-2) (4-3) (4-4),



*Fig. (4-2) FTIR spectra of SnO<sub>2</sub> films at (450 nm)*

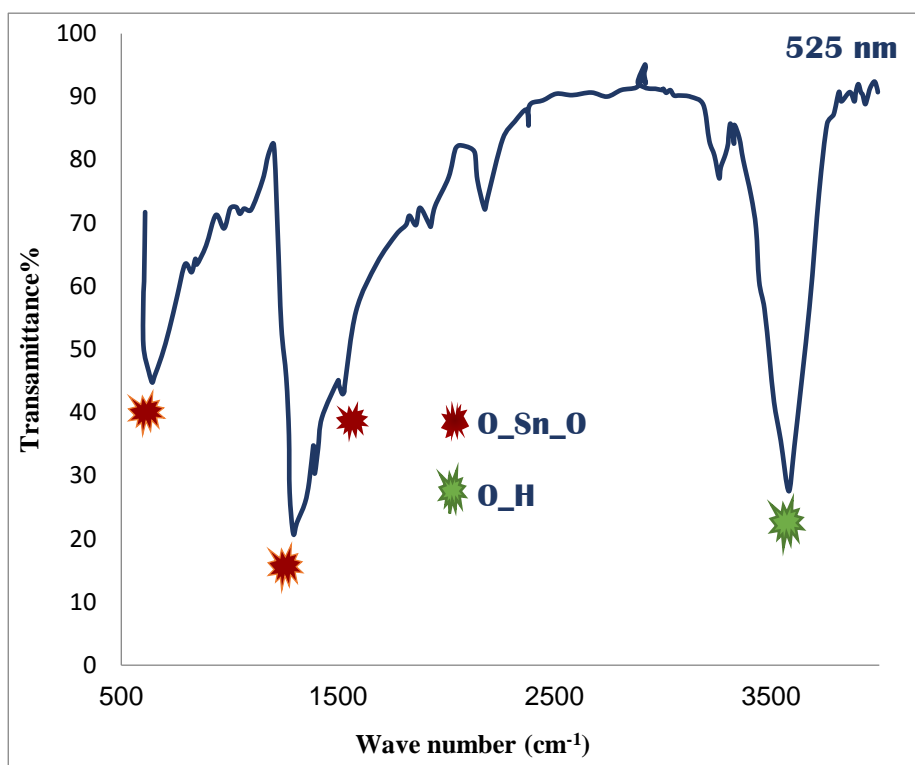


Fig. (4-3) FTIR spectra of SnO<sub>2</sub> films at (525 nm)

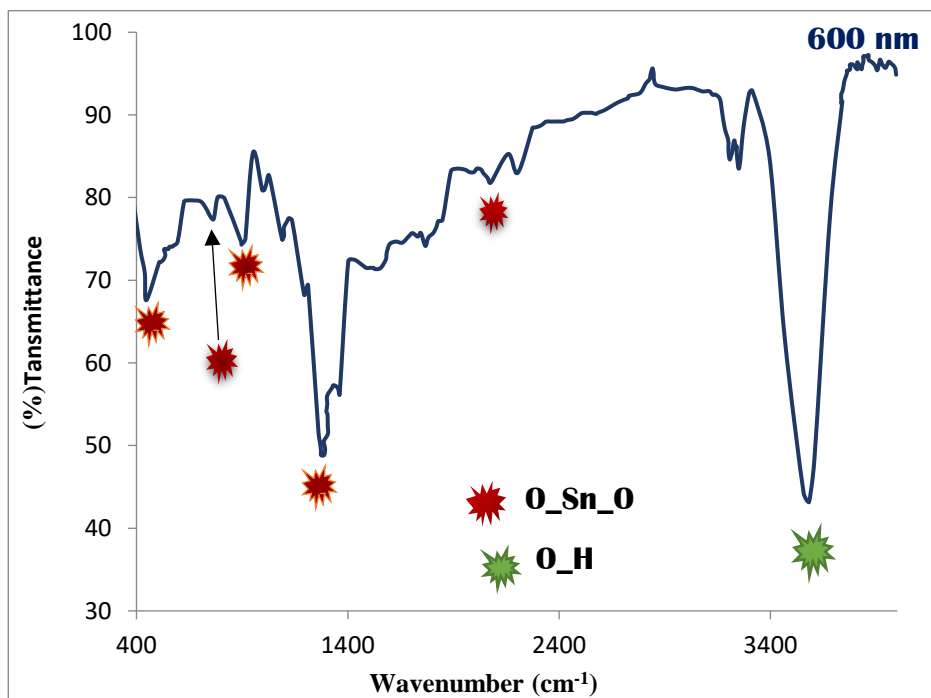


Fig. (4-4) FTIR spectra of SnO<sub>2</sub> films at (600 nm)

Table (4-3) FTIR spectra of SnO<sub>2</sub> for three Thickness

<i>Thickness (nm)</i>	<i>Wave number (cm<sup>-1</sup>)</i>
450	593
	735
	1263
	1328
	2066
525	642
	1293
	1530
600	447
	765
	910
	1288
	2077

### ***(4-3) Optical Properties***

#### ***(4-3-1) Absorptance spectrum***

To study of absorption and transmittance spectrum, an important benefit in determining the nature of practical application was harnessed the film in its service. Absorption depends on photons that falling on the material, the type of material and the nature of its crystalline structure, [81]. All absorption and transmittance spectroscopy measurements were carried out within wavelength range (300-1100) nm for all films thickness prepared from figure (4-5) which represents the change of the absorbance spectroscopy as a function of the wavelength for all samples. The figure shows the behavior of the absorption spectrum of any prepared thickness is as greater as possible at short wavelengths (high photonic energies) and then decreases when approaching long wavelengths, because the falling waves are photons have varying energies and absorbed only what the energy was equal to or greater than the value of the forbidden energy gap. Also the figure shows increases in absorbance due to increased crystallization of the films prepared by increment of thickness, then the increase in the particle size. The photon falling on the film's surface will suffer from successive absorption by the crystals within the granule, thus the possibility of reflection or transmitted without absorbed by atom's electron of the composite will be a few, especially increase the size of the granule one (increase the number of crystals by increasing thickness; by increment the thickness of the prepared film leads to increase the absorbance, this is called "Lambert's law in absorption").

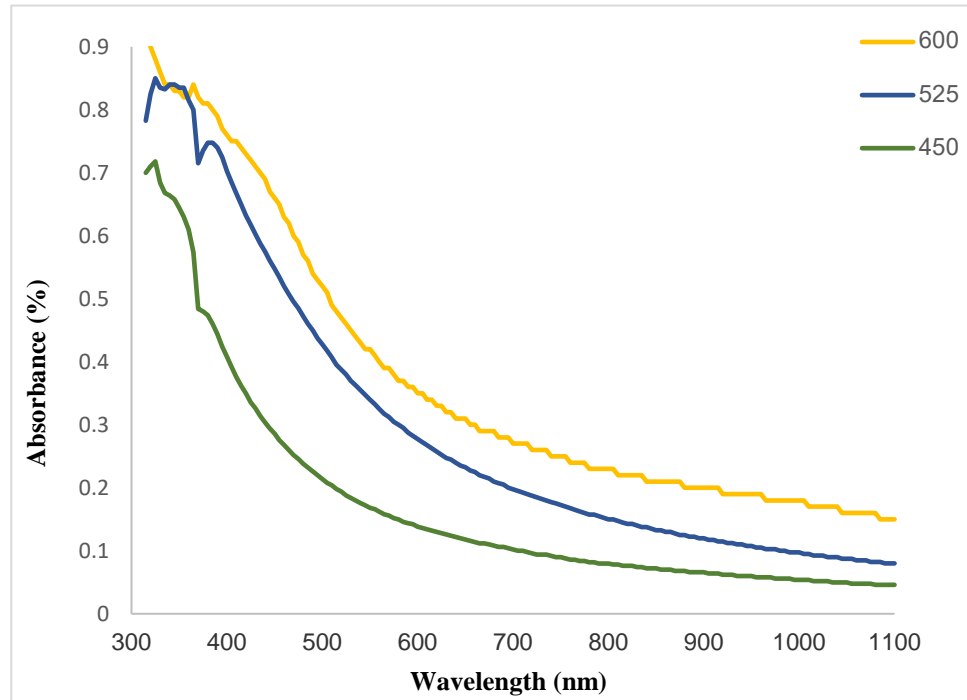


*Fig. (4-5) absorption spectrum of SnO<sub>2</sub> thin films as a function of wavelength*

### **(4-3-2) Transmittance spectrum**

Figure (4-6) represents the spectrum of the transmittance of tin oxide and the different thickness as a function of the wavelength of range (300-1100) nm. From the figure, there is no transmission in ultraviolet region, indicating that the material has an absorption spectrum under visible area region called (active material). According to Lambert's law transmission decreased with increasing thickness, at less 440 nm for all thicknesses we note transmission not exceed (0.4%) (semi-transparent). when the thickness at (450 and 525) nm, it is observing that the transmission spectrum is symmetric and reaches the transmission to 0.9 at thickness of (450) nm at a wavelength near infrared region (1020), a differentiated area

(remarkable area) is observed at the wavelength (365nm) indicating that the Plasmon region is due to the quantum size effect. The material has a quantitative effect as a result of the nanostructure, the homogenous gradient in the transmission spectrum was observed which indicates a uniform homogenous state opposite to the observed at thickness (600nm), it indicates that the material is heterogeneous and consistent with the results of AFM.

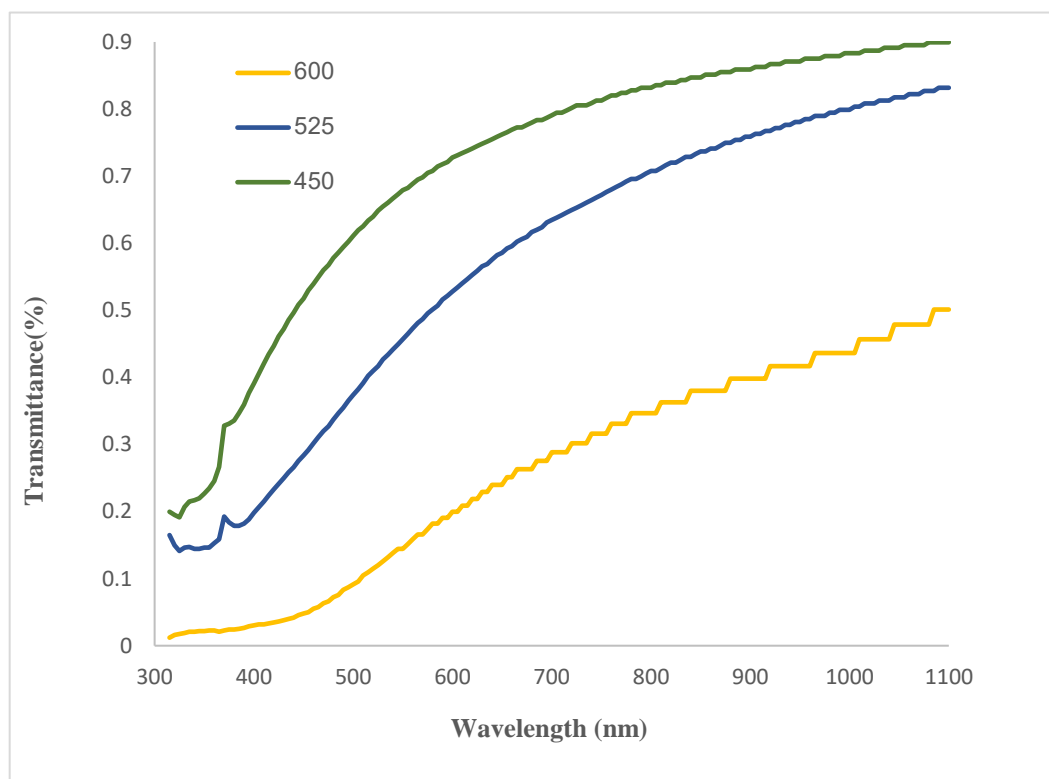


**Fig. (4-6) transmittance spectrum of SnO<sub>2</sub> thin films as a function of wavelength**

### **(4-3-3) The optical energy gap calculation**

The calculation of the energy gap was of great importance. Through the knowledge of its value, the appropriate electrophoresis application was determined for used prepared film, such as solar cells, and others. Figure (4-7) represents Tauc law's diagram, which represents the relationship between the  $(\alpha h\nu)^2$  on the y-axis and the photon energy on the x-axis, The tangent that intersects the x-axis of the zero point of the vertical axis represents the energy gap of the material which deposited on the glass substrate by vacuum evaporation. From the figure the energy gap at the thickness of (450) nm equals (3) eV, with increasing the thickness to (525) nm the gap energy was not more than (2.6) eV. When thickness is increased to (600) nm energy gap becomes (2.2) eV, because the quantum size effect; if the particle radius is much larger than Bohr's radius (0.5 Å). The quantitative effect will appear but the energy gap value will change inversely with square of granular radius according to Schrodinger equation of any energy level, the results of the structural tests on (AFM) showed that there was a clear increment in particle sizes of different film thicknesses, that leads to decrement in gap energy value with increasing film thicknesses, from the same Figure the values of the absorption coefficient of the prepared films are ( $\alpha > 10^4 \text{ cm}^{-1}$ ) which indicates that the electronic transition is direct.

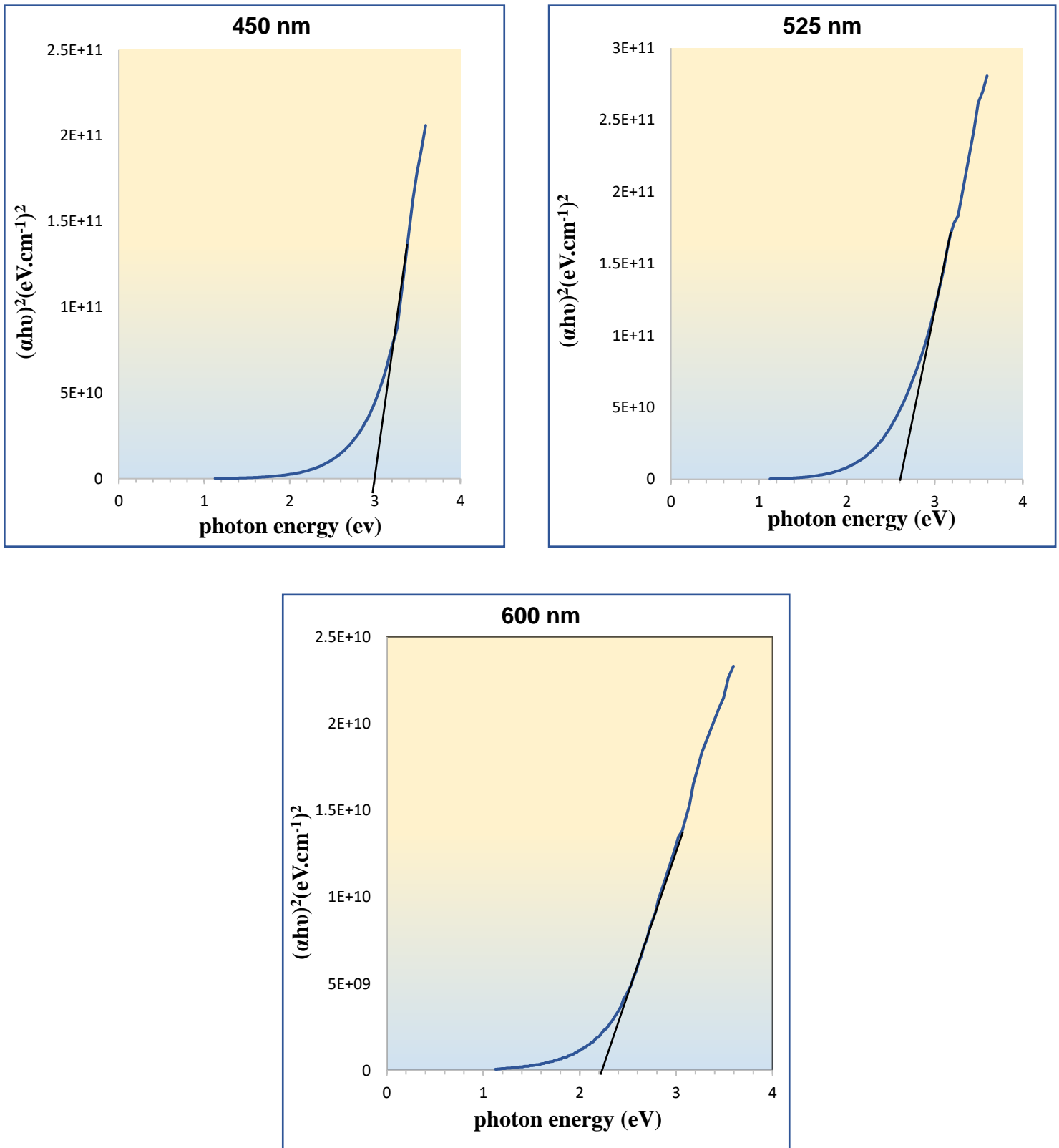
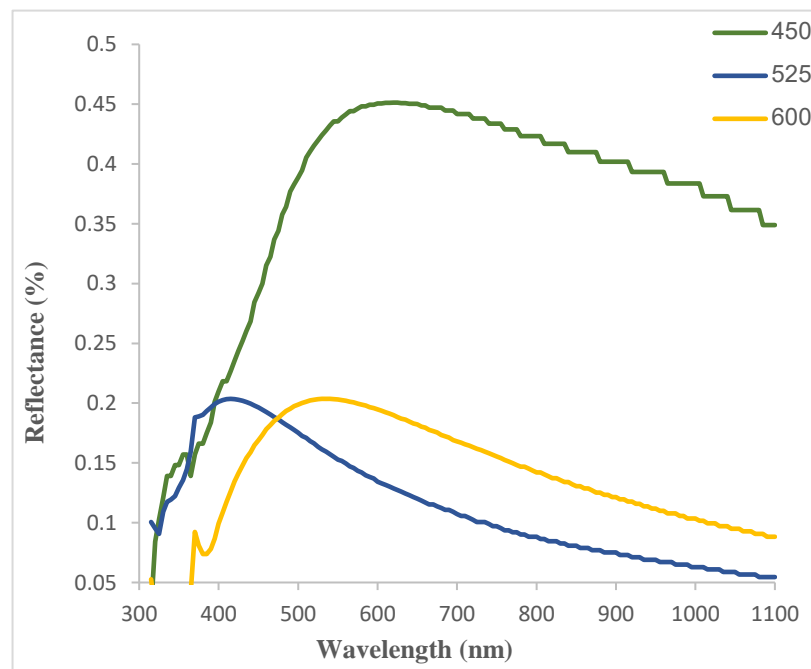


Fig. (4-7) relationship between  $(\alpha h\nu)^2$  and photon energy

#### (4-3-4) Reflectance & refractive spectrum

From absorbance and transmittance spectrum, reflectance was calculated according to the energy law conservation as in equation (2-25). Figure (4-8) shows the Reflectance spectrum as a function of wavelength, the reflection is zero in the ultraviolet region but with increasing thickness they are trending towards the short wavelengths and reaches its highest peak at wavelength between (400 - 500) nm for all thicknesses, this is the relative value to the material thickness, after that a gradual decrease is shown at a wavelength greater than (600) nm. Figure (4-8) also shows that reflection of the films decreases by increasing the thickness of the wavelengths within the visible area of the electromagnetic spectrum, and this is further evidence that the films roughness have increased, while refers to the surface roughness in the warp of the curves in the thicknesses.



*Fig. (4-8) reflective spectrum of SnO<sub>2</sub> thin films as a function of wavelength*

The refractive index of tin oxide ( $\text{SnO}_2$ ) prepared films from equation (2-28) was calculated and the refractive index was inverse of function (R). Thus, the results of spectral reflectivity and its wavelength change were reflected on the refractive index results. The behavior of the refractive index varies according to the preparation conditions and the technology adopted in the preparation. The value of the refractive index was determined from the change in the roughness coefficient of the prepared film surface. Figure (4-9) shows the change of refractive index as a function of the wavelength, where the refractive index decreases with the increase of thickness and increases with the increase of the wavelength of the fallen photon where increasing the thickness lead to the accumulation in atoms with an increase in crystalline arrangement. The refractivity at thicknesses (450, 525, 600) nm showed the highest refraction at wavelength greater than (450) nm and it starts decrease gradually, their behavior is similar to the behavior of reflectivity.

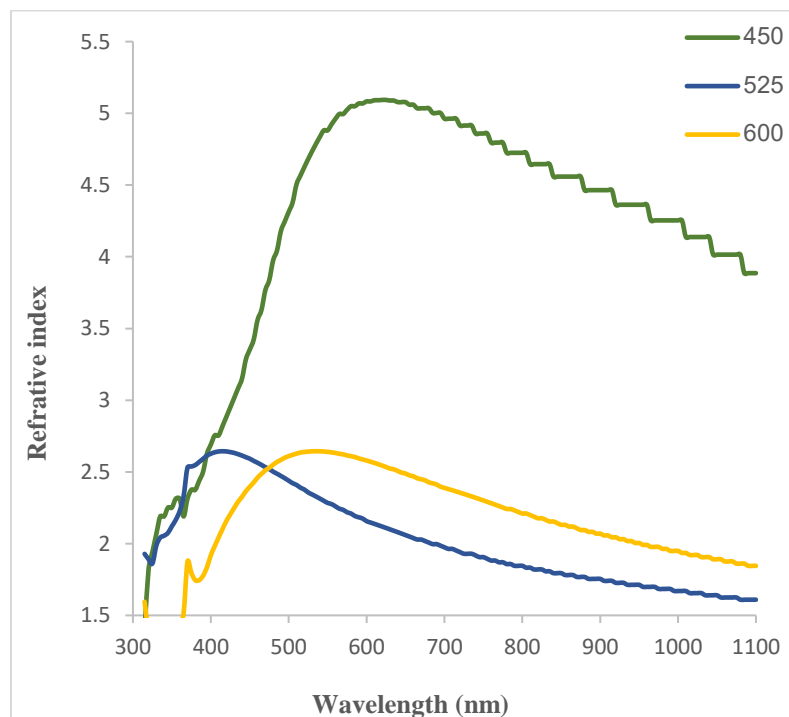


*Fig. (4-9) refractive index spectrum of  $\text{SnO}_2$  thin films as a function of wavelength*

## *Part two "Image processing"*

### **(4-4) Introduction**

In this section the surface roughness on a large scale using SEM images with aid of AFM image for SnO<sub>2</sub> thin surface was studied. The SEM images were captured with different zooming scales (1-50 μm). The surface roughness parameters of thin films were compared using AFM with calculated images from SEM for different scales which proved the validity of this approach to calculate the roughness parameter using the SEM images. Besides that, the calculated heights contrast parameter using the SEM images shows the homogeneity of the samples surface.

The algorithm (4-1) explains the calculation of roughness parameters using the Matlab program

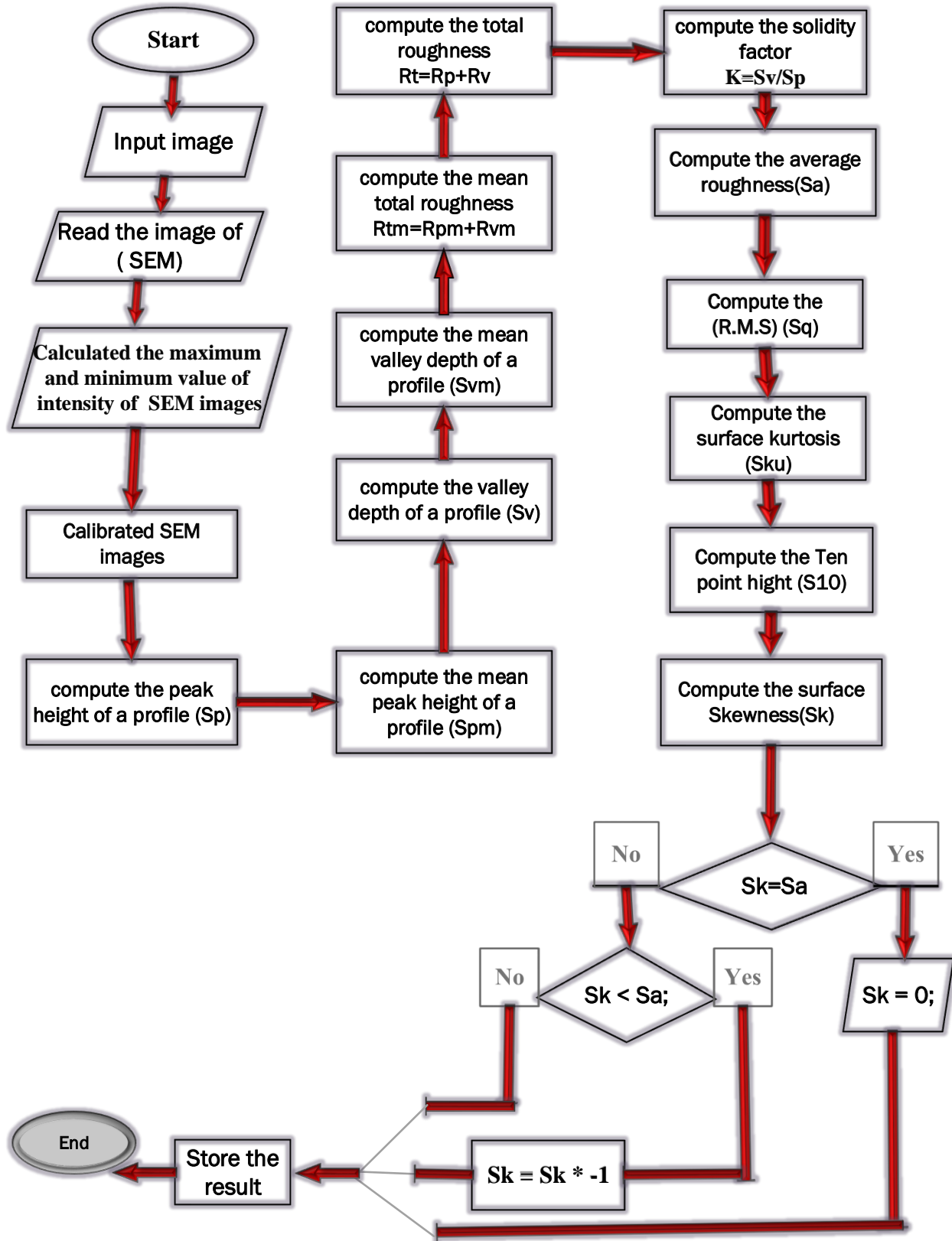


Figure (4-1) block diagram of roughness parameters

#### **(4-5) Atomic force microscope results (AFM)**

The Atomic force microscope (AFM) technique was used to study the topography of the prepared films and the film crystalline surface structure and the extent of the thickness change effect on the characteristics of the prepared film and to give very precise statistical values to the average number and distribution of grain size and the surface roughness based on the root mean square of roughness (RMS) [107, 108, 109]. The study of films material surfaces is important in explaining of the distribution and arrangement on the surfaces, it describes the differences or homogeneity of characteristics or features related to each crystallization separately [108, 110]. This microscope has a high analytical capacity for the surfaces as well as gives accurate roughness and root mean square values. Surface images examined by this microscope had two and three dimensions. So the thin surfaces of the (SnO<sub>2</sub>) films have studied by this technique. From figure (4-9), 3D AFM images for deposited SnO<sub>2</sub> films on glass substrate by thermal evaporation in vacuum method, it proved that the grains were uniformly distributed with individual columnar grains extending upwards. This surface characteristic is important for applications such as gas sensors and catalysts [111,112]. The particles were aligned horizontally spherical or semi-spherical with interstitial spaces (vacancies) separating them, but some particles adhered together giving different colors between brown to white on the peaks, indicating the difference in grain size shown in figure (4-9)

A change in the morphology of the films was shown when thickness increase to (525) and (600) nm due to good crystallinity in grown SnO<sub>2</sub> thin films. Also, all films display homogeneous, dense surfaces with pyramid-like shape reflected from

a well uniform surface with no pinholes or island structure, due to the accumulation of sediment atoms on the surface by increasing the thickness, thus forming the homogeneous film that has large granular size and improve its structural properties (especially the increase of crystallization), thus increasing the roughness of the surface and this is consistent with the results of X-ray diffraction tests. Table (4-3) shows surface roughness values, average diameter, and root mean square change at different thicknesses.

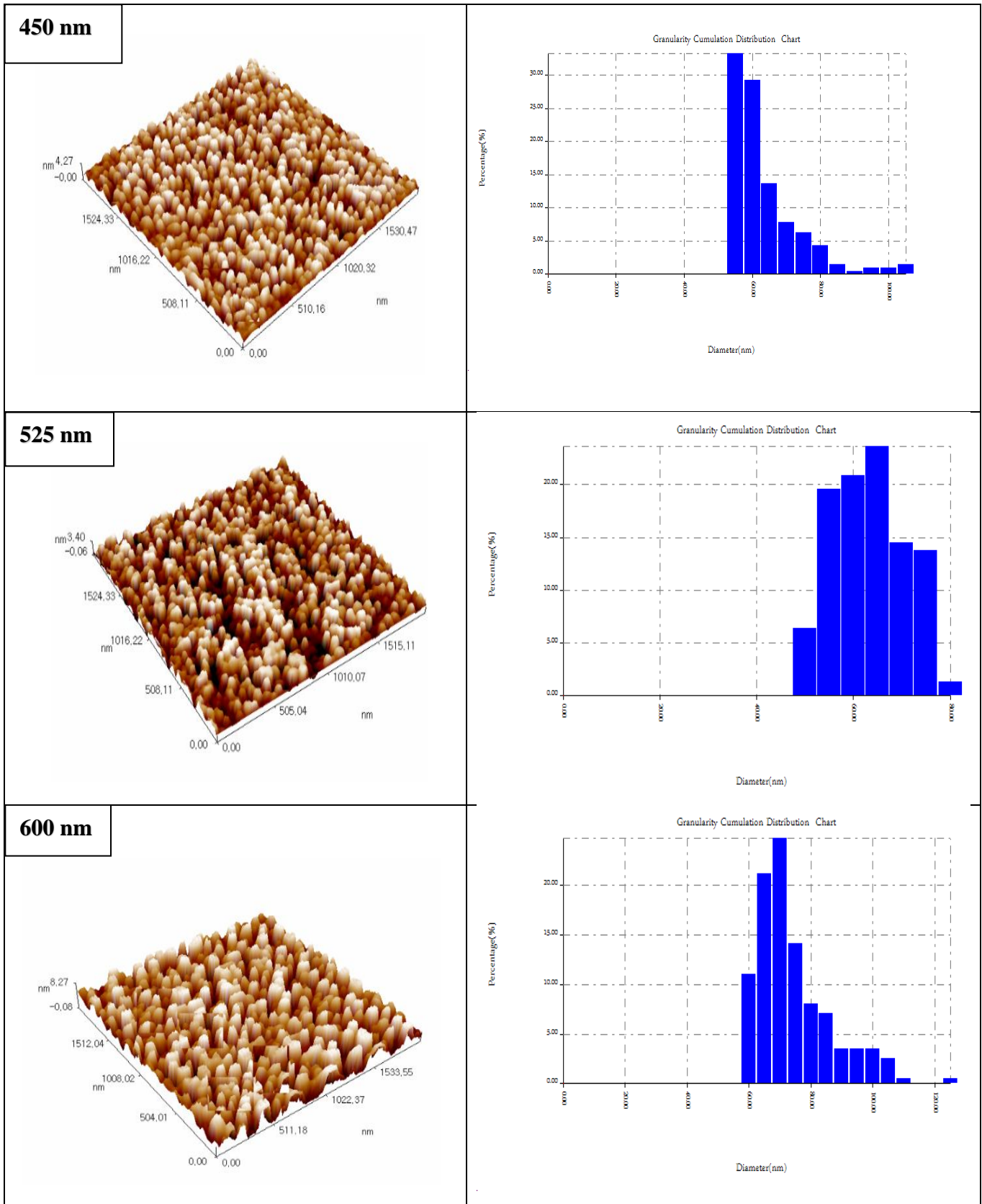


Fig. (4-9) AFM images for SnO<sub>2</sub> thin films

(AFM) measures the roughness coefficient of the surface from which (Root Mean Square) and the grain size can be obtained, as shown in Table (4-4).

**Table (4-4) the values of surface roughness, average diameter, and Root Mean Square for all thickness.**

<b>Thickness (nm)</b>	<b>Roughness (nm)</b>	<b>Grain size (nm)</b>	<b>R.M.S (nm)</b>
<b>450</b>	<b>0.949</b>	<b>60.88</b>	<b>1.12</b>
<b>525</b>	<b>0.878</b>	<b>60.90</b>	<b>1.02</b>
<b>600</b>	<b>1.91</b>	<b>71.78</b>	<b>2.24</b>

Table (4-5) shows the height of each thickness according to the AFM images used to find the roughness parameters.

**Table (4-5) the maximum height for each thickness**

<b>Thickness (nm)</b>	<b>Maximum Height (nm)</b>
<b>450</b>	<b>4</b>
<b>525</b>	<b>3.46</b>
<b>600</b>	<b>8</b>

**(4-6) Scanning Electron Microscopy results (SEM)**

The (SEM) device was used to examine and analyze sample surfaces the resulting signal was 2-D image, shows information about surface morphology, Figures (4-10), (4-11), (4-12) represent SEM images for 4-scales (1, 5, 10, 50)  $\mu\text{m}$  for 3-thicknesses of ( $\text{SnO}_2$ ), it is clear from the tests and images that increasing the thickness of the film has a significant impact on the profile formation of the surface structure of the prepared films. So, all prepared films had regular granules distribution. By increasing the thickness, the surface of the pure ( $\text{SnO}_2$ ) film became more homogeneous and uniform, thus improved the quality of the prepared film.

To calculate the roughness for large scale the following steps are adopted:

- 1- acquired SEM images for different scales (1-50 $\mu\text{m}$ ) for all tin oxide thicknesses.
- 2- transform the SEM intensity to heights (calibrating them) according to the highest AFM images.
- 3- calculate the adopted roughness parameters for each SEM image.

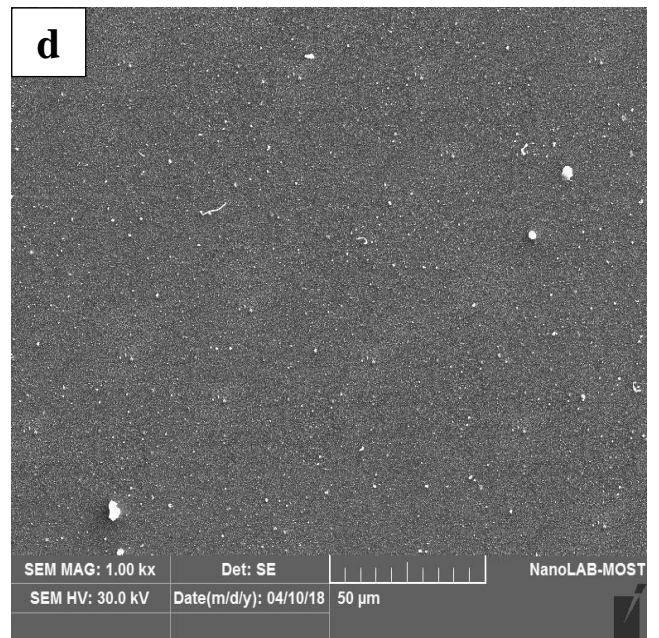
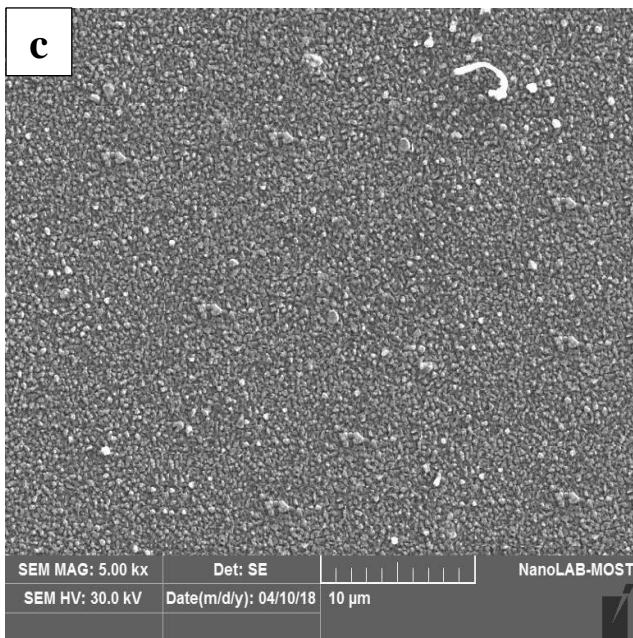
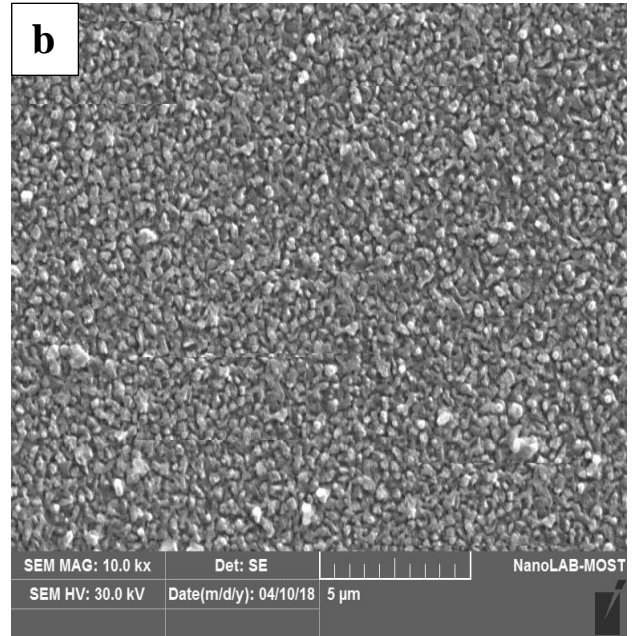
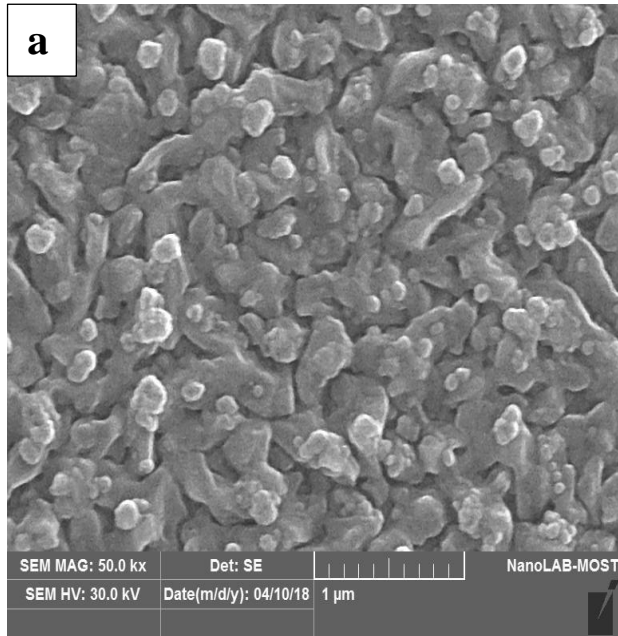


**Fig. (4-10) SEM images for 450 nm  
a- 1 μm b- 5 μm c- 10 μm d- 50 μm**

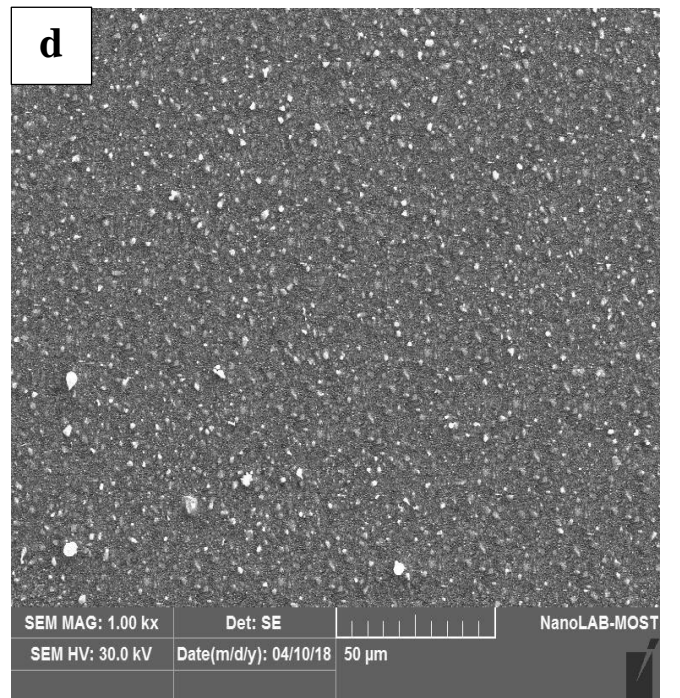
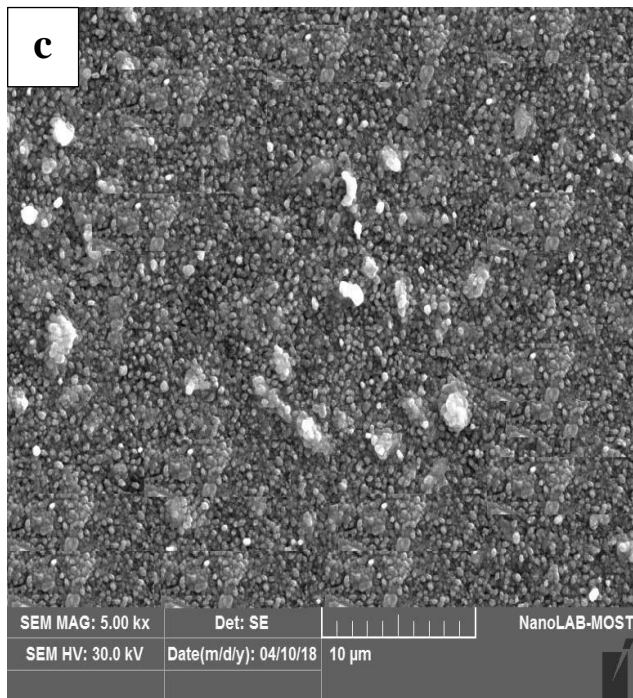
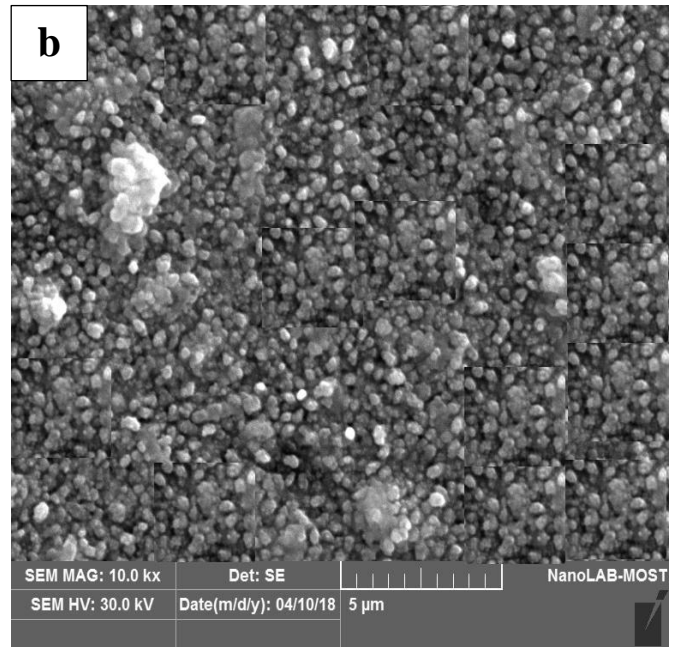
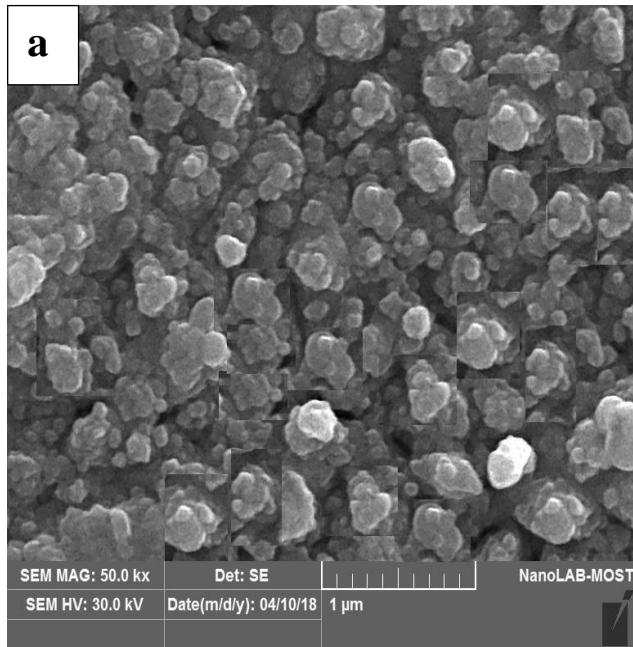


**Fig. (4-12) SEM images for 525 nm**  
**a- 1 μm b- 5 μm c- 10 μm d- 50 μm**

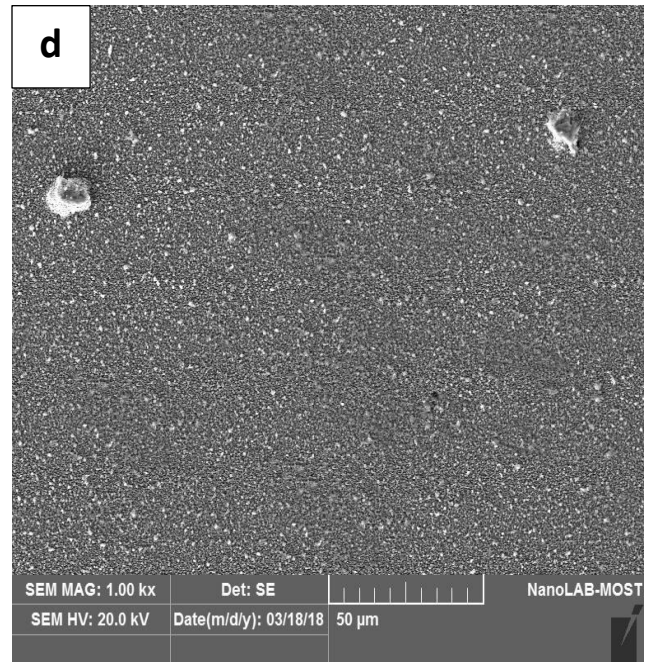
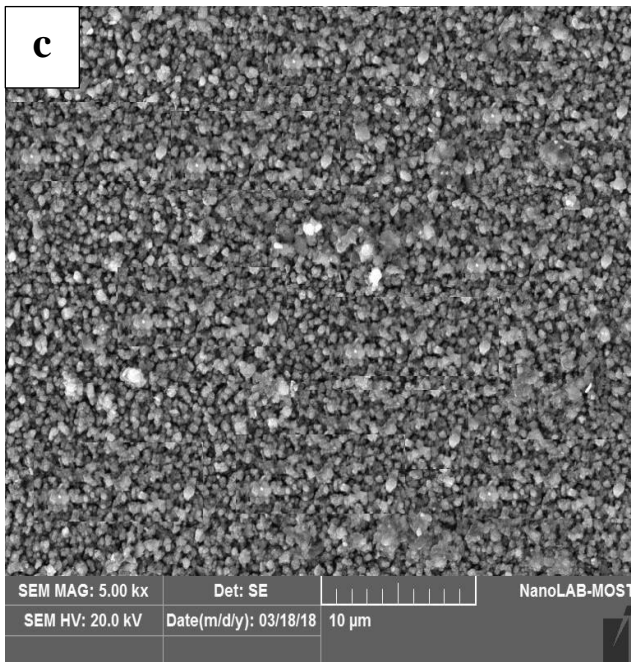
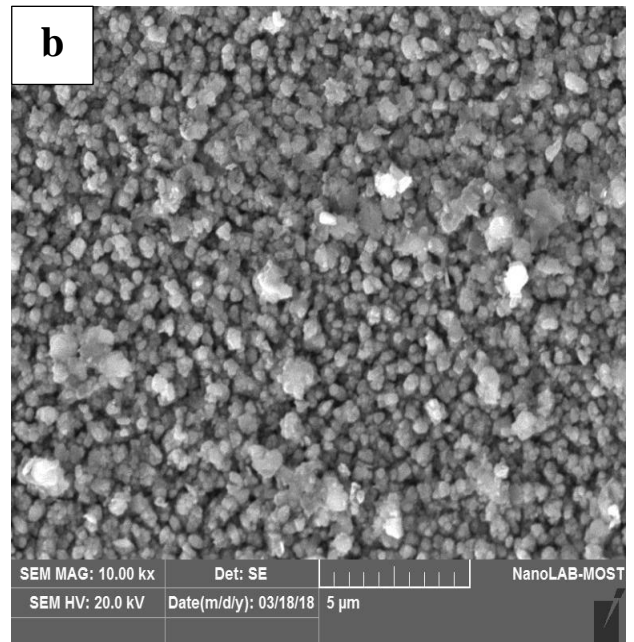
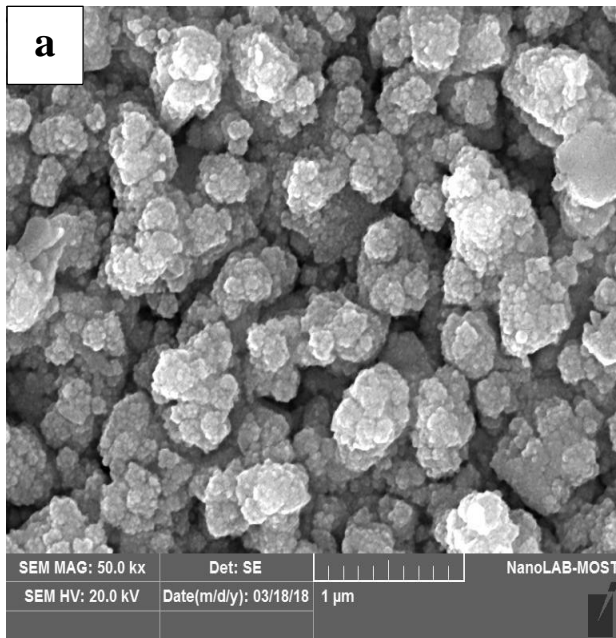


**Fig. (4-11) SEM images for 600 nm  
a- 1 μm b- 5 μm c- 10 μm d- 50 μm**

### (4-7) New method to calculation the surface roughness for SnO<sub>2</sub> films

The technique of using calibrated SEM image using AFM image to study large scale of the sample surface gives the ability to study more parameter doesn't exist in the AFM image, the highest peaks ( $S_p$ ) and the lowest valleys ( $S_v$ ) were calculated for the specimen, in addition to the average peaks heights ( $S_{pm}$ ) and the mean valleys depth ( $S_{vm}$ ) which give an indication for the depth of the samples surface scratches, beside that the total roughness ( $S_t$ ) and the mean of the total roughness ( $S_{tm}$ ) were calculated to give a numeric representation of the sample scratches which haven't measured by AFM image. Another parameter that hasn't calculated by AFM image was calculated, which the solidity factor represents the ratio of the peaks of the surface roughness to it's valleys, where this value was calculated for all spacement indicate that the number of peaks are greater than it's valleys ( $K > 1$ ) that can be easily observed visually in the AFM image.

Tables (4-6) (4-7) (4-8) show the roughness parameters values for thicknesses (450, 525, 600) nm in four scales (1, 5, 10, 50)  $\mu\text{m}$ , by comparing the parameters values obtained from the AFM scan with the calculated values from the SEM images, the variance in the values of one parameter was observed. In the case of (1 $\mu\text{m}$ ) the value of roughness increases, due to the smallness measured area and device accesses to a greater depth, in scale of (5  $\mu\text{m}$ ) the increase in the roughness value relative to the values of AFM was noticed because of the entry of peaks and valleys and increase the measured surface size, which leads to increase these values

**Table (4-6) values of roughness parameters for thickness (450) nm**

<b>Parameter</b>	<b>AFM 2 <math>\mu\text{m}</math></b>	<b>1<math>\mu\text{m}</math></b>	<b>5<math>\mu\text{m}</math></b>	<b>10<math>\mu\text{m}</math></b>	<b>50<math>\mu\text{m}</math></b>
$S_a$	0.949	2.0314	1.7441	1.6312	1.724
$S_q$	1.12	2.1924	1.8736	1.7871	1.8562
$S_{sk}$	-0.244	-0.1967	-0.1965	-0.2372	-0.2154
$S_{ku}$	2.03	1.5444	1.5603	1.6771	1.6347
$S_z$	4.27	4	3.9325	4	4
$S_p$		1.9686	2.2559	2.3688	2.276
$S_{pm}$		0.679	0.5722	0.6049	0.5934
$S_v$		2.0314	1.7441	1.6312	1.724
$S_{vm}$		0.679	0.5722	1.724	0.5934
$S_{tm}$		1.358	1.1444	1.2097	1.1868
$S_t$		4	4	4	4
$k$		1.0319	0.7731	0.6886	0.7574

Table (4-8) values of roughness parameters for thickness (525) nm

<i>Parameter</i>	<b>AFM 2<math>\mu</math>m</b>	<b>1<math>\mu</math>m</b>	<b>5<math>\mu</math>m</b>	<b>10<math>\mu</math>m</b>	<b>50<math>\mu</math>m</b>
$S_a$	0.878	1.2669	1.3246	1.3474	1.463
$S_q$	1.02	1.3415	1.4494	1.4645	1.5497
$S_{sk}$	-0.0547	-0.1862	-0.2755	-0.2654	-0.1962
$S_{ku}$	1.86	1.5769	1.8537	1.8327	1.6181
$S_z$	3.46	3.46	3.46	3.46	3.3749
$S_p$		2.1331	2.0754	2.0526	1.937
$S_{pm}$		0.3804	0.523	0.5165	0.4495
$S_v$		1.2669	1.3246	1.3474	1.463
$S_{vm}$		0.3804	0.523	0.5165	0.4495
$S_{tm}$		0.7609	1.0461	1.0329	0.8991
$S_t$		3.46	3.46	3.46	3.46
$k$		0.5939	0.6382	0.6564	0.7553

**Table (4-7) values of roughness parameters for thickness (600) nm**

<b>Parameter</b>	<b>AFM 2<math>\mu</math>m</b>	<b>1<math>\mu</math>m</b>	<b>5<math>\mu</math>m</b>	<b>10<math>\mu</math>m</b>	<b>50<math>\mu</math>m</b>
$S_a$	1.91	3.193	3.3261	3.3784	3.0313
$S_q$	2.24	3.3613	3.5973	3.6215	3.2266
$S_{sk}$	-0.2	-0.1624	-0.2371	-0.2157	-0.2122
$S_{ku}$	1.99	1.4912	1.716	1.6534	1.6799
$S_z$	8.53	7.8963	7.9158	7.9179	7.8504
$S_p$		4.807	4.6739	4.6216	4.9687
$S_{pm}$		0.8953	1.2068	1.1466	0.9754
$S_v$		3.193	3.3261	3.3784	3.0313
$S_{vm}$		0.8953	1.2068	1.1466	0.9754
$S_{tm}$		1.7907	2.4136	2.2931	1.9509
$S_t$		8	8	8	8
$k$		0.6642	0.7116	0.731	0.6101

From figures (4-13) a, (4-14) a, (4-15) a, the most calculated roughness parameters using the SEM images agree with that measured using AFM with acceptable error, the ( $S_k$ ) parameter that measured using AFM is negative which indicates that the sample has scratches more than peaks, the calculated ( $S_k$ ) parameter using the SEM image was negative, that means the sample had a small deep hole. The reason of that is due to the irregularities appears with changing the scale of the SEM images, where with increasing the SEM scales, more big grains appear in the SEM images. The differences between the measured and calculated roughness parameter was because of the change in the surface shape, where new structures appear with changing the acquired surface scale.

Finally, the unmeasured calculated roughness parameters that didn't measure by the AFM, such that the surface heights contrast. Figure (4-13 b) (4-14 b) (4-15 b) shows the results of the present work which is almost invariance with changing the acquired surface scale and that was due to the surface homogeneity. In fact, changing the sample thickness does not greatly effect on the roughness parameters behavior when the scale of the SEM acquired, image is changed.

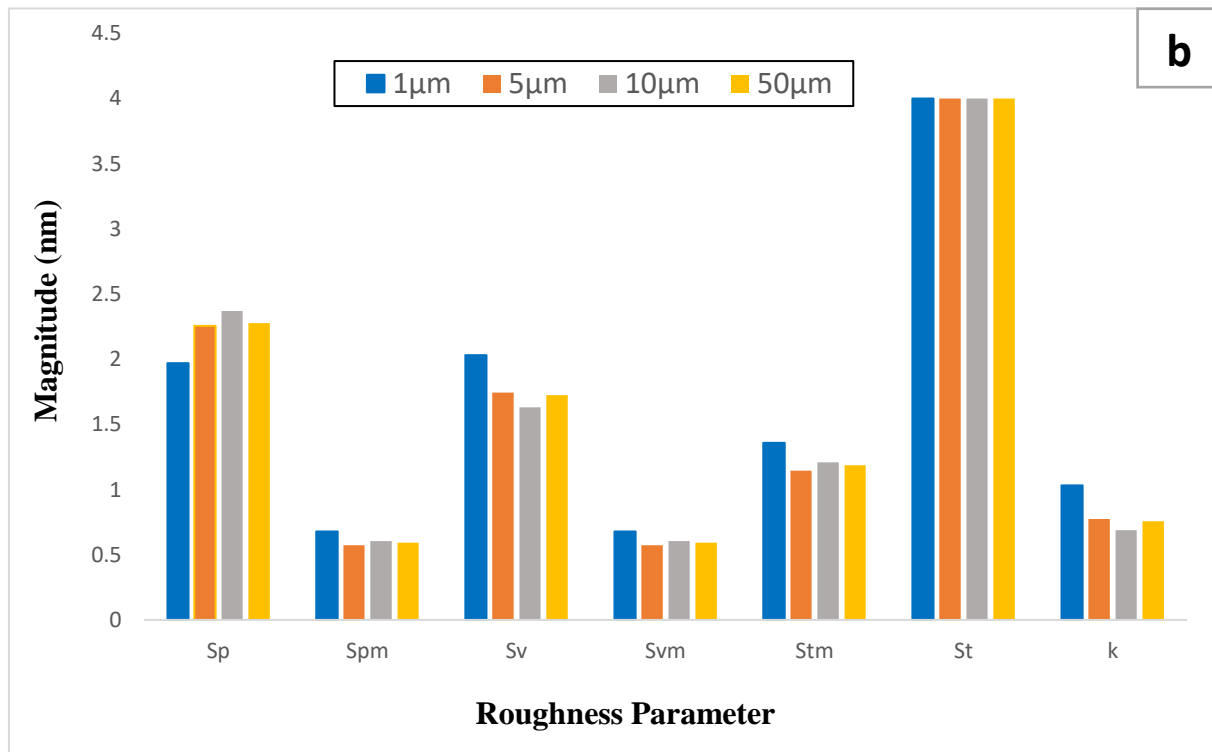
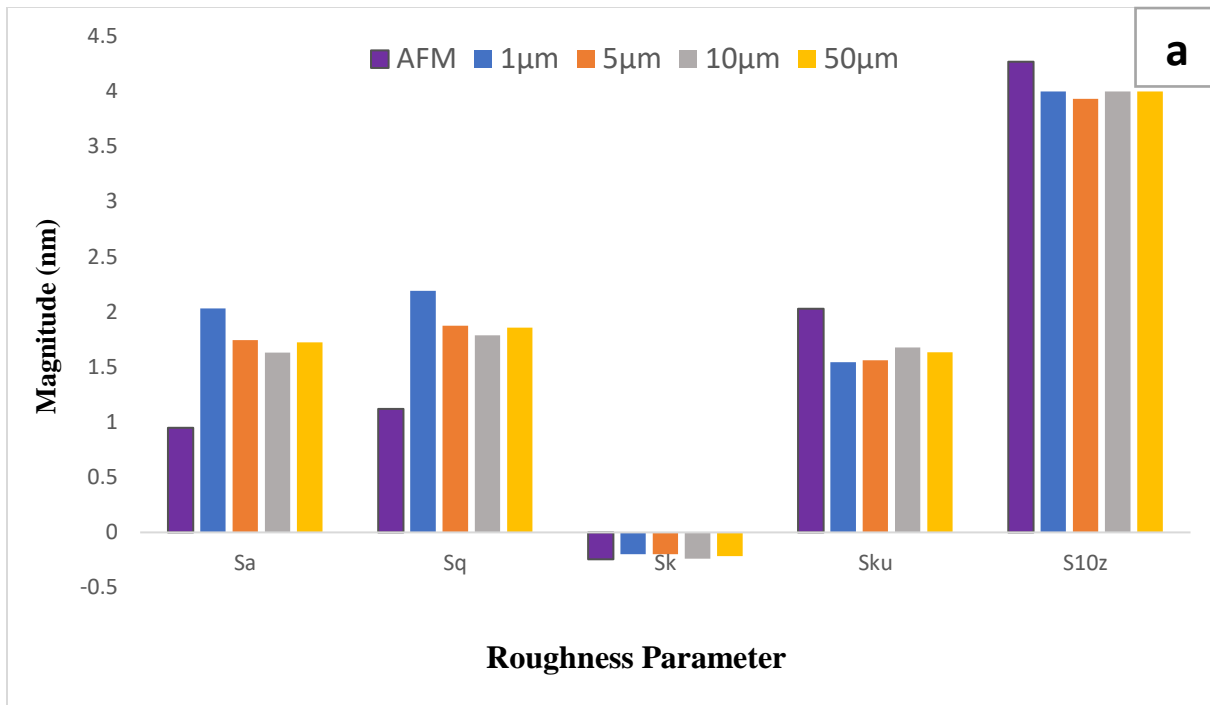


Fig. (4-13) SEM images for 450 nm

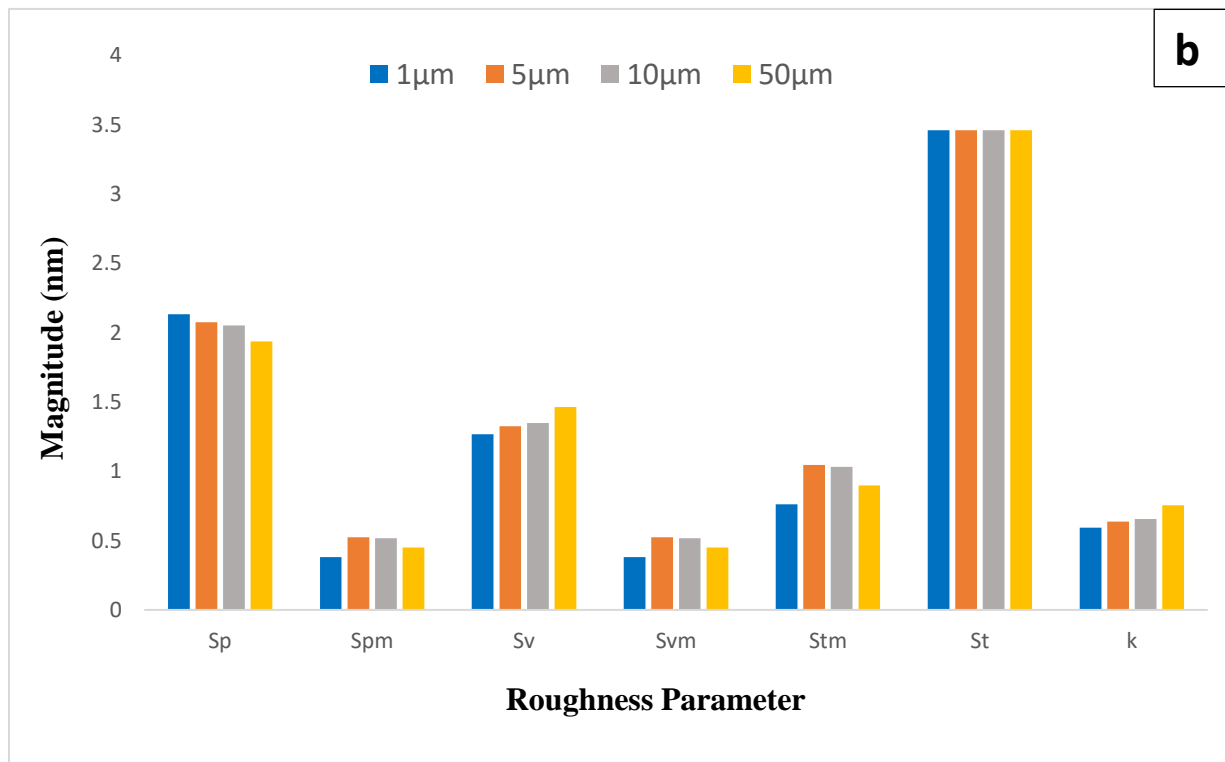
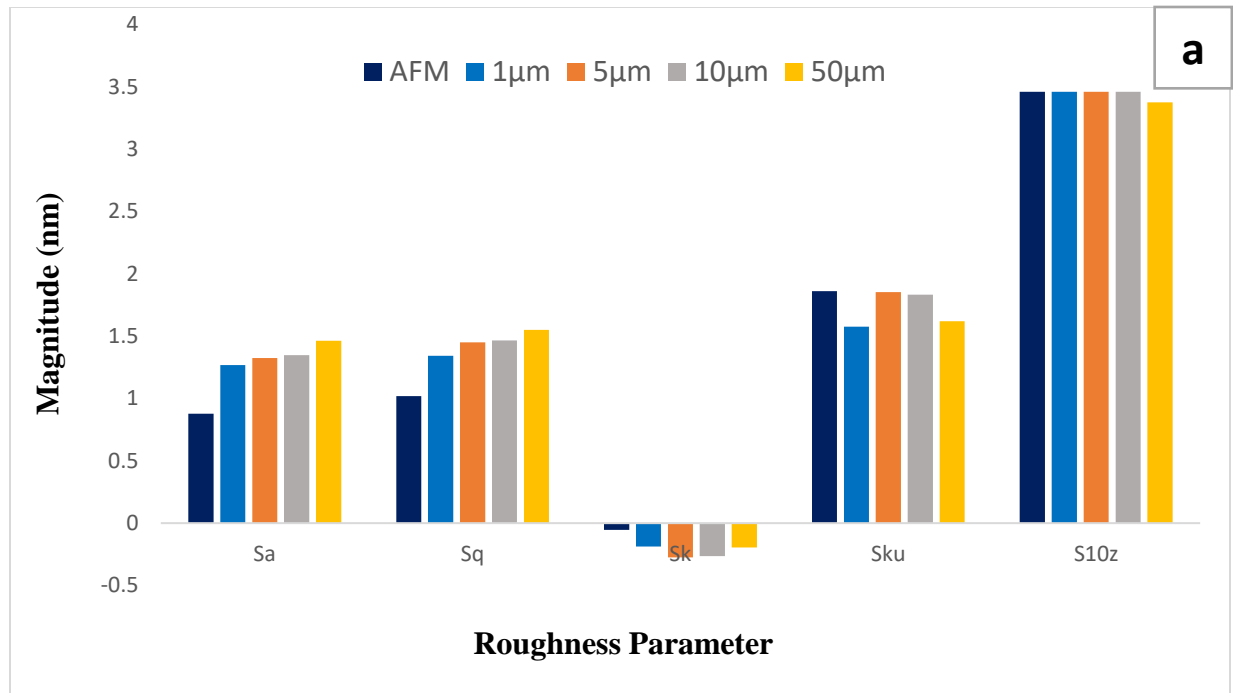


Fig. (4-15) SEM images for 525 nm

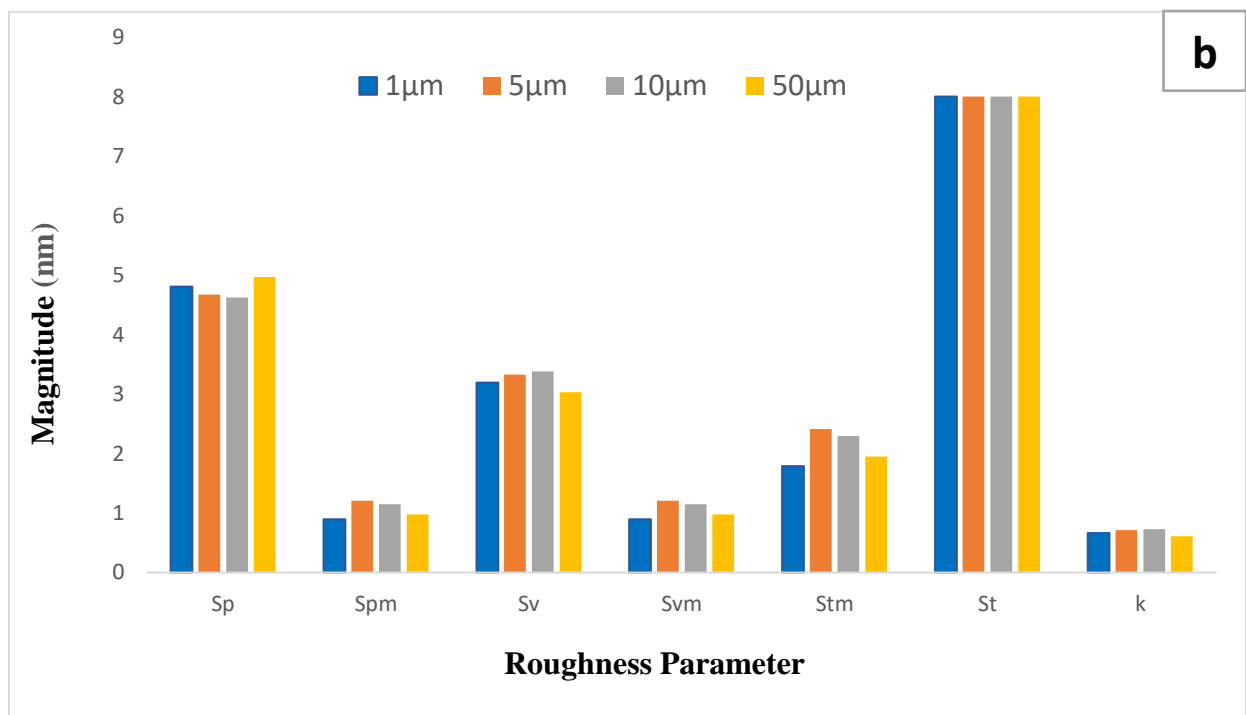
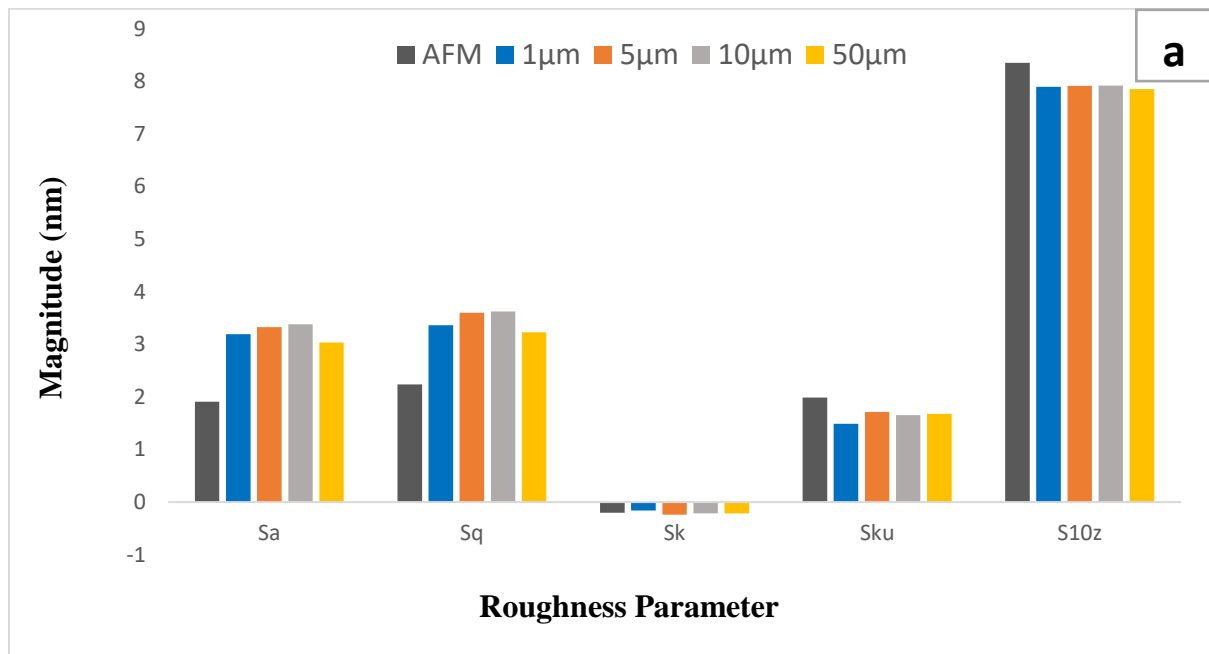


Fig. (4-14) SEM images for 600 nm

**(4-8) Conclusion:**

In this study we discussed the obtained results and reached to the most follow important:

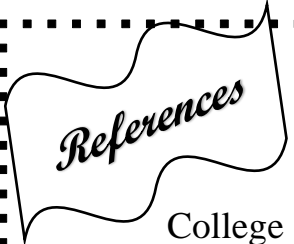
- ❖ (XRD) indication results, when the thickness of SnO<sub>2</sub> increased and at (400°) K oxidation lead to better crystallization and all the grown SnO<sub>2</sub> films are polycrystalline in nature with orthorhombic structure.
- ❖ (AFM) indication results, that the method of thermal evaporation was very suitable for depositing SnO<sub>2</sub> films on glass substrates so that no cracks or clusters were observed in specific locations without the other.
- ❖ The optical imaging techniques gave a good overview of the processes affecting the whole surface, (SEM) was used to visualize the nanoscale effects of reveal the full surface heterogeneity.
- ❖ It has from the (SEM) images that when the material thickness increased, the particles regravation in a way took clusters form with different surfaces and distributed regularly on the surface.
- ❖ The method proved the calculation validity sampling surfaces roughness. The results were similar to the roughness values obtained by the AFM test for the convergent scales between SEM and AFM. In addition, this method succeeded in calculation of other parameters such as ( $S_{ku}$ ,  $S_{sk}$ ,  $S_{vm}$ ,  $S_{pm}$ ,  $S_p$ ,  $S_v$  and  $K$ ) which gave a better description of surface roughness

**(4-9) Future works**

- i. Study the images of (SEM) for SnO<sub>2</sub> thin films doped with some impurities and annealing in different temperature.
- ii. Calculation of the porosity values for (SnO<sub>2</sub>) surface with surface roughness.
- iii. Calculation of the grain size and the inter grain distance and compare them with the surface roughness.
- iv. Develop a system with programming language on the computer in the service laboratory to read the surface roughness of the films when supplied with the images of the scanning electron microscope (SEM).
- v. Using conventional and widely accepted stylus type. Instrument for the components manufactured particularly using shaping, milling and grinding processes, indicating its effectiveness in quantification of surface roughness using SEM images.
- vi. Using the information of a top-down image obtained by Scanning Electron Microscopy (SEM) as an alternative edge boundary detection technique based on the wavelet framework.

## References

1. O. Ozatay, P. Chalsani, N.C. Emloy, I.N. Krivorotov, R.A. Buhrman, J. Appl. Phys. 95 (2004) 7315.
2. F. Meier, V. Cerletti, O. Gywat, D. Loss, D.D. Awschalom, Phys. Rev. B 69 (2004) 195315.
3. E. Roduner, Chem. Soc. Rev. 35 (2006) 583.
4. A. Dwayyan and M. Alsalhi **"Introduction to Nanotechnology"**, King Saud University Press, First Edition, (2007).
5. R. Blaunstein **"Nanotechnology"**, Guy Carpenter & Company, (2006).
6. O. S. Heavens ,**" Optical Properties of Thin Solid Films"** (1954) Copy right (1991) .
7. k. D. Lever , **" Thin Films "** London (1971) .
8. R.W. Berry and P. M. Hall ,**"Thin Films Technology"** , New York (1979) .
9. L. Eckertova, **"Physics of Thin Film "**, Plenum press, New York and London, 1977.
10. H. G. Rashid, **"Rashid" Design and optimization of thin Films optical filters With applications in the Visible and in Frared region"**, Ph. D. thesis, AL- Mustansiriyah University, 1996.
11. S. Perkins, A. Walker and E. Wolfart, **"Image Processing Operation Reference"** , Depart. Of Artificial Intelligence, Univ. of Edinburg, UK, the Hypermedia Image Processing Reference, (1994) Bob Fisher, [http://www.cee.hw.ac.ukhipr/html/hipr\\_top.html](http://www.cee.hw.ac.ukhipr/html/hipr_top.html).
12. P. Taylor, **"Computer aided detection"**, Centre for Health Information and Multiprofessional Education, Royal Free & University



## References

- College London Medical School, London, UK, Symposium Mammographicum (2002).
13. M. Batzill & U. Diebold, "**The surface and materials science of tin oxide**", progress in surface science, V. 79, P.147-154, 2005.
  14. M. Bagheri-Mohagheghi, M. Shokooh-Saremi "**Investigation on the physical properties of SnO<sub>2</sub>-ZnO transparent conducting binary \_ system deposited by spray pyrolysis technique** " Thin Film, Vol. 441, (2003) , P.(238-242).
  15. C. Chambers, A. Holliday, "**Modren Inorganic Chemistry**" Book, Translate by AL –Mousil , (1982) .
  16. D. R. Lide "**CRC Handbook of Chemistry and Physics**" , Boca Raton, Florida: CRC Press. 90<sup>th</sup> ed., PP .1-2804, (2009).
  17. H. Wang and A. L. Rogach "**Hierarchical SnO<sub>2</sub> Nanostructures: Recent Advances in Design, Synthesis, and Applications**" journal of chemistry of materials, Vol. 26, No. 1, PP.123-133, (2013) .
  18. M. M. Bagheri and M. Shokooh, "**Investigations on the Physical properties of SnO<sub>2</sub>-ZnO transparent conducting binary-binary system deposited by spray pyrolysis technique**", Thin Solid films, Vol. 441, No.1, PP.238-242, (2003).
  19. R. A. Casali, J. Lasave, M. A. Caravaca, S. Koval, C. A. Ponce and R. L. Migoni "**Ab initio and shell model studies of structural, thermoelastic and vibrational properties of SnO<sub>2</sub> under pressure**", journal of Phys, Vol.25, No.13, PP.1-11, (2013).
  20. A. House and K. House "**Descriptive Inorganic Chemistry**" Harcourt\_ Academic Press, (2001).

## References

21. ريم سامي، نادر فاضل الحبوبى وزيد محمد عبود " دراسة الخصائص التركيبية لأغشية أكسيد الكاديوم المشوب بالانتيمون باستخدام تقنيات معالجة الصور "
22. Jebor "Preparation and studying the physical Properties of SnO2 Sensor for (NO2,H2S,H2) gases detection " M.Sc thesis, College of Education ,University of Baghdad , (2010).
23. P. Saikia, A. Borthakur, P .K. Saikia, Indian J. phys., 2011, 85, 551-558.
24. Rana Osamah Mahdi "Optical Properties of Tin Oxide Nanostructure Thin Films Prepared by Simple and Classical Method" Eng. & Tech. Journal. Vol.30, No.20. 2012.
25. N. S. Sabri, M. S. M. Deni, A. Zakaria and M. K. Talari "Effect of Mn Doping on Structural and Optical Properties of SnO2 Nanoparticles Prepared by Mechanochemical Processing", Physics Procedia,Vol.25, PP.233-239 ,(2012).
26. G. R. Kandhasamy, S.Muruganand, and M.Pavithra "Surface Study of ZnO Thin Film using Image Processing Techniques" International Journal of Computer Application (0975-8887) Volume70- No.30, May 2013.
27. R. Bargougui, A. Oueslati, G. Schmerber, C. Ulhaq-Bouillet, S. Colis, F. Hlel, S. Ammar and A. Dinia "Structural, optical and electrical properties of Zn-doped SnO2 nanoparticles synthesized by the coprecipitation technique", Journal of Materials Science,Vol.25, No.5, PP.2066–2071,(2014).
28. A. R. Razeghizadeh, V. Rafee, and L. Zalaghi " Growth and Optical Properties Investigation of UN-Doped and Al-doped SnO2

## References

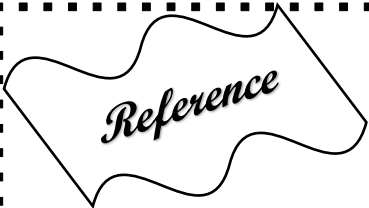
- Nanostructures by Sol-Gel Method"**, Mesoscale and Nanoscale Physics, PP.1-14(2015).
- 29.V.S. Jahnavi, S.K. Tripathy, Indian J. Res. Pharm. Biotechnol., 2014, 78-82.
30. C. Kittel " **Introduction to Solid State Physics**", 7th ed., John weily and Sons, Inc., New York, (1996).
31. M. S. El-Eskandarany " **Top-down approach accompanied with mechanical solid-state mixing for producing nanocomposite WC/Al<sub>2</sub>O<sub>3</sub> materials**", Journal of Nanoparticles, Vol.2, PP.13-22, (2009).
32. مارك ودانيال راتنر، "التقانة النانوية"، ترجمة، د. حاتم نجدي.
33. K. W. Boer " **Semiconductor Physics** " Second Edition., Vols. 1 and 2, Wiley, New York, (2001).
- 34.<http://www.makphys.com/vb3/showthread.php>
- 35.V. Pokropivny, R. Lohmus, I. Hussainova, A. Pokropivny and S. Vlassov " **Introduction in nanomaterials and nanotechnology**" MSc, postgraduates and specialists in nanotechnology University of Tartu. (2007).
36. R. N. Kostoff, R. G. Koytcheff and G. Y. Lau " **Global Nanotechnology Research Literature Overview on Research Gate**", Current Science, Vol.92, PP.1492-1499, (2008).
37. S. S. Al- Rawi , J. S. Jaber, Y. M. Hassan, " **Solid State Physics** ", Al-Mousul University, Arabic Version, (1988) .

## References

38. متي ناصر، " علم المواد " ، جامعة بغداد، (1990)
39. M. G. Yousif , " **Solid State Physics** " , Vol.1 ,  
Baghdad University , Arabic Version , (1989) .
40. محمد أمين سليمان، أحمد فؤاد باشا وشريف أحمد خيرى،  
فيزياء الجوامد " ، مطبعة الفكر العربي (2000).
41. J. S. Blakmore , " **Solid State Physics** " , Cambridge  
Press , 2nd Edition (1986) .
42. Y. N. Al-Jammal , " **Solid State Physics** " , Al-Mousul  
University , Arabic Version , (1990) .
43. K. Alexander , " **X-Ray Diffraction Procedures For  
Poly Crystalline Material** " , John Wiley and Sons ,  
(1974) .
44. M. N. Makadsi , " **Materials Science** " , High  
Education Publishing , Baghdad , Arabic Version , (1990).
45. S. Ben, " **Solid State Electronic Devices** " Hall  
International , Inc , U.S.A , (1990) .
46. M. E. Elangovan, K. Ramesh, K. Ramamurthi, (2004)  
,"**Solid State Comm.**", Ed. 130, p. 523,.
47. M. E. Elangovan, K. Ramesh, K. Ramamurthi, (2004) ,  
"**Solid State Comm.**" , Ed.130, P.523.
48. B. G. Streetman , S. Banerjee, (2000), "**Solid State  
Electronic Devices**", Prentice Hall, Inc., New Jersey, 5  
Ed.
49. مؤيد جبرائيل يوسف ، (1989) ، " فيزياء الحالة الصلبة " ، الجزء الأول .

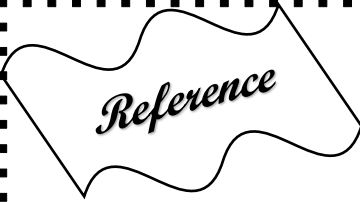
## References

50. AG. Tikle , " **Thin Film Transistor** " , John Wiley and Sons , New York , (1969) .
- 51.R. W. Hoffman , " **Physics of Thin Films** " , Vol. 3, P. 211, (1966).
- 52.K. L. Chopra , " **Thin Film Phenomena** " , Mc Graw – Hill , New York , (1969) .
- 53.Maissel and Glong , Hand Book of Thin Film Technology , Mc Graw - Hill, New York ,(1970) .
- 54.K. L. Chopra and I. Kaur , " **Thin Film Device Applications** " , Plenum Press, New York , (1983) .
55. R. W. Berry , P. M. Hall and T. Harris , " **Thin Film Technology** " , Litton Educational Publishing , New York , (1968) .
  
- 56.B. Mattes, L. Kazmarsk "**Polycrystalline and Amorphous Thin Film Device**", 2nd Ed, Academic press, (1980).
- 57.A. Beiser," **Concepts of Modern Physics** " Mc Graw-Hill Kogakusha , Ltd , 2nd Edition ,(1980).
- 58.M. G. Yousif, "**Solid state physics**", Baghdad University press, part I, (1987).
59. L. Pawlowski ,"**The Science and Engineering of Thermal Spray Coatings**", John Wiley and sons , 2nd. Edition, France , book, (2007).
60. Y. N .AL-Jammal " **Soild state physics** " , AL- Mousul University ,Arabic version , (1990).



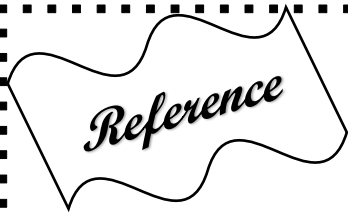
*Reference*

61. B. D. Cullity, " **elements of X-Ray diffraction** " 2<sup>nd</sup> edition , copyright © (1978) , by Addison – Wesley Publishing company , Inc.
62. F. Scholz , "**Compound Semiconductors**", (2000) .
63. C. Suryanarayana and M. G. Norton, "**X-ray Diffraction, A Practical Approach**". Plenum Press, New York, (1998).
64. R. L. Johnson, (2002) , "**Characterization of piezoelectric ZnO thin films and the fabrication of piezoelectric micro - cantilevers**" University-Ames, Iowa
65. G. Margaritondo, "**Electronic Structure of semiconductor Heterojunctions** ", London, (1988).
66. Tribble , "**Electrical Engineering Materials And Devices** ", University of Iowa , (2002).
67. Jalili, N. and Laxminarayana, K. 2004. A review of atomic force microscopy imaging systems: application to molecular metrology and biological sciences. *Mechatronics* 14(8), 907-945.
68. P. E. West, "**Introduction to Atomic Force Microscopy Theory Practice Applications** " .
69. B. Bhushan, "**Springer Handbook of Nanotechnology**", Springer Publisher, (2004).
70. Bindell, J.B. 1992 Scanning Electron Microscopy. In: Encyclopedia of Materials Characterization - Surfaces, Interfaces, Thin Films Edited by: Brundle, C.R., Evans, C.A., Wilson, S. Butterworth-Heinemann, MA, USA.



## Reference

71. Bhushan, B. 2001. Surface Roughness Analysis and Measurement Techniques. In book: Modern tribology handbook Volume I&II. EDS. Bhushan, B. CRC Press Inc., Boca Raton, Florida, USA.
72. R. J. Beane, (2004), "**Using the Scanning Electron Microscope for Discovery Based Learning in Undergraduate Courses**", Journal of Geoscience Education, Ed. 52, P.(250-253) .
73. J. Pattar , S.N.Sawant , M.Nagaraja , N.Shashank , K.M. alakrishna , G.Sanjeev , H.M.Mahesh , (2009) , "**Structural Optical and Electrical Properties of Vacuum Evaporated Indium Doped Zinc Telluride Thin Films**", Int. J. Electrochem. Sci., Ed.4 ,P.(369-376).
74. D. A. Neamen , "*Semiconductor Physics and Device*" University of New Mexico , (1992) .
75. S. M. Sze , "*Semiconductors Devices Physics and Technology* " , Translated to Arabic by F. G. Hayaty and H. A. Ahmed, Baghdad , (1990).
76. H. Bayhan, A.Sertap. and Kavasoglu, "**Admittance and impedance spectroscopy on Cu(In,Ga)Se<sub>2</sub> Solar cells** " Turk. J. Phys., 27 (2003), pp 529-535.
77. Zekai ,Sen "**Solar Energy Fundamentals and Modeling Techniques** " © Springer-Verlag London Limited.( 2008).
78. C. Kittel , "**Introduction to Solid State Physics** " , 6th Edition , Wiley (1986) .
79. A. H. Clark , "**Optical Properties of Polycrystalline and Amorphous Thin Films and Devices** " , Edited by Lawrence. L. Kazemerki , Academic Press, (1960) .



*Reference*

80. J. C. Phillips , " **Bonds and Bonds in Semiconductors** " , Academic Press ,New York and London , (1973) .
81. S. A. Tawfiq , " *A study of optical and electrical properties of the cadmium stannate material using the Co-Evaporation method* "PH.D. Thesis , Al –Mustansiriya University, (1996) .
82. M. A. Green , " *Solar Cells* " , Translated by Y. M. Hassan , Mousul University , (1989) .
83. J. I. Pankove , " **Optical Processes in Semiconductors** " , Prentice – Hall Englewood Cliffs , New Jersey , (1971) .
84. Z. M. Jarzberzki , " **Oxide Semiconductors** " , Pergamon Press , London (1973) .
85. R . A. Smith , " *Semiconductors* " , 2nd Edition , Cambridge University Press , London , (1987) .
86. M. S. Dresselhaus ," **Optical Properties of Solids** " , Part II , (1998) .
87. R. A. Levy, " **Principles of Solid State Physics** " , 5th Edition, New York, (1972).
88. S. M. Sze ," **Semiconductors Devices**", John Wiley and Sons , Ins ,(2002) .
89. C. Kittel , " *Introduction to Solid State Physics* " , John Wiley and Sons , Inc , 7th Edition , (1997).
90. M. A. Omer, (1975) , "Elementary Solid State Physics", Addison - Wesley Publishing .



## References

91. B . Saporal and C . Herman , " **Physics of Semiconductors** " , Springer Verlag , New York , Inc , ( 1995 ) .
- 92.E. Bacaksiz , S.Aksu , B.M.Basol , M.Altunbas , M.parlak and E. Yanmaz , " **Structural , Optical and Magnetic Properties Of Zn<sub>1-x</sub>CoxO Thin Films Prepared by Spray Pyrolysis** " Thin Films , Vol.516 , PP.7899-79029 ,(2008).
- 93.A. N. Abd," Quantum dots CdSe/PSi/Si Photodetector", Ph. D. thesis, AL-Mustansiriyah University,(2015).
- 94.Song, J.F. and Vorburger, T. V. 1992. Surface Texture. ASM Handbook vol. 18: Friction, Lubrication and Wear Technology, ASM International, Materials Park, OH.
- 95.Amaral Ron. Ho Chong Leonel, "**Surface Roughness**". December 2, 2002.
- 96." **Quick Guide to Surface Roughness Measurement** " , Reference guide for laboratory and workshop , Bulletin No.2229 , USA , Dec, 2016.
- 97."**SURFACE ROUGHNESS**".
- 98.Taylor Hobson , " **Exploring Surface Texture** " , A fundamental guide to the measurement of surface finish , list No. 600- 14/03 , England (2011).  
[www.taylor-hobson.com](http://www.taylor-hobson.com).
- 99.E. S. Gadelmawla , M. M. Koura , T. M. A. Maksoud , I. M. Elewa , H. H. Soliman " **Roughness Parameter** " Journal of Materials Processing Technology 123 (2002) 133-145.

## References

100. Thomas, T.R. 1999. Rough surfaces 2nd edition, London Imperial College Press, UK
101. J. A. Venaables ,"*Introduction to Surface and Thin Film Processes* " ,Cambridge University Press ,(2003) .
102. L. B. Freund and S. Suresh ,"*Thin Films Materials* " ,Brown University (2003) .
103. P. Joseph , C. Charles and J. Igor , Pump Handbook , 3rd Edition , Mc Graw – Hill , New York ,(2001) .
104. P. Prashanth ,"*Presentation of Thermal Evaporator* " , Indian Institute of Science Publication,
105. A. Kinbara , S. Baba , and N. Matuta, "*Mechanical Properties of Metal and Component Films* " , Journal of Thin Solid Films , Vol. 141 , P. 222 , (1986).
106. A. A. Shehab, S. A. Maki and Ayad A. Salih, "*The Structural and Surface Morphology Properties of Aluminum Doped CdO Thin Films Prepared by Vacuum Thermal Evaporation Technique*", Ibn Al-Haitham J. for Pure & Applied Science, 27(2): 158-169, (2014).
107. P. Miller and R. Yang, "*Scanning Tunneling and atomic force microscopy combined*", Applied Physics Letters,52: 2233-2235, (1988).



## References

108. G. Haugstad, "*Atomic Force Microscopy: Understanding Basic Modes and Advanced Applications*", John Wiley & Sons, Inc., (2012).
109. P. Eaton and P. West, "*Atomic Force Microscopy*", Oxford University Press Inc., New York, (2010).
110. E. Gyogy, E. Axente, " *Doped thin metal oxide films for catalytic gas sensors* ", Applied Surface Science, 2030, PP.4123, (2000).
111. N. Al-Hardan, M.Abdulllah, "*The gas response enhancement from ZnO film for H<sub>2</sub> gas detection*", Applied Surface Science, 255:7749-7, (2009).

## الخلاصة

في هذا البحث، تم تحضير أغشية ( $\text{SnO}_2$ ) الرقيقة غير المشوبة بطريقة التبخير الحراري بالفراغ، حيث تم ترسيب هذه الأغشية على ارضيات زجاجية ذات سمك مختلف  $[450, 525, 600]$  nm.

تمت دراسة طوبوغرافية وطبيعة السطح للأغشية المحضرة باستخدام المجهر الإلكتروني الماسح SEM ومجهر القوة الذرية AFM. أظهرت الدراسة أن التركيب السطحي للأغشية المرسبة كانت نانوية، ويتراوح قيمة الحجم الحبيبي (60-71) nm، من ناحية أخرى، وجد أن خشونة السطح تزداد (0.9 - 1.9) nm مع زيادة السمك، ويتضمن الوصف العام دراسة طوبوغرافيا السطح (حجم الحبيبات والخشونة) باستخدام صور AFM واستكشاف العلاقة مع مجموعة من معلمات الخشونة التي تم الحصول عليها من صور SEM، وهذه المعلمات ( $S_a, S_q, S_p, S_v, S_z$ ) تعطي معلومات عن ارتفاع السطح. أما المعلمات ( $S_{sk}, S_{ku}$ ) فتعطي معلومات حول توزيع الاتساعات وتناظر ارتفاعات السطح حول المستوى المتوسط.

وأظهرت نتائج حيود الأشعة السينية (XRD) لجميع الأغشية المحضرة انها ذات تركيب متعدد التبلور نوع معيني قائم وان الاتجاه السائد (111)، وتناقص قيم عرض المنحني عند منتصف القمة (FWHM) لأغشية ثنائي أكسيد القصدير بزيادة السمك.

أوضحت الخصائص البصرية المتمثلة بدراسة طيفي النفاذية والامتصاصية بصفتهما دالة للطول الموجي ضمن المدى (300 - 1100) nm ان النفاذية تقل عند زيادة سمك الغشاء. أما فجوة الطاقة البصرية للانتقال المباشر المسموح فقد لاحظنا نقصان قيم فجوة الطاقة من (2.2-3) eV مع زيادة السمك.



جمهورية العراق  
وزارة التعليم العالي والبحث العلمي  
جامعة بغداد  
كلية التربية للعلوم الصرفة / (ابن الهيثم)  
قسم الفيزياء

## دراسة الخصائص التركيبية والبصرية لغشاء ثاني أكسيد القصدير

### الرقيق وتحليلها باستخدام تقنية المعالجة الصورية

رسالة مقدمة إلى مجلس كلية التربية للعلوم الصرفة-ابن الهيثم وهي جزء من

متطلبات نيل درجة ماجستير في علوم الفيزياء

تقدم بها

نور علي حميد

بكالوريوس علوم فيزياء / جامعة بغداد 2013

بإشراف

د. إنشاق محمد علي